

ISSN 1881-7831 Online ISSN 1881-784X

DD & T

Drug Discoveries & Therapeutics

Volume 6, Number 3
June, 2012



www.ddtjournal.com

DD & T

Drug Discoveries & Therapeutics



ISSN: 1881-7831
Online ISSN: 1881-784X
CODEN: DDTRBX
Issues/Year: 6
Language: English
Publisher: IACMHR Co., Ltd.

Drug Discoveries & Therapeutics is one of a series of peer-reviewed journals of the International Research and Cooperation Association for Bio & Socio-Sciences Advancement (IRCA-BSSA) Group and is published bimonthly by the International Advancement Center for Medicine & Health Research Co., Ltd. (IACMHR Co., Ltd.) and supported by the IRCA-BSSA and Shandong University China-Japan Cooperation Center for Drug Discovery & Screening (SDU-DDSC).

Drug Discoveries & Therapeutics publishes contributions in all fields of pharmaceutical and therapeutic research such as medicinal chemistry, pharmacology, pharmaceutical analysis, pharmaceuticals, pharmaceutical administration, and experimental and clinical studies of effects, mechanisms, or uses of various treatments. Studies in drug-related fields such as biology, biochemistry, physiology, microbiology, and immunology are also within the scope of this journal.

Drug Discoveries & Therapeutics publishes Original Articles, Brief Reports, Reviews, Policy Forum articles, Case Reports, News, and Letters on all aspects of the field of pharmaceutical research. All contributions should seek to promote international collaboration in pharmaceutical science.

Editorial Board

Editor-in-Chief:

Kazuhisa SEKIMIZU
The University of Tokyo, Tokyo, Japan

Co-Editors-in-Chief:

Xishan HAO
Tianjin Medical University, Tianjin, China

Norihiro KOKUDO
The University of Tokyo, Tokyo, Japan

Hongxiang LOU
Shandong University, Ji'nan, China

Yun YEN
City of Hope National Medical Center, Duarte, CA, USA

Chief Director & Executive Editor:

Wei TANG
The University of Tokyo, Tokyo, Japan

Managing Editor:

Hiroshi HAMAMOTO
The University of Tokyo, Tokyo, Japan
Munehiro NAKATA
Tokai University, Hiratsuka, Japan

Senior Editors:

Guanhua DU
Chinese Academy of Medical Science and Peking Union Medical College, Beijing, China

Xiao-Kang LI
National Research Institute for Child Health and Development, Tokyo, Japan

Masahiro MURAKAMI
Osaka Ohtani University, Osaka, Japan

Yutaka ORIHARA
The University of Tokyo, Tokyo, Japan

Tomofumi SANTA
The University of Tokyo, Tokyo, Japan

Wenfang XU
Shandong University, Ji'nan, China

Web Editor:

Yu CHEN
The University of Tokyo, Tokyo, Japan

Proofreaders:

Curtis BENTLEY
Roswell, GA, USA
Thomas R. LEBON
Los Angeles, CA, USA

Editorial and Head Office:

Pearl City Koishikawa 603,
2-4-5 Kasuga, Bunkyo-ku,
Tokyo 112-0003, Japan
Tel.: +81-3-5840-9697
Fax: +81-3-5840-9698
E-mail: office@ddtjournal.com

Drug Discoveries & Therapeutics

Editorial and Head Office

Pearl City Koishikawa 603, 2-4-5 Kasuga, Bunkyo-ku,
Tokyo 112-0003, Japan

Tel: +81-3-5840-9697, Fax: +81-3-5840-9698
E-mail: office@ddtjournal.com
URL: www.ddtjournal.com

Editorial Board Members

Alex ALMASAN (Cleveland, OH)	Yu HUANG (Hong Kong)	Xiao-Ming OU (Jackson, MS)	Yasuko YOKOTA (Tokyo)
John K. BUOLAMWINI (Memphis, TN)	Hans E. JUNGINGER (Marburg, Hesse)	Weisan PAN (Shenyang, Liaoning)	Takako YOKOZAWA (Toyama, Toyama)
Shousong CAO (Buffalo, NY)	Amrit B. KARMARKAR (Karad, Maharashtra)	Rakesh P. PATEL (Mehsana, Gujarat)	Rongmin YU (Guangzhou, Guangdong)
Jang-Yang CHANG (Tainan)	Toshiaki KATADA (Tokyo)	Shivanand P. PUTHLI (Mumbai, Maharashtra)	Guangxi ZHAI (Ji'nan, Shandong)
Fen-Er CHEN (Shanghai)	Gagan KAUSHAL (Charleston, WV)	Shafiqur RAHMAN (Brookings, SD)	Liangren ZHANG (Beijing)
Zhe-Sheng CHEN (Queens, NY)	Ibrahim S. KHATTAB (Kuwait)	Adel SAKR (Cairo)	Lining ZHANG (Ji'nan, Shandong)
Zilin CHEN (Wuhan, Hubei)	Shiroh KISHIOKA (Wakayama, Wakayama)	Gary K. SCHWARTZ (New York, NY)	Na ZHANG (Ji'nan, Shandong)
Chandradhar DWIVEDI (Brookings, SD)	Robert Kam-Ming KO (Hong Kong)	Yuemao SHEN (Ji'nan, Shandong)	Ruiwen ZHANG (Amarillo, TX)
Mohamed F. EL-MILIGI (6th of October City)	Nobuyuki KOBAYASHI (Nagasaki, Nagasaki)	Brahma N. SINGH (New York, NY)	Xiu-Mei ZHANG (Ji'nan, Shandong)
Hao FANG (Ji'nan, Shandong)	Toshiro KONISHI (Tokyo)	Tianqiang SONG (Tianjin)	Yongxiang ZHANG (Beijing)
Marcus L. FORREST (Lawrence, KS)	Chun-Guang LI (Melbourne)	Sanjay K. SRIVASTAVA (Amarillo, TX)	
Takeshi FUKUSHIMA (Funabashi, Chiba)	Minyong LI (Ji'nan, Shandong)	Hongbin SUN (Nanjing, Jiangsu)	(As of June 2012)
Harald HAMACHER (Tübingen, Baden-Württemberg)	Jikai LIU (Kunming, Yunnan)	Chandan M. THOMAS (Bradenton, FL)	
Kenji HAMASE (Fukuoka, Fukuoka)	Xinyong LIU (Ji'nan, Shandong)	Murat TURKOGLU (Istanbul)	
Xiaojiang HAO (Kunming, Yunnan)	Yuxiu LIU (Nanjing, Jiangsu)	Fengshan WANG (Ji'nan, Shandong)	
Kiyoshi HASEGAWA (Tokyo)	Xingyuan MA (Shanghai)	Hui WANG (Shanghai)	
Waseem HASSAN (Rio de Janeiro)	Ken-ichi MAFUNE (Tokyo)	Quanxing WANG (Shanghai)	
Langchong HE (Xi'an, Shaanxi)	Sridhar MANI (Bronx, NY)	Stephen G. WARD (Bath)	
Rodney J. Y. HO (Seattle, WA)	Tohru MIZUSHIMA (Tokyo)	Yuhong XU (Shanghai)	
Hsing-Pang HSIEH (Zhunan, Miaoli)	Abdulla M. MOLOKHIA (Alexandria)	Bing YAN (Ji'nan, Shandong)	
Yongzhou HU (Hangzhou, Zhejiang)	Yoshinobu NAKANISHI (Kanazawa, Ishikawa)	Yonghua YANG (Shanghai)	

Reviews

- 112 - 122 **Monoamine oxidases in major depressive disorder and alcoholism.**
Jeremy Duncan, Shakevia Johnson, Xiao-Ming Ou
- 123 - 132 **Improved treatment of nicotine addiction and emerging pulmonary drug delivery.**
Nazrul Islam, Shafiqur Rahman

Brief Report

- 133 - 139 **Synthesis and anticancer activity of novel 5-(indole-2-yl)-3-substituted 1,2,4-oxadiazoles.**
Peng Wang, Jianzhen Liu, Hualu Xing, Yang Liu, Wencheng Xie, Guisen Zhao

Original Articles

- 140 - 146 **Time and dose-response effects of honokiol on UVB-induced skin cancer development.**
Ruth F. Guillermo, Chandeshwari Chilampalli, Xiaoying Zhang, David Zeman, Hesham Fahmy, Chandradhar Dwivedi
- 147 - 156 **Ameliorating effect of DL- α -lipoic acid against cisplatin-induced nephrotoxicity and cardiotoxicity in experimental animals.**
Asmma Hussein, Amany A. E. Ahmed, Samia A. Shouman, Sabry Sharawy
- 157 - 162 **Evaluation of skin surface hydration state and barrier function of stratum corneum of dorsa of hands and heels treated with PROTECT X2 skin protective cream.**
Takahiro Kubota
- 163 - 168 **Effect of surfactant on lycopene-loaded nanostructured lipid carriers.**
Pornthida Riangjanapatee, Siriporn Okonogi

CONTENTS

(Continued)

Guide for Authors

Copyright

Monoamine oxidases in major depressive disorder and alcoholism

Jeremy Duncan, Shakevia Johnson, Xiao-Ming Ou*

Department of Psychiatry and Human Behavior, University of Mississippi Medical Center, Jackson, MS, USA.

ABSTRACT: Monoamine oxidases play an integral role in brain function. Both monoamine oxidase A (MAO-A) and monoamine oxidase B (MAO-B) regulate neurochemistry by degrading monoamine neurotransmitters (serotonin, dopamine, and norepinephrine). Any alteration in MAO levels can have devastating effects on the brain and behavior by lowering or raising neurotransmitter levels and producing toxic reactive oxygen species. In this review article, MAO is examined in terms of function and genetic organization, with special focus on recent discoveries related to the transcriptional regulation of MAO. In recent studies, transcriptional regulation involves a repressor protein, R1, for MAO-A and an activator protein, KLF11 (a Krüppel-like factor; also referred to as transforming growth factor-beta early inducible gene 2, TIEG2), for both MAO-A and MAO-B, by binding to Sp/KLF sites in the core promoters of *MAO* and regulating *MAO* gene expression. Furthermore, KLF11 may influence MAO-B expression and augment glyceraldehyde-3 phosphate dehydrogenase (GAPDH) to upregulate MAO-B transcription upon exposure to ethanol. Finally, we review recent progress in MAO research and highlight the roles that MAOs play in several psychiatric conditions, including chronic stress, major depressive disorder and alcohol dependence. Further research in this area is needed to better understand MAOs, their transcription factors and signaling pathways in psychiatric illnesses in order to develop new strategies for pharmacological advancement.

Keywords: Monoamine oxidase, major depressive disorder, alcohol dependence, chronic stress, gene transcription, transcription factor, Krüppel-like factor 11 (transforming growth factor-beta-inducible early gene 2)

*Address correspondence to:

Dr. Xiao-Ming Ou, Division of Neurobiology & Behavioral Research G-109, Department of Psychiatry and Human Behavior, University of Mississippi Medical Center, 2500 N. State Street, Jackson, MS 39216, USA.

E-mail: xou@umc.edu

1. Introduction

Psychiatric illness, including mood disorders and alcohol dependence, causes disturbance in personality, interferes with daily routines and damages personal relationships. Not since the advent of monoamine oxidase inhibitors (MAOIs) have we realized the important role monoamine oxidase (MAO) has in psychiatric conditions. In the 1950-60's, the discovery of MAO's impact on neurotransmitter metabolism followed by an upsurge in MAO research attempted to decipher the mechanisms underlying mental disorders, such as depression.

MAO has two isoforms, MAO-A and MAO-B. Serotonin (5-HT) and norepinephrine (NE) are preferentially deaminated by MAO-A while MAO-B primarily targets phenylethylamine (PEA) and benzylamine; however, both monoamine oxidases can degrade dopamine (DA). Though its role has been thoroughly documented in major depressive disorder, only recently have scientists discovered that MAO is also impacted in stress disorders and alcoholism. Additionally, aberrant MAO levels can result in other behavioral changes in addition to depressive moods; downregulation of MAO can manifest as aggressiveness as seen in MAO-knockout studies (1). Contrarily, upregulation of MAO results in rapid metabolism of neurotransmitters and consequently damages neurons partially through its byproduct, hydrogen peroxide. This holds implications for the neuronal damage seen in alcoholism, neurodegenerative disorders, and possibly one explanation for reduced cortical volume in chronically depressed patients. In this review study, we discuss MAO in terms of genetic organization and function, and emphasize recent discoveries on the transcriptional regulation of MAO and their implications in major depressive disorder and alcohol dependence.

2. Monoamine oxidase background

2.1. Function

Monoamine oxidase oxidizes amines from both endogenous and exogenous sources, thereby influencing the concentration of neurotransmitter amines as well as

many xenobiotics by controlling their availability and physiological activity (2). MAO-A and MAO-B belong to a family of flavin-containing amine oxidoreductases; both are located in the outer membrane of mitochondria (3), but are encoded by different genes (4). Although dopamine is primarily oxidized by MAO-B in humans and by MAO-A in rodents, in most species dopamine can be oxidized by both forms of the enzyme (1), just as serotonin can also be oxidized by MAO-B – though MAO-A has preference. MAO-A has higher affinity for serotonin, norepinephrine, dopamine, and the MAO inhibitor, clorgyline, whereas MAO-B has a higher affinity for phenylethylamine (a monoamine alkaloid that regulates the release of norepinephrine and dopamine), benzylamine (a common precursor of organic compounds), and the MAO inhibitors, deprenyl (1) and rasagiline (5,6). Exogenous sources of PEA and benzylamine require regulated entry into brain suggesting a functional role for MAO-B predominance at glial cells as a component of the blood-brain-barrier.

In light of the vital role that MAO plays in the metabolism of neurotransmitters, MAO-A dysfunction have been implicated in a variety of neuropsychiatric disorders such as depression, social anxiety, autism, and attention deficit hyperactivity disorder (7). Furthermore, MAO-A deficiency caused by a spontaneous mutation in the *MAO-A* gene in a Dutch family resulted in impulsive aggressive behavior and mild mental retardation in affected males (8). In addition, *MAO-A*, specifically, may act as a pro-apoptotic gene. MAO-A expression was shown to be increased in cells during nerve growth factor withdrawal-induced apoptosis, which inhibited neuronal proliferation and accelerated cell apoptosis through the p38 mitogen-activated protein kinase pathway (9).

These harmful effects of MAO-A (also MAO-B) are produced partially through the byproducts of their enzymatic activity (monoamine degradation) which include a number of neurotoxic species, such as hydrogen peroxide, ammonia, and MPP⁺ (1-methyl-4-phenylpyridinium, a neurotoxin that dysregulates NADH dehydrogenase). In particular, hydrogen peroxide can elicit the production of reactive oxygen species (ROS) and induce mitochondrial damage and neuronal apoptosis (10).

Unlike MAO-A, significant age-related increases in MAO-B activity may contribute to cellular degeneration in the brain due to corresponding increases in the production of ROS (5,11). However, MAO-A emerges first (1) and is near adult levels at birth while a several-fold increase in MAO-B activity occurs with aging (12-14). An increase in MAO-B with age has also been verified in human positron emission tomography (PET) studies in all brain regions examined (15). Abnormally elevated levels of MAO-B are well known to be associated with neurodegenerative diseases, such as Parkinson disease and Alzheimer disease (16,17).

A consequence of increased MAO-B could result in elevated dopamine oxidation and byproducts, such as hydrogen peroxide, which form highly reactive hydroxyl radicals that subsequently damage proteins, membrane lipids, and nucleic acids leading to neuronal degeneration (5). In fact, hydrogen peroxide produced during the oxidative deamination of catecholamines produces damage to the mitochondrial membrane and DNA, which appears to be involved in the progression of neurodegenerative disorders, such as Parkinson disease (11).

2.2. MAO genetic studies

MAO-A and MAO-B share genetic homology and are highly conserved among species. Located in the outer mitochondrial membrane, MAO-A and MAO-B are encoded by two independent genes on chromosome Xp11.23-11.4 (1,4,18,19). These two genes consist of 15 exons and have identical exon-intron organization, which suggests that both *MAO-A* and *MAO-B* are derived from the duplication of a common ancestral gene (1). Interestingly, exon 12 products of *MAO-A* and *MAO-B* share 93.9% amino acid identity (4). Conversely, the arrangement of transcriptional promoters differs between the two monoamine oxidases. The *MAO-A* core promoter (0.14 kb) fragment lacks a TATA box, consists of three Sp1 (Sp/KLF) elements (20,21), and exhibits bidirectional promoter activity (21) whereas the *MAO-B* core promoter (0.15 kb) fragment consists of two clusters of overlapping Sp/KLF-binding sites separated by a CACCC element (21). The different promoter organization of *MAO-A* and *MAO-B* genes may underlie their different tissue- and cell-specific expression (1). Moreover, the conservation of these two genes indicates the biological importance of neurotransmitter regulation. This can be verified through the study of transgenic knockout (KO) mice.

In brains of MAO-A KO pups, serotonin concentrations were increased up to nine-fold compared with wild-type mice and in adult brains, serotonin levels were only increased two-fold due to the development of MAO-B (1). In the brains of MAO-A KO pups and adults, norepinephrine concentrations were increased up to two-fold, and a small increase in dopamine levels was observed in pup brains (22). Not surprisingly, the behavioral ramifications mimic the expression of neurotransmitters on a cellular level. Both MAO-A-deficient and MAO-B-deficient mice show an increased reactivity to stress in the forced-swim test (1). As norepinephrine and dopamine mediate the stress response and are further potentiated by phenylethylamine, these findings are consistent with elevated brain levels of norepinephrine and dopamine in MAO-A KO mice (22), and phenylethylamine in MAO-B KO mice (23). In addition to aberrant stress responses, MAO-A KO pups also exhibit aggressive behavior comparable to adults due to increased levels of serotonin; and this may

also be important for enhanced emotional learning that is exhibited by adult MAO-A KO mice (24). MAO-A and MAO-B double knockout mice exhibit reduced body weight, increased anxiety-like behavior and brain levels of serotonin, norepinephrine, dopamine, and phenylethylamine (25), increased baroreceptor response (26), and abnormal heart rate dynamics (27) compared to wild type mice. These studies illustrate a critical role of maintaining proper balance of MAO expression for normalcy in behavior and physiological responses. Additionally, forebrain-specific MAO-A transgenic mice generated from MAO KO mice using the calcium-dependent kinase II α promoter showed restored axonal, cellular, and dendritic patterning in the forebrain similar to wild type mice and displayed decreased aggressive behavior compared to MAO-A KO mice without forebrain-specific MAO-A expression (28). These transgenic studies provide foundational knowledge of behavioral outcomes precipitated by gene knockout and results from these studies document the importance of monoamine oxidase not only for behavior, but for many other physiological functions.

3. Transcription factors for MAO-A and MAO-B

As with any gene expression, MAO regulation is determined by transcription factor interaction within the core promoter of *MAO*. The transcription factors can be activators, co-activators, or repressors depending on their influence on RNA polymerase. Ultimately, transcription factors will determine the level of gene expression by binding to unique domains inside the promoter with RNA polymerase II to form transcription initiation complexes.

3.1. *MAO-A* transcription factors

For *MAO-A*, an extensive repeat structure contained in two 90 bp repeats within the promoter sequence (1.2 kb upstream of the *MAO-A* coding sequences) downregulates human *MAO-A* promoter activity across ethnic groups and has been shown to affect the transcriptional activity of the *MAO-A* gene promoter in a luciferase assay system (29). This polymorphism constitutes a 30 bp repeated sequence, with 3-5 copies each for different individuals. Alleles with 3.5 or 4 copies of the repeat sequence are transcribed 2-10 times more efficiently than those with 3 or 5 copies of the repeat, suggesting an optimal length for the regulatory region (29). This is also shown *in vitro*, as median MAO-A activity in cell cultures with three repeats was significantly lower than that in cultures with four repeats (20), consistent with published evidence that *MAO-A* promoter constructs bearing three repeats have lower transcriptional activity in transfected neuroblastoma and choriocarcinoma cells (29). In fact, several studies have reported other various polymorphisms of *MAO-A*, including a GA repeat polymorphism in intron 2 and

a G/T single-nucleotide polymorphism in exon 8 (7) on the X chromosome which may impact psychiatric or cognitive disorders. *MAO-A* may also have other genetic regulators not present on the X chromosome. Wu *et al.* recently found that *MAO-A* was regulated by a transcription factor encoded by the sex-determining region Y (SRY) gene located on the Y chromosome and that SRY and Sp1 form a transcriptional complex and synergistically activate *MAO-A* transcription (7). This occurs as Sp1 recruits SRY through physiological interaction, forming a transcriptional regulatory complex within the *MAO-A* core promoter capable of enhancing SRY-induced *MAO-A* gene expression. The influence of SRY on *MAO-A* expression shows sexual dimorphism, and this divergence has an important feature on neuronal activity, structure, and dysfunction with possible implications for neurodevelopmental disorders (7).

The human *MAO-A* core promoter region (-303/-64) contains four imperfect tandem repeats, with each repeat containing an Sp/KLF-binding site in reverse orientation with positive correlation existing between cellular Sp1 concentrations and *MAO-A* promoter and catalytic activities (30). This suggests *MAO-A* gene expression can be upregulated by Sp1. Sp1 is expressed ubiquitously in mammals (31,32) and is a key activator of the *MAO-A* promoter (30) by binding to GC-rich regions (27). Besides Sp1, two Sp-family proteins, Sp3 and Sp4, have also been shown to regulate the *MAO-A* promoter *via* the same Sp/KLF-binding sites (7). Sp4 activates the *MAO-A* core promoter like Sp1, while Sp3 may compete with Sp1 and Sp4 to repress *MAO-A* activation (33). A recently discovered novel transcription repressor, R1, has been shown to downregulate *MAO-A* gene expression by competing with Sp1 for binding to Sp/KLF-binding sites as well (34).

3.2. Novel *MAO-A* repressor, R1

R1 (RAM2/CDCA7L/JPO2) is expressed widely in the human brain and peripheral tissues and includes a nuclear targeting sequence (aa 301-318) with a subcellular distribution in the nucleus, consistent with its functional role in the transcriptional regulation of MAO-A (34). R1, consisting of 454 amino acids with 77 amino acid residues in the C-terminal, shares 87% homology with the c-Myc target protein, JPO1 (34). c-Myc can act as a transcription factor and also plays a pivotal role in global chromatin structure by regulating histone acetylation. Therefore, R1 may interact with c-Myc in tumor genesis and cell division.

R1 directly impacts MAO-A expression. R1 binds to Sp/KLF-binding sites in the *MAO-A* core promoter and inhibits *MAO-A* promoter and catalytic activities (34). This notion is supported as Ou *et al.* demonstrated that R1 mRNA decreased 70%, 60%, and

45%, and MAO-A mRNA levels were increased by 2.5, 3.8, and 4.3-fold on days 1, 2, and 3, respectively, following serum starvation-induced apoptosis (35). R1 overexpression increases cell proliferation and decreases MAO-A activity whereas R1 knockdown by siRNA decreases proliferation and increases MAO-A mRNA (35), suggesting that R1 is upstream to MAO-A. Therefore, R1 overexpression prevents apoptosis, an event mediated by its repression of MAO-A. Thus, the pendulum shift between R1 and MAO-A has imperative roles in regulating the cell cycle and are negatively correlated in function and expression.

R1's role in cellular proliferation is further verified by immunostaining showing its colocalization with c-Myc, and that overexpression of c-Myc increases R1 mRNA. This increase is further escalated by inhibiting p38 MAPK in a concentration-dependent manner (35) as R1 is downstream to both c-Myc and p38. The interaction between R1 and c-Myc is co-operative in cell-cycle regulation. Furthermore, RT-PCR results show that cells transfected with R1 and/or c-Myc exhibited decreased MAO-A mRNA and increased E2F1 or cyclin D1 by 350-500%, demonstrating that E2F1 and cyclin D1 are also downstream of R1 (35).

These results show that MAO-A is not only involved in the oxidation of neurotransmitters but also plays a significant role in cellular development. Since the byproduct of MAO-A activity is hydrogen peroxide (H_2O_2) resulting in cytotoxic stress which causes cell death, R1 may therefore prevent cells from undergoing apoptosis. Understanding the mechanics of up/downstream signaling pathways will allow greater

insight into MAO-mediated apoptosis. Further research to elucidate this transcription factor, R1, its signaling pathway, and regulators in detrimental conditions such as mental illness could explain morphological changes in the brain that have been unaccounted for.

3.3. Novel MAO-A activator, KLF11 (TIEG2)

Krüppel-like factor 11 (KLF11), also referred to as transforming growth factor-beta-inducible early gene 2 (TIEG2), is a member of the Sp/KLF family of transcription factors. KLF11 can inhibit cell growth by acting as a potential effector of the transforming growth factor β (TGF β) signaling pathway and increases the rate of apoptosis in KLF11 transgenic pancreatic cells (36). Aside from its role in cell-cycle regulation, KLF11 has recently been reported to act as a transcriptional activator of MAO-A. In addition, glucocorticoid exposure can further amplify KLF11 expression and influence KLF11-induced MAO-A transcriptional activation (Figure 1A). In brain-derived SH-SY5Y cell lines, treatment with dexamethasone, a synthetic glucocorticoid, resulted in a 2.3-fold increase in KLF11 expression and 3.3-fold increase in nuclear fraction (37), suggesting increases in both KLF11 protein levels and translocation to the nucleus in the presence of dexamethasone. Examining the significance of KLF11 action on MAO-A, cells stably transfected with KLF11 showed a 2-fold increase in MAO-A mRNA levels and a 4.2-fold increase in MAO-A mRNA following dexamethasone treatment compared to control vector (37). Interestingly, when cells were treated with KLF11-

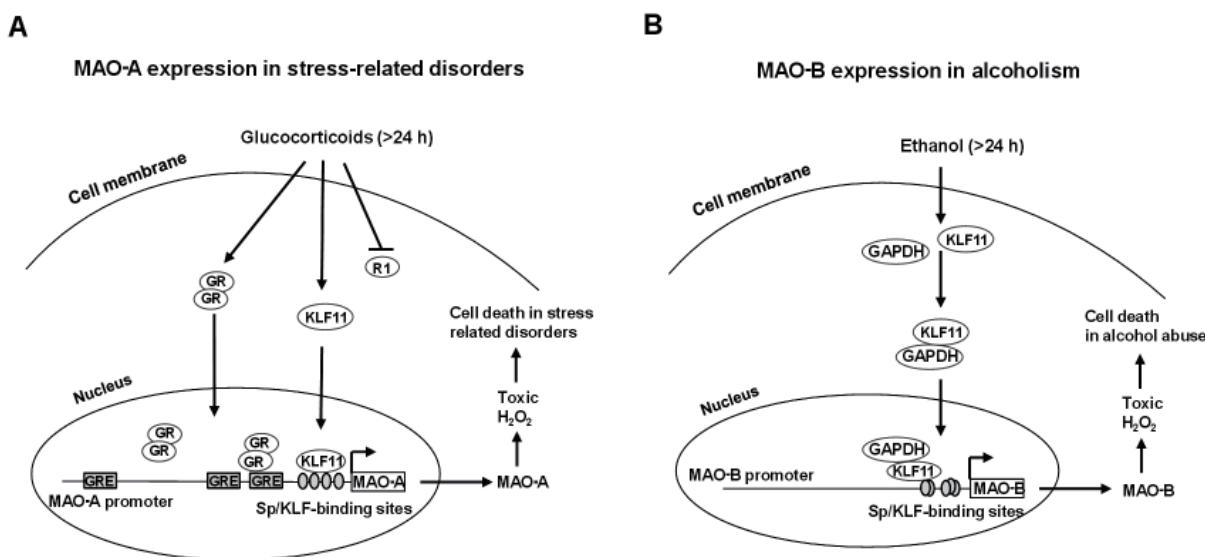


Figure 1. A representative structure of the transcriptional regulation of MAO-A gene expression (A) in stress-related disorders and MAO-B gene expression (B) in alcohol-related disorders. (A) The human MAO-A promoter contains glucocorticoid response element (GRE) and Sp/KLF-binding sites, both of which are independently responsive to the impact of glucocorticoids on MAO-A upregulation. **(B)** The human MAO-B promoter contains Sp/KLF-binding sites, which are responsive to ethanol-induced GAPDH/KLF11-mediated upregulation of MAO-B and subsequent cellular toxicity. Arrows and dashed line indicate activation and repression of the following targets, respectively. R1: a transcriptional repressor; GR: glucocorticoid receptor; GAPDH: glyceraldehyde-3-phosphate dehydrogenase; KLF11: Krüppel-like factor 11 (also called TIEG2).

siRNA to deplete endogenous KLF11, dexamethasone-induced MAO-A expression was reduced by 30% compared to control-siRNA cells showing that KLF11 mediates corticoid-induced upregulation of MAO-A (37).

KLF transcription factors have been shown to interact with histone acetyl transferases (HATs), such as p300, to regulate transcription. To further evaluate how KLF couples to chromatin remodeling machines, cells were transiently co-transfected with a p300 and KLF11 expression constructs in the *MAO-A* promoter-luciferase reporter gene which showed that activation of *MAO-A* by KLF11 was greatly increased when co-transfected with p300 (37). Therefore, successful augmentation of KLF11 by this particular HAT shows that glucocorticoids act through KLF11 to upregulate *MAO-A* promoter activity, and this pathway is mediated by a p300-dependent mechanism. Furthermore, rats exposed to chronic social defeat stress revealed a significant increase of both MAO-A and KLF11 levels in the brain cortex compared to the untreated control rats, providing further *in vivo* data that KLF11 is a novel activator for *MAO-A* (37).

3.4. MAO-B transcription factors

The human *MAO-B* core promoter (0.15 kb) fragment contains two clusters of overlapping Sp/KLF-binding sites separated by a CACCC element, and a TATA box (21,38). Among others, modulators of MAO-B expression include DNA status and hormonal influence. DNA methylation of CpG sites in the *MAO-B* promoter epigenetically inhibits *MAO-B* gene expression (39) as these regions become silenced. In addition, glucocorticoids and glucocorticoid receptors upregulate MAO-B transcription through the fourth glucocorticoid response element of the *MAO-B* promoter, which has been recently found to overlap with a consensus retinoic acid response (RAR) element suggesting the potential regulation of MAO-B by retinoic acid (40). Moreover, retinoic acid activates MAO-B transcription through RAR- α and the third RAR element in the *MAO-B* promoter as RAR- α physically interacts with Sp1 *via* zinc finger domains in Sp1 (40). Collectively, these known regulators exhibit the complexity underlying MAO-B expression. Still, many elements are unknown about the functionality of these regulators in different environmental conditions, such as retinoic acid/*MAO-B* interaction during development and Sp-family/*MAO-B* interactions in psychiatric illness.

MAO-B gene expression can also be regulated through signaling pathways. For example, phorbol-12-myristate-13-acetate (PMA), an extracellular stress inducer, increases human MAO-B expression. PMA transiently increases *Egr-1* and *c-Jun* gene expression *via* protein kinase C and MAPK signaling pathways, including Ras, MEK1, MEK3, MEK7, ERK2, JNK1, and p38/RK (41). Site directed mutations show that

Egr-1 and *c-Jun* then transactivate the *MAO-B* promoter and increase endogenous MAO-B transcripts *via* the Sp1/Erg-1/Sp1 overlapping binding sites (41). Additionally, protein kinase C inhibitor blocks the PMA dependent activation of *MAO-B* indicating that MAO expression is selectively induced by the activation of protein kinase C and MAPK signaling pathways and that *c-Jun* and *Egr-1* appear to be the ultimate targets of this regulation (41).

The Sp-family proteins also demonstrate a significant impact on MAO-B transcriptional regulation. Analysis of nine site-directed mutations exhibiting the highest activity at -246/-99 region reveals that both clusters of Sp/KLF-binding sites contribute positively whereas the CACCC element contributes negatively to transcriptional activity (42). Sp1 can activate the *MAO-B* core promoter *via* Sp/KLF-binding overlapping sites, and its activation is repressed by Sp3 interaction as determined by gel shift analysis (34,42) just as *MAO-A*. Furthermore, Sp4 can trans-activate *MAO-B* promoter activity *via* Sp1 clusters suggesting that the binding to overlapping Sp1 sites by various members of the Sp family is important for the upregulation of *MAO-B* gene expression, whereas over-expression of Sp3 or BTEB2, an Sp3-related family member, can repress activation (38). Sp3 is a ubiquitously expressed transcription factor, closely related to Sp1 but, unlike Sp1, often functions as a transcriptional repressor by means of interacting with GC-rich Sp/KLF-binding sites (43,44). Sp3 has no net effect on *MAO-B* gene expression as it *i*) represses the transcription of the human *MAO-B* gene by interaction with the CACCC box, *ii*) activates *MAO-B* through proximal overlapping Sp1 sites, and *iii*) has bi-functional regulation with independent modular repressor and activator domains (42). KLF11 also influences the expression of MAO-B (42).

3.5. Novel MAO-B activator, KLF11 (TIEG2)

Studies have shown that KLF11 (TIEG2) represses gene transcription and regulates cell growth, development and differentiation (45) by binding to GC-rich Sp/KLF-binding sites (46,47). In addition to *MAO-A* transcriptional activation, KLF11 has recently been shown to activate *MAO-B* gene expression (42), which implicates that one function of MAO-B may serve as an anti-proliferating mechanism. KLF11 reportedly inhibits cell growth (46) and mediates caspase-3-dependent apoptosis (48). Depending on where KLF11 binds within the promoter will influence how MAO-B is expressed. KLF11 serves as a repressor when binding through the CACCC element but as an activator when binding through proximal Sp/KLF-binding sites (42). Thus, KLF11 serves dual functions as both a regulator of cell-cycle-dependent activities and as a transcriptional activator for both *MAO-A* and *MAO-B*.

4. Implications for MAO in psychiatric illness

4.1. Impact of stress on MAO

Chronic stress encompasses the psychological perturbations that affect the normal physiological state of the body and interferes with emotional, cognitive, and physical aspects of health. Often, stress may precipitate or present comorbidly with depression. A major response to stress is the production of glucocorticoids, steroid hormones secreted from the adrenal zona fasciculata, which play a crucial role in sympathetic arousal, immunity, and behavior. Excessive glucocorticoid exposure can result in neuronal cell death and dysregulation as an abnormal increase of glucocorticoid levels has been associated with atrophy of the hippocampus (49) and major depression (50). Additionally, stress has been correlated with increased salivary activity of MAO-A and MAO-B (51). Stress may also impact the expression of monoamine oxidases, further decreasing monoamine availability in depression.

As MAO and glucocorticoid hypersecretion are associated with depression, the synthetic glucocorticoid, dexamethasone, has been documented to increase MAO-A activity but decrease the MAO-transcriptional repressor, R1, in human neuroblastoma and glioblastoma cells through its role as a cellular stressor (52) (Figure 1A). For example, dexamethasone administration to older Sprague-Dawley rats can increase MAO-A density in the brain by 300% (53), and dexamethasone has been shown to increase MAO-A mRNA, protein, and enzymatic activity in human skeletal muscle cells (54). Furthermore, dexamethasone increases MAO-A in the dorsal raphe nucleus in rats (55), induces MAO-B expression and activity in both neuronal cells (56) and astrocytes (57), and ultimately reduces the number of viable brain cells (58).

The biological action of glucocorticoids and androgens are mediated through their respective receptors, glucocorticoid receptor (GR) and androgen receptor (AR) (12). GR and AR undergo dimerization before binding to a specific region in their promoter responsible for gene expression, the glucocorticoid response element (GRE) and the androgen response element (ARE), respectively. There are three consensus GRE/AREs and a core promoter with four Sp/KLF-binding sites that have been identified within the human *MAO-A* 2 kb promoter region (Figure 1A); Ou *et al.* reported that deleting the third GRE/ARE reduced the glucocorticoid effect compared to that of wild type upon dexamethasone exposure, yet still showed an increase in *MAO-A* promoter activity as compared to cells not treated with dexamethasone. These results suggested that the third GRE/ARE element was important for the GR activation (52). In the case of MAO-B, four consensus GREs have been identified in the *MAO-B* 2

kb promoter and GRs directly bind to GRE4 (59). Much like *MAO-A*'s third GRE, glucocorticoid complexes may target a particular region within the promoter. In addition, Sp/KLF-binding sites in the *MAO-B* core promoter are also necessary for glucocorticoid activation of the *MAO-B* promoter as deletion of Sp/KLF-binding sites downstream of GRE4 reduced *MAO-B*'s response to glucocorticoids (59). Indeed, Sp1 appears to be a key player in glucocorticoid regulation over MAO-B as removal of GRE in the core promoter still results in glucocorticoid-inducible MAO-B upregulation (59). Glucocorticoids also show an ability to directly interact with basal transcription factors, such as TATA-binding protein, transcription factor IIB (TFIIB) and other co-activators. To counteract the effect of glucocorticoids, R1 is shown to compete with Sp1 for binding to Sp/KLF-binding sites in the *MAO-B* core promoter, thereby exerting repressing effects on MAO-B (59). In fact, overexpression of E2-F associated phosphoprotein (EAPP), a ubiquitous nuclear protein, and R1 reduces both basal and Sp1-enhanced glucocorticoid activation (59), suggesting cell-specific events may supersede the action of glucocorticoids.

Chronic stress may result in long-lasting changes in the brain due to elevated levels of MAO including increased cell death due to the presence of ROS. As a result, an MAO inhibitor prevents cell death related to this manner of toxicity (60). M30, a new inhibitor of MAO, has recently demonstrated its effectiveness in neuroprotection by significantly decreasing the enzymatic activity of both MAO-A and MAO-B in human neuroblastoma cells while also decreasing the amount of fragmented DNA due to ROS production and increasing cell viability in stressful environments (61). Compared to rasagiline and selegiline, which are irreversible MAO-B inhibitors, M30 had the highest neuroprotectivity by providing the greatest decrease in cell death rates and MAO-A activity following dexamethasone-induced toxicity (61). In light of the neuroprotective advantages MAO inhibitors provide, newer generations of MAO inhibitors, currently used for the treatment of depression and neurodegenerative diseases, may be potential drug candidates for alleviating the toxic, pejorative effects of increased MAO-A and MAO-B in chronic stress.

4.2. MAO-A in depression

Major depressive disorder (MDD) has a lifetime prevalence of 16.6% (62), making it an important topic of research and necessitating new pharmacological targets in clinical treatment. Since resistance to treatment and recurrence of major depressive episodes constitute a large portion of the MDD burden, it is important to evaluate monoamine dysregulation during and after selective serotonin re-uptake inhibitor (SSRI) treatment. Moreover, the MAO theory of depression is

bolstered since SSRI's have no direct effect on MAO's and work secondarily on transporters that are responding to changes in monoamine concentration. Meyer *et al.* were able to demonstrate that greater MAO-A binding during major depressive episodes persists after short-term SSRI treatment and is greater during recovery from MDD (63). This supports an ongoing monoamine-lowering process due to pathological conditions that is not entirely counterbalanced by SSRI treatment. From the perspective of the monoamine theory, SSRIs raise serotonin levels vigorously (64), whereas elevated MAO-A levels would be expected to metabolize serotonin and other monoamines readily. The high recurrence rates of major depressive episodes following short-term SSRI treatment indicate the power of MAO-A on the monoamine-lowering process. With MAO-A binding greater during recovery, an underlying impaired ability to regulate monoamines is present competing to lower monoamine concentrations which have been increased by SSRI treatment. Hence, the mismatch between monoamine levels raised by treatment and monoamine levels lowered by disease processes might, at times, contribute to a lack of response to SSRI treatment (63). Another aspect to consider in MAO theory is that MAO-A metabolism creates ROS that are potentially neurotoxic if present in excess, such as hydrogen peroxide. This could be one explanation for dendritic loss, cortical shrinkage, and neuronal apoptosis associated with MDD.

A promising avenue to depict human MAO-A density and distribution *in vivo* during a major depressive episode is using positron emission tomography (PET) with harmine-labeled carbon 11 ([¹¹C]harmine), a selective, reversible PET radio tracer with high affinity for the MAO-A enzyme, showing high brain uptake in humans with the greatest uptake in regions with the highest MAO-A density. Meyer *et al.* reported that MAO-A density was elevated throughout the brain on average by 34% in MDD patients compared to controls, with the highest densities in the thalamus and cingulate cortex (65). These areas are of great significance as the thalamus, particularly the ventral posterolateral segment, has many acetylcholinergic projections containing MAO-A. The anterior nucleus has connections with the cingulate gyrus and the dorsomedial nucleus projects to the frontal lobe, both of which are implicated in mood processes. With no other studies explaining why monoamine levels are lower during a depressive episode, it is thereby plausible that an elevation in brain MAO-A density is the primary monoamine-lowering process during major depressive episodes (65).

Genetic polymorphisms may also contribute to MAO-A expression and lower levels of neurotransmitters seen in depression. The MAO-A coding gene (Xp11.4-Xp11.3) presents a well-characterized variable number tandem repeat (VNTR) functional polymorphism in the

promoter region, which has two common alleles that selectively influence protein transcription and, hence, enzymatic activity (66). Beyond environmental factors, proof exists that innate genetic polymorphisms may ultimately impact susceptibility of psychiatric illness.

The role of R1 in MDD has only recently been investigated. As R1 is a novel repressor of MAO-A and is also involved in cell cycle regulation, further research to elucidate their activity in mental illness is needed to determine whether morphological changes in the brain are contributed by R1. To support this notion, Johnson *et al.* reported a decrease in R1 by 37.5% and an increase in MAO-A levels by 40% in human postmortem prefrontal cortices diagnosed with major depressive disorder (MDD) who had not undergone antidepressant drug therapy (67). Additionally, R1 levels in depressed individuals receiving antidepressants had comparable levels of R1 to that of non-medicated depressed, suggesting that current antidepressants do not significantly modulate R1 levels. These results corroborate the notion reported by Meyer *et al.* that antidepressant treatments do not adjust MAO-A binding even after 6 weeks of SSRI treatment but only compensate increased MAO-A expression by amplifying neurotransmitter levels at the synapse. With results indicating elevated MAO-A-binding and reduced R1 levels *in vivo*, and that current antidepressant treatments have no significant impact on the oxidation of monoamines, future research on R1 as a diagnostic tool and pharmacological target is justified.

4.3. MAO-B in alcoholism

Alcoholism is a substance use disorder with a lifetime prevalence of 14.6% (62) that results in cognitive impairments and brain cell loss. It is also a major psychiatric condition that causes approximately one-half of alcoholics to suffer from neuropsychological difficulties (68,69) that affect physical health and memory along with social, family, and job responsibilities (70,71). Ethanol also induces neuronal cell death and cell cycle delay in cell model systems *in vitro* (72-74). Furthermore, alcohol-use disorders have been shown to reduce prefrontal cortex volume as compared to healthy controls (75) and lower densities of neuronal and glial cells in brains from human subjects with alcohol dependence (76,77). In addition, MAO-B has been implicated in alcoholism (78) and until recently, it was unclear exactly how MAO-B was involved. As previously discussed, MAO-B can generate ROS from the breakdown of biogenic amines, and is upregulated in response to KLF11 (TIEG2) binding at the core promoter region of MAO-B promoter. Therefore, the KLF11(TIEG2)-MAO-B cascade has a role in cell dysfunction and damage (79) related to alcohol use disorders.

Glyceraldehyde-3-phosphate dehydrogenase (GAPDH) is a multifunctional protein that catalyzes and breaks down glucose with the release of energy and carbon (80), occurring during the 6th step of glycolysis. Recently, GAPDH has been implicated in other non-metabolic roles involving the initiation of apoptosis and transcriptional regulation. Furthermore, the protein level of GAPDH was not only increased in the prefrontal cortex of brains from human alcoholics (81), but also elevated in rat brains that were exposed to ethanol (79). To examine the relationship between GAPDH and the KLF11-MAO-B cascade, Ou *et al.* treated human brain cell lines with ethanol and found that MAO-B mRNA levels were significantly increased by 4-fold and GAPDH was increased 3.5-fold in the nucleus with a 1.8-fold increase overall following ethanol treatments (79). Under these conditions, GAPDH-KLF11 co-immunoprecipitation was increased in the nucleus, levels of GAPDH interacting with KLF11 were increased, and KLF11-elicited *MAO-B* gene transcription is enhanced more by the coexpression of GAPDH (79). These results indicate that GAPDH can increase MAO-B *via* KLF11 in the presence of ethanol by translocating to the nucleus where it binds to KLF11 and augments KLF11-mediated gene transcription for *MAO-B* at Sp/KLF binding sites (79), thereby resulting in subsequent cell damage in neuronal cells exposed to ethanol due to increased MAO-B-mediated oxidative stress (Figure 1B). Remarkably, ethanol exposure in the presence of an MAO-B inhibitor (deprenyl) reduced the expression of both KLF11 and MAO-B and increased cell viability (60). Moreover, a new MAO-B inhibitor (rasagiline) and its metabolite could decrease ethanol-induced cell death by preventing nuclear translocation of GAPDH in cell cultures *in vitro* (80).

In vivo studies examining the prefrontal cortex (PFC) from postmortem subjects with alcohol dependence showed a significant increase in protein levels of GAPDH and MAO-B compared to normal subjects while ethanol-preferring rats showed a two-fold increase in GAPDH and a 1.7-fold increase in MAO-B protein in the PFC when exposed to ethanol for 4 weeks (82). Interestingly, rats treated chronically with ethanol not only showed an increase in GAPDH and MAO-B protein levels, but also resulted in a 1.6-fold increase of KLF11, a 1.37-fold increase in MAO-B catalytic activity, and a 1.8-fold increase in active caspase 3, an apoptotic protein, in the PFC compared to control rats (74). Conversely, the anti-apoptotic protein, Bcl-2, was decreased by 41% in rats exposed to ethanol compared to controls (82). The decrease in anti-apoptotic Bcl-2 and increase in apoptotic caspase 3 in the PFC of rat brains upon ethanol exposure suggest that ethanol induces apoptosis that may be mediated by an increase in the KLF11-MAO-B cell death cascade (82). The GAPDH-KLF11-MAO-B cascade is a novel approach for explaining ethanol-induced neuronal death due to

chronic alcoholism. However, the precise mechanism for GAPDH-mediated damage in alcoholism and upstream effectors of GAPDH in this context remains elusive.

5. Conclusion and future directions

Monoamine oxidases play a fundamental role in brain homeostasis by regulating neurotransmitters which has been substantially documented in literature. However, improper levels of monoamine oxidase can otherwise damage the brain and impact behavior. Because finding the proper balance in MAO expression is paramount, any deviation can result in significant impairment or psychiatric illness. For example, since MAO-A and MAO-B catalytic activity produces neurotoxic hydrogen peroxide and nitrogen species resulting in oxidative damage to mitochondrial DNA, they hold implications for apoptosis, neuronal aging, neurodegenerative diseases, mental illness, and developmental disorders. Furthermore, if R1 acts as an anti-apoptotic force and reduced levels of R1 have been verified in postmortem brains of individuals diagnosed with major depressive disorder, then it is plausible that decreased R1 could attribute to not only a loss of monoamines, but increased neuronal apoptosis and dendritic loss associated with depression. Further studies to investigate the extent of cortical shrinkage as a result of R1 are necessary. Likewise, studies to measure the extent of brain tissue injury and axonal deterioration as a result of increased KLF11, MAO activity and oxidative stress associated with alcohol dependence are also warranted. Many important MAO transcription factors have been recently discovered; however, it remains unclear how these factors function in response to many physiological changes, hormonal influences, age, cortical organization and neurodevelopment, metabolic changes, downstream neurotransmitter pathways, cellular signaling pathways, and current antidepressant medications.

Since MAO downregulation does not adequately occur with current antidepressant treatment regimens, it could be possible that maintaining a normal level of neurotransmitter at the synapse for an extended period of time could adjust or "reset" MAO expression *via* upstream or downstream regulatory pathways, endocrine responses, or neuronal resurgence, and also involve individual genetic backgrounds. If MAO upregulation is the first step towards a monoamine-lowering process during depressive disorders, such as major depressive disorder, it makes sense that MAO downregulation would be the last step involved in a pathological recovery process. To elucidate this notion, many signaling and second messenger pathways would need to be studied in relation to their impact on MAO transcription factors. Finally, pharmacological targeting of aforementioned molecular pathways in major depressive disorder and alcoholism could provide

tremendous benefits for treatment and prognosis. Alternative pharmacological approaches could involve gene therapy with siRNAs, specific drug targeting of transcription factors and the development and application of newer generation MAO inhibitors. Much work is still needed in the field of MAO research; although, new advancements in our understanding of MAO related to psychiatric illness will be fruitful for future research directions and clinical outcomes.

Acknowledgements

This research was supported by National Institutes of Health Grant (NIH/NIAAA) R01AA020103, Public Health Service Grants P20 RR 017701, The Brain & Behavior Research Foundation (NARSAD) and an Intramural Research Support grant from the University of Mississippi Medical Center.

References

- Shih JC, Chen K, Ridd MJ. Monoamine oxidase: From genes to behavior. *Annu Rev Neurosci.* 1999; 22:197-217.
- Fowler JS, Logan J, Volkow ND, Wang GJ. Translational neuroimaging: Positron emission tomography studies of monoamine oxidase. *Mol Imaging Biol.* 2005; 7:377-387.
- Green AR, Youdim MB. Effects of monoamine oxidase inhibition by clorgyline, deprenil or tranylcypromine on 5-hydroxytryptamine concentrations in rat brain and hyperactivity following subsequent tryptophan administration. *Br J Pharmacol.* 1975; 55:415-422.
- Grimsby J, Chen K, Wang LJ, Lan NC, Shih JC. Human monoamine oxidase A and B genes exhibit identical exon-intron organization. *Proc Natl Acad Sci U S A.* 1991; 88:3637-3641.
- Youdim MB, Edmondson D, Tipton KF. The therapeutic potential of monoamine oxidase inhibitors. *Nat Rev Neurosci.* 2006; 7:295-309.
- Youdim MB, Gross A, Finberg JP. Rasagiline [N-propargyl-1R(+)-aminoindan], a selective and potent inhibitor of mitochondrial monoamine oxidase B. *Br J Pharmacol.* 2001; 132:500-506.
- Wu JB, Chen K, Li Y, Lau YF, Shih JC. Regulation of monoamine oxidase A by the *SRY* gene on the Y chromosome. *Faseb J.* 2009; 23:4029-4038.
- Brunner HG, Nelen M, Breakefield XO, Ropers HH, van Oost BA. Abnormal behavior associated with a point mutation in the structural gene for monoamine oxidase A. *Science.* 1993; 262:578-580.
- De Zutter GS, Davis RJ. Pro-apoptotic gene expression mediated by the p38 mitogen-activated protein kinase signal transduction pathway. *Proc Natl Acad Sci U S A.* 2001; 98:6168-6173.
- Naoi M, Maruyama W, Youdim MB, Yu P, Boulton AA. Anti-apoptotic function of propargylamine inhibitors of type-B monoamine oxidase. *Inflammopharmacology.* 2003; 11:175-181.
- Mallajosyula JK, Kaur D, Chinta SJ, Rajagopalan S, Rane A, Nicholls DG, Di Monte DA, Macarthur H, Andersen JK. Mao-B elevation in mouse brain astrocytes results in Parkinson's pathology. *PLoS One.* 2008; 3:e1616.
- Diez JA, Maderdrut JL. Development of multiple forms of mouse brain monoamine oxidase *in vivo* and *in vitro*. *Brain Res.* 1977; 128:187-192.
- Lewinsohn R, Glover V, Sandler M. Development of benzylamine oxidase and monoamine oxidase A and B in man. *Biochem Pharmacol.* 1980; 29:1221-1230.
- Saura J, Luque JM, Cesura AM, Da Prada M, Chan-Palay V, Huber G, Loffler J, Richards JG. Increased monoamine oxidase B activity in plaque-associated astrocytes of Alzheimer brains revealed by quantitative enzyme radioautography. *Neurosci.* 1994; 62:15-30.
- Fowler JS, Volkow ND, Wang GJ, Logan J, Pappas N, Shea C, MacGregor R. Age-related increases in brain monoamine oxidase B in living healthy human subjects. *Neurobiol Aging.* 1997; 18:431-435.
- Hauptmann N, Grimsby J, Shih JC, Cadenas E. The metabolism of tyramine by monoamine oxidase A/B causes oxidative damage to mitochondrial DNA. *Arch Biochem Biophys.* 1996; 335:295-304.
- Fowler CJ, Wiberg A, Oreland L, Marcusson J, Winblad B. The effect of age on the activity and molecular properties of human brain monoamine oxidase. *J Neural Transm.* 1980; 49:1-20.
- Bach AW, Lan NC, Johnson DL, Abell CW, Bembenek ME, Kwan SW, Seeburg PH, Shih JC. cDNA cloning of human liver monoamine oxidase A and B: Molecular basis of differences in enzymatic properties. *Proc Natl Acad Sci U S A.* 1988; 85:4934-4938.
- Lan NC, Heinzmann C, Gal A, Klisak I, Orth U, Lai E, Grimsby J, Sparkes RS, Mohandas T, Shih JC. Human monoamine oxidase A and B genes map to Xp 11.23 and are deleted in a patient with Norrie disease. *Genomics.* 1989; 4:552-559.
- Denney RM, Koch H, Craig IW. Association between monoamine oxidase A activity in human male skin fibroblasts and genotype of the MAOA promoter-associated variable number tandem repeat. *Hum Genet.* 1999; 105:542-551.
- Zhu QS, Grimsby J, Chen K, Shih JC. Promoter organization and activity of human monoamine oxidase (MAO) A and B genes. *J Neurosci.* 1992; 12:4437-4446.
- Cases O, Seif I, Grimsby J, Gaspar P, Chen K, Pournin S, Muller U, Aguet M, Babinet C, Shih JC, De Maeyer E. Aggressive behavior and altered amounts of brain serotonin and norepinephrine in mice lacking MAOA. *Science.* 1995; 268:1763-1766.
- Grimsby J, Toth M, Chen K, Kumazawa T, Klaidman L, Adams JD, Karoum F, Gal J, Shih JC. Increased stress response and beta-phenylethylamine in MAOB-deficient mice. *Nat Genet.* 1997; 17:206-210.
- Kim JJ, Shih JC, Chen K, Chen L, Bao S, Maren S, Anagnostaras SG, Fanselow MS, De Maeyer E, Seif I, Thompson RF. Selective enhancement of emotional, but not motor, learning in monoamine oxidase A-deficient mice. *Proc Natl Acad Sci U S A.* 1997; 94:5929-5933.
- Chen K, Holschneider DP, Wu W, Rebrin I, Shih JC. A spontaneous point mutation produces monoamine oxidase A/B knock-out mice with greatly elevated monoamines and anxiety-like behavior. *J Biol Chem.* 2004; 279:39645-39652.
- Holschneider DP, Scremin OU, Roos KP, Chialvo DR, Chen K, Shih JC. Increased baroreceptor response in mice deficient in monoamine oxidase A and B. *Am J Physiol Heart Circ Physiol.* 2002; 282:H964-972.
- Holschneider DP, Scremin OU, Chialvo DR, Chen K, Shih JC. Heart rate dynamics in monoamine oxidase-A-

- and -B-deficient mice. *Am J Physiol Heart Circ Physiol.* 2002; 282:H1751-1759.
28. Chen K, Cases O, Rebrin I, Wu W, Gallaher TK, Seif I, Shih JC. Forebrain-specific expression of monoamine oxidase A reduces neurotransmitter levels, restores the brain structure, and rescues aggressive behavior in monoamine oxidase A-deficient mice. *J Biol Chem.* 2007; 282:115-123.
 29. Sabol SZ, Hu S, Hamer D. A functional polymorphism in the monoamine oxidase A gene promoter. *Hum Genet.* 1998; 103:273-279.
 30. Zhu QS, Chen K, Shih JC. Bidirectional promoter of human monoamine oxidase A (MAO A) controlled by transcription factor Sp1. *J Neurosci.* 1994; 14:7393-7403.
 31. Ryu S, Zhou S, Ladurner AG, Tjian R. The transcriptional cofactor complex CRSP is required for activity of the enhancer-binding protein Sp1. *Nature.* 1999; 397:446-450.
 32. Li R, Knight JD, Jackson SP, Tjian R, Botchan MR. Direct interaction between Sp1 and the BPV enhancer E2 protein mediates synergistic activation of transcription. *Cell.* 1991; 65:493-505.
 33. Chen K. Organization of mao A and mao B promoters and regulation of gene expression. *Neurotoxicology.* 2004; 25:31-36.
 34. Chen K, Ou XM, Chen G, Choi SH, Shih JC. R1, a novel repressor of the human monoamine oxidase A. *J Biol Chem.* 2005; 280:11552-11559.
 35. Ou XM, Chen K, Shih JC. Monoamine oxidase A and repressor R1 are involved in apoptotic signaling pathway. *Proc Natl Acad Sci U S A.* 2006; 103:10923-10928.
 36. Cook T, Urrutia R. TIEG proteins join the Smads as TGF-beta-regulated transcription factors that control pancreatic cell growth. *Am J Physiol Gastrointest Liver Physiol.* 2000; 278:G513-521.
 37. Grunewald M, Johnson S, Lu D, *et al.* Mechanistic role for a novel glucocorticoid-KLF11 (TIEG2) pathway in stress-induced monoamine oxidase A expression. *J Biol Chem.* 2012. PMID:22628545
 38. Wong WK, Chen K, Shih JC. Regulation of human monoamine oxidase B gene by Sp1 and Sp3. *Mol Pharmacol.* 2001; 59:852-859.
 39. Wong WK, Chen K, Shih JC. Decreased methylation and transcription repressor Sp3 up-regulated human monoamine oxidase (MAO) B expression during Caco-2 differentiation. *J Biol Chem.* 2003; 278:36227-36235.
 40. Wu JB, Chen K, Ou XM, Shih JC. Retinoic acid activates monoamine oxidase B promoter in human neuronal cells. *J Biol Chem.* 2009; 284:16723-16735.
 41. Wong WK, Ou XM, Chen K, Shih JC. Activation of human monoamine oxidase B gene expression by a protein kinase C MAPK signal transduction pathway involves c-Jun and Egr-1. *J Biol Chem.* 2002; 277:22222-22230.
 42. Ou XM, Chen K, Shih JC. Dual functions of transcription factors, transforming growth factor-beta-inducible early gene (TIEG)2 and Sp3, are mediated by CACCC element and Sp1 sites of human monoamine oxidase (MAO) B gene. *J Biol Chem.* 2004; 279:21021-21028.
 43. De Luca P, Majello B, Lania L. Retinoblastoma protein tethered to promoter DNA represses TBP-mediated transcription. *J Cell Biochem.* 1998; 70:281-287.
 44. Ammanamanchi S, Brattain MG. 5-azaC treatment enhances expression of transforming growth factor-beta receptors through down-regulation of Sp3. *J Biol Chem.* 2001; 276:32854-32859.
 45. Tachibana I, Imoto M, Adjei PN, Gores GJ, Subramaniam M, Spelsberg TC, Urrutia R. Overexpression of the TGFbeta-regulated zinc finger encoding gene, TIEG, induces apoptosis in pancreatic epithelial cells. *J Clin Invest.* 1997; 99:2365-2374.
 46. Cook T, Gebelein B, Belal M, Mesa K, Urrutia R. Three conserved transcriptional repressor domains are a defining feature of the TIEG subfamily of Sp1-like zinc finger proteins. *J Biol Chem.* 1999; 274:29500-29504.
 47. Zhang JS, Moncrieffe MC, Kaczynski J, Ellenrieder V, Prendergast FG, Urrutia R. A conserved alpha-helical motif mediates the interaction of Sp1-like transcriptional repressors with the corepressor mSin3A. *Mol Cell Biol.* 2001; 21:5041-5049.
 48. Wang Z, Spittau B, Behrendt M, Peters B, Kriegelstein K. Human TIEG2/KLF11 induces oligodendroglial cell death by downregulation of Bcl-XL expression. *J Neural Transm.* 2007; 114:867-875.
 49. Lee AL, Ogle WO, Sapolsky RM. Stress and depression: Possible links to neuron death in the hippocampus. *Bipolar Disord.* 2002; 4:117-128.
 50. Duval F, Mokrani MC, Monreal-Ortiz JA, Fattah S, Champeval C, Schulz P, Macher JP. Cortisol hypersecretion in unipolar major depression with melancholic and psychotic features: Dopaminergic, noradrenergic and thyroid correlates. *Psychoneuroendocrinology.* 2006; 31:876-888.
 51. Doyle A, Hucklebridge F, Evans P, Clow A. Salivary monoamine oxidase A and B inhibitory activities correlate with stress. *Life Sci.* 1996; 59:1357-1362.
 52. Ou XM, Chen K, Shih JC. Glucocorticoid and androgen activation of monoamine oxidase A is regulated differently by R1 and Sp1. *J Biol Chem.* 2006; 281:21512-21525.
 53. Slotkin TA, Seidler FJ, Ritchie JC. Effects of aging and glucocorticoid treatment on monoamine oxidase subtypes in rat cerebral cortex: Therapeutic implications. *Brain Res Bull.* 1998; 47:345-348.
 54. Manoli I, Le H, Alesci S, McFann KK, Su YA, Kino T, Chrousos GP, Blackman MR. Monoamine oxidase-A is a major target gene for glucocorticoids in human skeletal muscle cells. *Faseb J.* 2005; 19:1359-1361.
 55. Jahng JW, Kim NY, Ryu V, Yoo SB, Kim BT, Kang DW, Lee JH. Dexamethasone reduces food intake, weight gain and the hypothalamic 5-HT concentration and increases plasma leptin in rats. *Eur J Pharmacol.* 2008; 581:64-70.
 56. Tazik S, Johnson S, Lu D, Johnson C, Youdim MB, Stockmeier CA, Ou XM. Comparative neuroprotective effects of rasagiline and aminoindan with selegiline on dexamethasone-induced brain cell apoptosis. *Neurotox Res.* 2009; 15:284-290.
 57. Carlo P, Violani E, Del Rio M, Olasmaa M, Santagati S, Maggi A, Picotti GB. Monoamine oxidase B expression is selectively regulated by dexamethasone in cultured rat astrocytes. *Brain Res.* 1996; 711:175-183.
 58. Yu S, Patchev AV, Wu Y, Lu J, Holsboer F, Zhang JZ, Sousa N, Almeida OF. Depletion of the neural precursor cell pool by glucocorticoids. *Ann Neurol.* 2010; 67:21-30.
 59. Chen K, Ou XM, Wu JB, Shih JC. Transcription factor E2F-associated phosphoprotein (EAPP), RAM2/CDCA7L/JPO2 (R1), and simian virus 40 promoter factor 1 (Sp1) cooperatively regulate glucocorticoid activation of monoamine oxidase B. *Mol Pharmacol.* 2011; 79:308-317.
 60. Lu D, Johnson C, Johnson S, Tazik S, Ou XM. The neuroprotective effect of antidepressant drug *via* inhibition of TIEG2-MAO B mediated cell death. *Drug Discov Ther.*

- 2008; 2:289-295.
61. Johnson S, Tazik S, Lu D, Johnson C, Youdim MB, Wang J, Rajkowska G, Ou XM. The new inhibitor of monoamine oxidase, M30, has a neuroprotective effect against dexamethasone-induced brain cell apoptosis. *Front Neurosci.* 2010; 4:180.
 62. Kessler RC, Berglund P, Demler O, Jin R, Merikangas KR, Walters EE. Lifetime prevalence and age-of-onset distributions of DSM-IV disorders in the national comorbidity survey replication. *Arch Gen Psychiatry.* 2005; 62:593-602.
 63. Meyer JH, Wilson AA, Sagrati S, Miler L, Rusjan P, Bloomfield PM, Clark M, Sacher J, Voineskos AN, Houle S. Brain monoamine oxidase A binding in major depressive disorder: Relationship to selective serotonin reuptake inhibitor treatment, recovery, and recurrence. *Arch Gen Psychiatry.* 2009; 66:1304-1312.
 64. Meyer JH, Kapur S, Eisfeld B, Brown GM, Houle S, DaSilva J, Wilson AA, Rafi-Tari S, Mayberg HS, Kennedy SH. The effect of paroxetine on 5-HT(2A) receptors in depression: An [(18)F]setoperone PET imaging study. *Am J Psychiatry.* 2001; 158:78-85.
 65. Meyer JH, Ginovart N, Boovariwala A, Sagrati S, Hussey D, Garcia A, Young T, Praschak-Rieder N, Wilson AA, Houle S. Elevated monoamine oxidase A levels in the brain: An explanation for the monoamine imbalance of major depression. *Arch Gen Psychiatry.* 2006; 63:1209-1216.
 66. Cerasa A, Cherubini A, Quattrone A, Gioia MC, Magariello A, Muglia M, Manna I, Assogna F, Caltagirone C, Spalletta G. Morphological correlates of MAO A VNTR polymorphism: New evidence from cortical thickness measurement. *Behav Brain Res.* 2010; 211:118-124.
 67. Johnson S, Stockmeier CA, Meyer JH, Austin MC, Albert PR, Wang J, May WL, Rajkowska G, Overholser JC, Jurjus G, Dieter L, Johnson C, Sittman DB, Ou XM. The reduction of R1, a novel repressor protein for monoamine oxidase A, in major depressive disorder. *Neuropsychopharmacology.* 2011; 36:2139-2148.
 68. Ducci F, Enoch MA, Funt S, Virkkunen M, Albaugh B, Goldman D. Increased anxiety and other similarities in temperament of alcoholics with and without antisocial personality disorder across three diverse populations. *Alcohol.* 2007; 41:3-12.
 69. Dupont RM, Rourke SB, Grant I, Lehr PP, Reed RJ, Challakere K, Lamoureux G, Halpern S. Single photon emission computed tomography with iodoamphetamine-123 and neuropsychological studies in long-term abstinent alcoholics. *Psychiatry Res.* 1996; 67:99-111.
 70. Caldwell TM, Rodgers B, Jorm AF, Christensen H, Jacomb PA, Korten AE, Lynskey MT. Patterns of association between alcohol consumption and symptoms of depression and anxiety in young adults. *Addiction.* 2002; 97:583-594.
 71. Rodgers B, Korten AE, Jorm AF, Christensen H, Henderson S, Jacomb PA. Risk factors for depression and anxiety in abstainers, moderate drinkers and heavy drinkers. *Addiction.* 2000; 95:1833-1845.
 72. Johnson S, Williams AN, Johnson C, Ou XM. The effects of antidepressant drug on ethanol-induced cell death. *Drug Discov Ther.* 2007; 1:130-135.
 73. Chen CP, Kuhn P, Chaturvedi K, Boyadjieva N, Sarkar DK. Ethanol induces apoptotic death of developing beta-endorphin neurons via suppression of cyclic adenosine monophosphate production and activation of transforming growth factor-beta1-linked apoptotic signaling. *Mol Pharmacol.* 2006; 69:706-717.
 74. Luo J, Miller MW. Transforming growth factor beta1-regulated cell proliferation and expression of neural cell adhesion molecule in B104 neuroblastoma cells: Differential effects of ethanol. *J Neurochem.* 1999; 72:2286-2293.
 75. Paul CA, Au R, Fredman L, Massaro JM, Seshadri S, Decarli C, Wolf PA. Association of alcohol consumption with brain volume in the Framingham study. *Arch Neurol.* 2008; 65:1363-1367.
 76. Miguel-Hidalgo JJ, Overholser JC, Meltzer HY, Stockmeier CA, Rajkowska G. Reduced glial and neuronal packing density in the orbitofrontal cortex in alcohol dependence and its relationship with suicide and duration of alcohol dependence. *Alcohol Clin Exp Res.* 2006; 30:1845-1855.
 77. Miguel-Hidalgo JJ, Wei J, Andrew M, Overholser JC, Jurjus G, Stockmeier CA, Rajkowska G. Glia pathology in the prefrontal cortex in alcohol dependence with and without depressive symptoms. *Biol Psychiatry.* 2002; 52:1121-1133.
 78. Carlsson A, Adolfsson R, Aquilonius SM, Gottfries CG, Oreland L, Svennerholm L, Winblad B. Biogenic amines in human brain in normal aging, senile dementia, and chronic alcoholism. *Adv Biochem Psychopharmacol.* 1980; 23:295-304.
 79. Ou XM, Stockmeier CA, Meltzer HY, Overholser JC, Jurjus G, Dieter L, Chen K, Lu D, Johnson C, Youdim MB, Austin MC, Luo J, Sawa A, May W, Shih JC. A novel role for glyceraldehyde-3-phosphate dehydrogenase and monoamine oxidase B cascade in ethanol-induced cellular damage. *Biol Psychiatry.* 2010; 67:855-863.
 80. Ou XM, Lu D, Johnson C, Chen K, Youdim MB, Rajkowska G, Shih JC. Glyceraldehyde-3-phosphate dehydrogenase-monoamine oxidase B-mediated cell death-induced by ethanol is prevented by rasagiline and 1-R-aminoindan. *Neurotox Res.* 2009; 16:148-159.
 81. Alexander-Kaufman K, James G, Sheedy D, Harper C, Matsumoto I. Differential protein expression in the prefrontal white matter of human alcoholics: A proteomics study. *Mol Psychiatry.* 2006; 11:56-65.
 82. Ou XM, Johnson C, Lu D, Johnson S, Paul IA, Austin MC, Iyo AH, Miguel-Hidalgo JJ, Luo J, Bell RL, Grunewald M, Wang J, Sittman DB. Ethanol increases TIEG2-MAO B cell death cascade in the prefrontal cortex of ethanol-preferring rats. *Neurotox Res.* 2011; 19:511-518.

(Received May 2, 2012; Revised June 12, 2012; Accepted June 13, 2012)

Improved treatment of nicotine addiction and emerging pulmonary drug delivery

Nazrul Islam^{1,2}, Shafiqur Rahman^{3,*}

¹ Pharmacy Discipline, Faculty of Science and Technology, Queensland University of Technology, Brisbane, QLD, Australia;

² Institute of Health and Biomedical Innovation, Kelvin Grove, QLD, Australia;

³ Department of Pharmaceutical Sciences, College of Pharmacy, South Dakota State University, Brookings, SD, USA.

ABSTRACT: Nicotine addiction remains the leading cause of death and disease in developed and developing nations and a major cause of mortality around the world. Currently, nicotine replacement therapies (NRTs), bupropion, and varenicline are approved by the regulatory agencies as first-line treatments for nicotine addiction. Emerging evidence indicates that varenicline and bupropion have some therapeutic limitations for treating nicotine addiction with oral route of administration. Thus, continued investigation of innovative drug delivery for nicotine addiction remains a critical priority. This review will discuss some novel strategies and future directions for pulmonary drug delivery, an emerging route of administration for smoking cessation. It is anticipated that the advancement of knowledge on pulmonary drug delivery will provide better management for nicotine addiction and other addictive disorders.

Keywords: Nicotine addiction, bupropion, varenicline, nicotinic receptor, pulmonary drug delivery, dry powder inhaler (DPI), metered dose inhaler (MDI), nebulizer

1. Introduction

Tobacco smoking and nicotine addiction is a growing public health problem in the developing and developed world. The World Health Organization (WHO) estimates that about 30% of the adult male global population smokes (1). It is estimated that each year tobacco smoking accounts for about 3 million deaths worldwide. Unless the current trends are reversed, by

the year 2030, this figure will be increased to 10 million deaths every year. Seventy percent of these deaths are predicted to be in developing nations. In the USA alone, tobacco smoking causes 440,000 deaths annually (2). Approximately, 50% of long-term tobacco smokers die prematurely from adverse effects of smoking, including cancer, cardiovascular disease, lung disease or other illness (3). The risk of tobacco smoking can be reduced significantly by smoking cessation with multiple strategies including pharmacotherapy. Current pharmacotherapies (Table 1) include nicotine replacement therapy (NRT) in the form of gum, transdermal patch, sublingual tablet, nasal spray, and vapor inhaler formulations; however, each therapy has its advantages as well as some significant drawbacks (details in the section 5.1.). There are two non-nicotine based medications which have been approved by the US Food and Drug Administration which are bupropion (Zyban) and varenicline (Chantix) (4-6). Recent data suggest that varenicline and bupropion have some therapeutic limitations or adverse effects for treating nicotine addiction with current delivery system. Like other brain disorders (Table 2), continued investigation of innovative drug delivery for nicotine dependence remains a critical priority. In this review, we will discuss novel strategies and future directions for smoking cessation using a suitable inhaler for deep lung delivery of nicotine, an emerging route of drug administration. The currently available nicotine inhaler delivers nicotine into the mouth for buccal absorption and there is no ideal inhaler to deliver nicotine into the deep lung. The pulmonary route of nicotine delivery would be expected to mimic the effects of tobacco smoking and would significantly reduce cravings and withdrawal symptoms. It is anticipated that the advancement of knowledge on pulmonary drug delivery will provide novel therapeutic formulations for better management of nicotine addicted population. Improvement of nicotine addiction treatment depends on the novel pharmacotherapeutic approaches, including new drugs or new formulation of current drugs and/or novel delivery technique, like deep lung delivery, which is discussed in the following sections.

*Address correspondence to:

Dr. Shafiqur Rahman, Department of Pharmaceutical Sciences, College of Pharmacy, South Dakota State University, Avera Health and Science Center, SAV 265, Brookings, SD 57007, USA.
E-mail: shafiqur.rahman@sdstate.edu

Table 1. Currently approved medications for smoking cessation (4,57)

Pharmacotherapy	Common side effects	Delivery methods
NRT*	Skin reaction, insomnia, irritation of mouth and throat	Oral, nasal, skin, nicotine cartridges in an inhaler, pMDI
Bupropion (Zyban®)	Insomnia, dry mouth, suicide ideation	Oral
Varencline (Chantix®)	Headache, mood changes, insomnia, constipation, suicide ideation	Oral

* NRT: nicotine replacement therapy.

Table 2. Drugs administered as aerosols against smoking cessation and other neurological diseases

Active drugs	Indication	Formulation	Delivery system	References
Nicotine	Smoking cessation	Aqueous solution	MDI (AERx Essence®)	(72,73)
Nicotine	Smoking cessation	Suspension	MDI	(70,71,83)
Nicotine	Smoking cessation	Micronized powder	DPI	(67)
Nicotrol®, Nicorette® (Nicotine)	Smoking cessation	Nicotine cartridge/Liquid	DPI & MDI	(64,68)
Dihydroergotamine mesylate	Migraine, Vascular cephalgia	HFA 134a based suspension	MDI	(84)
Ergotamine tartrate	Migraine, Vascular cephalgia	Suspension	Unavailable	(50)
Detorelix	Migraine, Vascular cephalgia	Suspension of liposomal drugs	Intratracheal (<i>i.t.</i>) instillation	(85)
Dopamine D-1 agonist, ABT-431	Parkinson's disease	HFA based suspension	MDI (AERx)	(86,87)
L-Dopa	Parkinson's disease	Micronized powder	Alkermes AIR/DPI	(52,88)
Dopamine agonist	Parkinson's disease	Suspension in propellant and poloxamer	MDI	(89)

MDI: metered dose inhaler; HFC is hydrofluoro alkane; AERx is a DPI device that deliver aerosolized drugs from a dosage form that consists of liquid drug formulation.

2. Pulmonary delivery technology

Aerosol delivery of drugs, formulated as liquid solutions, suspensions, emulsions, or micronized dry powders, are aerosolized *via* some commonly used different types of delivery devices *i.e.*, nebulizers, metered dose inhaler (MDI), and dry powder inhaler (DPI). Nebulizers deliver large volumes of drug solutions or suspensions and are used for those drugs which are difficult to be formulated into pressurized metered dose inhalers (pMDIs) or DPIs. Nebulizers are suitable for drugs with high dose and little patient coordination or skill; however, treatment using nebulizer is time consuming and less efficient, resulting in the waste of active medicaments. They are not portable devices and have been limited to the treatment of hospitalized patients only.

Metered dose inhalers/pMDIs are the most commonly used delivery devices (Figure 1), which deliver drug. In this delivery method, drug is either dissolved or suspended in liquefied propellents. The propellents used in pMDI formulations are liquefied gases of chlorofluorocarbons (CFC), which are not environmental friendly. This is the reason why currently hydrofluoroalkanes (HFAs), which have no remarkable effects on the ozone layers, are used in the formulation for MDIs. On spraying, drug formulation with propellants is expelled and aerosolized (Figure 1). Although pMDIs are widely used in respiratory drug delivery, some problems have been associated with these devices, including the need for coordination of inspiratory inhalation with valve actuation and the use of a propellant, which has possible adverse effects on the stratospheric ozone layer.

In addition, pMDIs have some other disadvantages such as oropharyngeal deposition of drugs. On actuation, the particles aerosolized from the MDIs have a high velocity, which exceeds the patients' inspiratory force, therefore, a large number of particles deposit onto the oropharyngeal areas. Thus a small fraction of drug deposits into the patients lungs due to a lack of coordination between actuation and inhalation (7). To overcome this difficulty several inhalation aids like spacers incorporated with MDIs have been developed (8) to improve the delivery; however, bacterial contamination of spacer devices are very common if the devices are not cleaned and dried appropriately (9).

Dry powder inhalation formulations contain the drug in a powder form and the drug particles (< 5 µm) are blended with a suitable large carrier (*i.e.*, lactose) to improve flow properties and dose uniformity (10) and drug powders are delivered into the deep lung *via* DPI devices (Figure 2). Powder de-agglomeration and aerosolisation from these formulations are achieved by the mechanical force provided by the device and patient's inspiratory airflow, which needs to be sufficient to create an aerosol containing respirable drug particles for lung deposition. Good flow properties of the formulation are necessary to ensure accurate dose metering of the drug. Advantages of DPI over other inhaler systems (pMDIs) are independence of breathing co-ordination with dose actuation, the absence of propellants, low innate initial velocity of particles (reducing inertial impaction at the back of the throat), and solid state drug stability. Drug dispersion from the powder formulation can be enhanced by the addition of fine excipients in the formulation (11,12). Drug particle size and powder formulation, breathing patterns, and complex physiology of respiratory

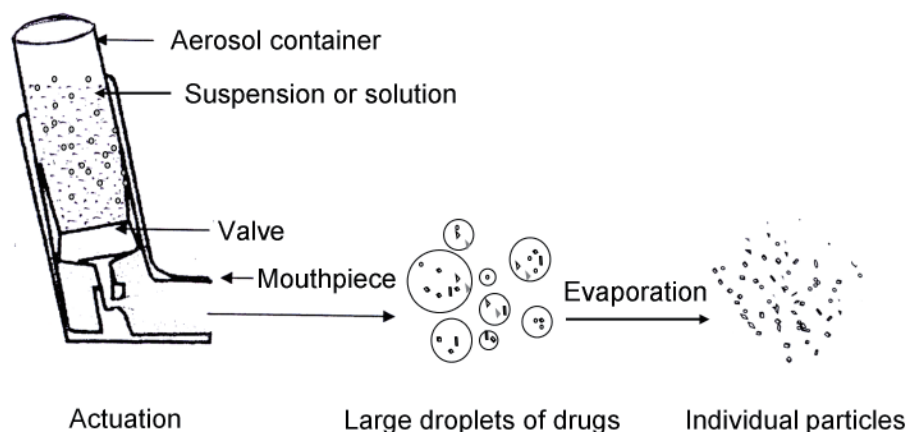


Figure 1. Schematic diagram of aerosol delivery of drugs from pMDI. Modified form Dalby *et al.* (94).

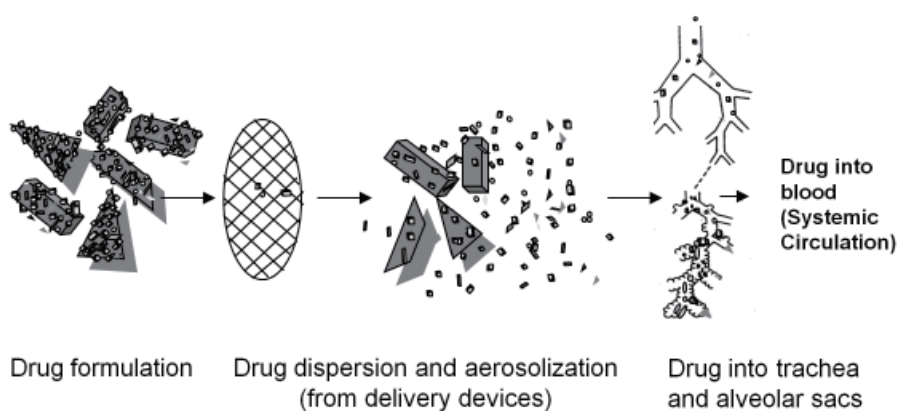


Figure 2. Schematic diagram of the pulmonary delivery of drugs from DPI formulation. The formulation consists of micronized drugs adhered on the surface of large carrier particles. Drug particles detached from the surface of large carriers and deposits into the patients airways by inhalation.

tract are major factors affecting delivery of drugs into the deep lung. DPIs are highly portable, breath activated, and relatively less expensive. Since drugs are kept in solid state in DPIs, they exhibit high physicochemical stability of drugs particularly proteins and peptides. In DPI formulation the device is an important factor in achieving adequate delivery of inhaled drug to lungs. The device must provide an environment where the drug can maintain its physicochemical stability and produce reproducible drug dosing.

On inhalation, drugs are dispersed and delivered into deep lungs. To achieve a desired therapeutic effect from aerosols, an adequate amount of drug must reach the alveolar sacs of the respiratory airways. The dynamic behavior of aerosol particles is governed by the laws of aerosol kinetics (13). The dominant mechanisms of depositing aerosol particles into the respiratory tract include inertial impaction, sedimentation (gravitational deposition), Brownian diffusion, interception, and electrostatic precipitation (14). The distribution of the inhaled drug particles in the lung depends on the characteristics of the inhaled particles, such as drug particle diameter, mass, shape, density and hygroscopicity, the physiology of the respiratory tract,

and breathing patterns of the patients (15-17). Inertial impaction and sedimentation are the most important for large particle deposition ($1 \mu\text{m} < \text{MMAD} < 10 \mu\text{m}$). Large particles ($> 5 \mu\text{m}$) with high velocity (due to higher mass) are mainly deposited by impaction (18). Particles of smaller size ($0.5\text{-}3.0 \mu\text{m}$), which have tendency to escape from deposition by inertial impaction, may be deposited by sedimentation. Deposition of small particles by sedimentation mainly occurs in the smaller airways and alveolar regions and increased sedimentation is observed during breath-holding or slow steady breathing (18). Deposition of particles less than $0.5 \mu\text{m}$ occurs in the lower airway of lungs by diffusion due to Brownian movement. Generally, the deposition of particles larger than $1.0 \mu\text{m}$ is dominated by inertial impaction and particles smaller than $0.1 \mu\text{m}$ are deposited by diffusion. Both sedimentation and diffusion are important for the particle size ranging between $0.1\text{-}1.0 \mu\text{m}$ (19). The maximum pulmonary deposition of particles of $1.5\text{-}2.5 \mu\text{m}$ and $2.5\text{-}4 \mu\text{m}$ diameters occurred with and without breath holding, respectively. However, rapid breathing showed maximum deposition of particles between $1.5\text{-}2 \mu\text{m}$ in the tracheobronchial region with breath holding and particles between $2\text{-}3 \mu\text{m}$ deposited in the pulmonary

region without breath holding (15). Therefore, slow inhalation is desirable to obtain maximum deposition of aerosol particles in the lower airways of lung. Although particles less than 1 μm have challenging dispersion behavior due to the strength of the inter-particle forces, inhaled nanoparticles or nanoagglomerates of various drugs showed better dispersion (20-24), rapid absorption (25), and avoidance of mucociliary clearance (26). Recently, a formulation containing carrier lactose and salbutamol sulphate nanoparticles, which demonstrated a 2- to 3-fold increase in total lung deposition compared to a formulation containing the same drug as micronized form (20) has been reported.

Electrostatic charges may be generated in a DPI on particles of an aerosol and a charged particle may induce an image charge of opposite polarity on the airway walls during inhalation. This image charge attracts the particle which is subsequently deposited by electrostatic precipitation (18,27). Only fibrous particles are believed to be deposited by this mechanism, therefore, this mechanism may not be significant for DPI formulations.

3. Pulmonary delivery of various drugs

Currently, local delivery of medicaments to the alveoli of lungs from both DPIs and pMDIs are mainly used for the treatment of lung disorders including asthma and chronic obstructive pulmonary disorders (COPD) and a limited number of therapeutic compounds such as β -adrenoceptor agonist, muscarinic agonist, corticosteroids, and mast cell stabilizers are available. Recently certain combinations of drugs are also formulated due to a synergistic therapeutic benefit. Zanamavir, an antiviral agent has been introduced in the market as an aerosol product for the treatment of influenza (28). Aerosol delivery of recombinant human deoxyribonuclease (rhDNase) and tobramycin are available as nebulizer for the treatment of cystic fibrosis (28,29). The very first approved aerosol delivery of insulin as DPI formulation (Exubera[®], Pfizer) was introduced in the market, however, the production has been discontinued from market because the sales of this product were disappointing as the product failed to gain acceptance of patients and physicians. The manufacturer failed to demonstrate the clinical benefits of the inhaled insulin over the currently available self-injection insulin products to the doctors and patients. Although the DPI product is stable (compared to the liquid injectable product) and easy to use; however, due to the higher cost of Exubera[®], clumsy design of the device and poor marketing are also responsible for this breakdown.

Using DPI technique respiratory delivery of other potent drugs or other agents, such as hormone (30), antibiotics (31,32), drugs for Parkinson's disease (33), gene delivery (34,35), vaccine delivery (36-38), antituberculosis (39,40), antihypertensive nifedipine (21), anticoagulant heparin (41), drugs for sexual dysfunction (42), opioids (fentanyl) for cancer pain (43-45), and

atropine sulphate nanoparticle as an antidote for organophosphorus poisoning with better bioavailability have been reported (46). The inhaled dry powders of levodopa showed to produce a therapeutic effect within 10 min of administration for the treatment of Parkinson's disease (47). Using a mouse model, deep lung delivery of poorly water soluble drug, ibuprofen nanoparticle showed 3-5 orders of magnitude less dose than that required for oral administration of the drug to achieve the same analgesic effect (48). Deep lung delivery of various drugs has been investigated and the pulmonary route has been found to be more effective compared to those of other routes. Aerosol delivery offers the greatest potential to delivery drugs into the lower airway of lungs of a wide range of molecules for systemic diseases.

4. Pharmacokinetics of some inhaled drugs

Very little is known about the pharmacokinetics of inhaled drugs. Recently, the bioavailability of levonorgestrel after pulmonary and oral administration has been investigated and pulmonary delivery of liposome encapsulated levonorgestrel produced prolonged effective concentration of the drug in the plasma over a period of 16-60 h with reduced side effects compared to that of orally administered drug (49). Higher plasma concentration of ergotamine tartrate was found when delivered *via* pulmonary route compared to that of orally administered tablet (50). This study revealed the superiority of inhaled route to the oral route of drug delivery. In another study, inhaled L-dopa produced at least 2-fold fewer doses compared to that of oral dose (51). Using a rat model, lung delivery of L-dopa dry powder formulation, developed by Alkerm's Advanced Inhalation Research (AIR), showed rapid and higher plasma levels (C_{max} , 4.8 ± 1.10 mg/mL in 2 min) compared to that of oral administration where the drug produced delayed and lower plasma level (C_{max} , 1.8 ± 0.40 mg/mL) in 30 min (52).

Deep lung delivery of Ergotamine tartrate (ET) *via* an inhaler (Medihaler[®]) produced 9-fold higher peak plasma concentration (C_{max} , 1,109 pg/mL at 4 min) compared to that of sublingual ET formulation (C_{max} , 134.0 pg/mL at 37 min) (53). Inhaled testosterone in postmenopausal women delivered by AREx (a novel handheld aerosol delivery system) produced a dose dependent increase in plasma drug concentration (54). After administering the maximum dose of 3.0 mg, plasma concentration (C_{max}) of free testosterone was increased from 0.6 nmol/L to a maximum level of 62.6 nmol/L achieved within 1-2 min after dosing. The authors demonstrated that the administration of inhaled testosterone was safe and no adverse effects related to the treatment occurred. Inhalation route can be an alternative route with safety profile to consider for many therapeutic agents (55). Thus the lung delivery of drugs has a lot of potential in managing various diseases with excellent pharmacokinetic profiles.

5. Medications for smoking cessation

5.1. Nicotine replacement therapy

Nicotine replacement therapy (NRT) may facilitate smoking cessation in several ways. The primary action is believed to be the relief of craving and withdrawal symptoms when a person stops tobacco use (56). The second critical effect of NRT is being positive reinforcement. The third possible mechanism of benefit has been suggested to be the potential for nicotine based medications to desensitize brain nicotinic acetylcholine receptors (nAChRs). A desensitized state of nAChRs such as alpha4beta2 subtype and/or other subtypes may cause in reduced receptor responsiveness to endogenously released acetylcholine which may be relevant to general mood stabilizing effect (57). Currently, NRT is available in 5 different formulations with different pharmacokinetic profiles, *i.e.*, chewing gum, lozenges, sublingual tablets, transdermal patch, and/or nasal spray inhale. The gum is available in two doses (2 or 4 mg) and the amount of drug absorbed from nicotine gum is much lower (~50%) than nicotine content in the formulation. With regards to the lozenges chewing is not required but like gum, nicotine from this preparation is absorbed very slowly through the buccal mucosa. A significant amount of nicotine is swallowed when using sublingual tablets, gum or lozenges and undergoes hepatic first pass metabolism and thus reduced bioavailability (20-45%) (58,59). The transdermal patch is much easier to use; however, the rate of nicotine delivery from this formulation is very slow and has an initial lag time of about 1 h before nicotine appears in the blood stream and a very slow rise (2-6 h) (60). Nicotine absorption from sublingual tablets are somewhat higher than that of gum; however, efficacy rates appeared to be consistent with gum and lozenge preparation (61). Absorption of nicotine from capsules or solutions is not promising and peak plasma concentrations are achieved in about 1 h after oral administration (59,62). Nicotine is ionized at low pH (stomach) and thus poorly absorbed from the stomach but it is well absorbed from intestine due to alkaline pH. The pharmacokinetics of currently available nicotine dosage forms are presented in Table 3, which indicates that the absorption of nicotine from orally administered formulations is slower and peak plasma concentrations are gradual compared to that of smoking. No significant difference in efficacy has been shown between formulations (3). Nicotine absorption from nasal spray is very rapid (C_{max} 8.6-10.5 ng/mL at 2.5-5 min) (63) compared to that of gum; however, it has some unavoidable drawbacks like burning nose and throat, watery eyes, runny nose, sneezing, and coughing (64), which limit its application in smoking cessation. The nicotine vapor inhaler (inhaled by mouth) containing nicotine cartridge (10 mg each) deliver nicotine more

into the oral cavity, stomach and very little into lungs (65). This is not a real inhaler that delivers drug into the deep lungs for better absorption. In addition, the nicotine delivery from this type of inhaler is temperature dependent (to vaporize the nicotine) and the inhaler is required to be kept warm before inhalation. From the above discussion, it is evident that each of the above mentioned nicotine based therapy has its advantages as well as some unavoidable limitations.

Although these products are alternatives of the nicotine associated with tobacco consumption, none of these found to produce rapid absorption and quick onset of action that can be achieved with cigarette. It is assumed that these products do not show the ability to effectively relieve the craving for cigarettes associated with nicotine withdrawal. Therefore, this intense craving drives smokers back to cigarettes. New delivery method such as pulmonary drug delivery may enhance the efficacy of some NRT formulations. The pulmonary route is known as one of the efficient methods of delivering drugs to the body due to large surface area of the pulmonary alveoli, small airways, and dissolution of nicotine products in the fluid of pH 7.4 in the lungs facilitates transfer across membrane. A unique inhaler (DPI or MDI) would deliver nicotine to the lung in a manner comparable to nicotine intake through smoking. It is anticipated that this new method like lung delivery of nicotine would reduce background cravings and withdrawal symptoms for rapid relief of cravings (57,66). Thus pulmonary drug delivery technology may revolutionize the effective treatment by right NRT formulations and the following section is dedicated to demonstrate the current status and future direction of developing inhalable nicotine formulation.

Table 3. Pharmacokinetics (average values) of different dosage forms of Nicotine products

Dosage forms and administration	C_{max} (ng/mL)	T_{max}	Ref.
Smoking			
1.1 mg/cigarette	25.9	2.0 min	(71)
0.9 mg/cigarette	38.9	4.0 min	(90)
MDI			(71)
50 µg /puff (0.5 mg dose)	12.5	6.0 min	
100 µg /puff (1.0 mg dose)	9.4	5.0 min	
Vapor Inhaler (10 mg cartridge)	8.1	30 min	(91)
Nasal spray (2.0 mg)	8.6-10.5	2.5-5 min	(63)
Nicotine vapor inhaler (1.1 mg)	5.8	10 min	(90)
Nicotine Gum (2.0 mg)	6-9	30 min	(92)
Lozenge			(93)
2.0 mg	4.4	60 min	
4.0 mg	10.8	66 min	
Transdermal patch			(60)
15 mg/16 h	11.9	6.5 h	
21.0 mg/24 h (Novartis)	17.0	10 h	
21.0 mg/24 h (Alza)	21.9	3.8 h	
Oral solution 2.0 mg	4.7	52 min	(62)
Oral capsules 3-4 mg	6-8	90 min	(59)
Sublingual tablet 2.0 mg	13.2	20 min	(61)

5.2. Deep lung delivery of nicotine

No DPI/MDI formulations for pulmonary delivery of nicotine have been approved yet for the management of nicotine addiction. Only two products, *i.e.*, Nicotrol[®] and Nicorette[®] Inhalers (Pfizer) of nicotine are available as nicotine vapor inhaler; however, these devices deliver nicotine into buccal areas, not into the deep lungs, resulting in lowering plasma maximum concentration and delayed time to reach maximum concentration. In 1997, Rose *et al.*, patented a DPI formulation of nicotine bitartrate with lactose powders for lung delivery with a view to manage smoking cessation; however, no further details are accessible (67). In an early study, a nicotine pMDI formulation containing nicotine in ethanol with hydrofluoroalkane (HFA), produces a microaerosol of fine droplet size that mimics the nicotine delivered *via* tobacco smoke (68). The author emphasized the nicotine pMDI offered safer delivery compared to that of smoked tobacco where heat, carcinogens, and carbon monoxide produce various adverse effects. Delivery of nicotine to the deep lung was comparable to cigarette smoking and this method showed to reduce cravings and nicotine withdrawal symptoms (69). A breath-activated MDI nicotine formulation, that produced a fine particle dose (FPD) up to 60%, would rapidly produce maximum plasma concentration to reduce smoking urges (70). This type of nicotine delivery is encouraging and suitable for relieving nicotine addiction; however, no further details are available. Very recently, using a large spacer with MDI lung delivery of nicotine produced a median maximum plasma concentration, which was about 50% of the amount that was obtained by smoking a cigarette (71). This formulation produced higher peak plasma levels and was achieved rapidly compared to those of many current forms of nicotine replacement therapy. In addition, inhaled MDI formulation showed self-satisfaction and reduce urge to smoke similar to a cigarette. Gonda *et al.*, delivered clean nicotine aqueous solution to the deep lung for tobacco smoking cessation treatment using a promising device, AERx Essence[®] inhaler (72,73) and produced a rapid and dose proportional increase in plasma nicotine concentration within 1 min (data not accessible). Although nicotine was eliminated rapidly from the blood stream, prolonged craving reduction was observed without administering another dose. The craving reduction could be due to changes in brain nicotinic receptor regulation and neuroadaptation associated with brain reward circuitry (3-5). These studies suggested that deep lung delivery of nicotine using inhaler devices with better formulation would be an effective way to eliminate the craving for cigarettes and other tobacco products.

Nicotine absorption *via* lung from smoking is very rapid and currently available nicotine products (Table 3) deliver nicotine more slowly compared to that of smoking, which indicates that the pulmonary delivery is

advantageous over other routes. The typical steady-state plasma concentrations of nicotine from gum, inhaler, sublingual tablets, and nasal spray is in the range of 5-15 ng/mL and from nicotine patches (according to the design and dose of nicotine in patches) in the range of 10-20 ng/mL (Table 3). Administration of nicotine capsules or solution found to produce peak plasma concentrations in about 1 h (59,62). The absorption of nicotine from gum is not fast and frequent dosing is required to achieve good absorption from the oral mucosa to achieve peak plasma levels of nicotine. Nicotine absorption from transdermal patch is very slow and plasma concentration rises gradually over 6-10 h (depending on the type of product). The nicotine absorption from nasal spray was rapid and peak plasma concentration achieved within 5 min after administration (63) with a high individual variability. Hence, from the table it is evident that pulmonary delivery confirmed promising outcome compared to those of currently available non-inhaled nicotine products (tablets, capsules, nasal spray, gums, *etc.*).

5.3. Non-nicotine based medications

Currently there are some non-nicotine based drugs, such as bupropion (Zyban[®]) and varenicline (Chantix[®]) available for the treatment of nicotine addiction and these drugs are considered better for the management of smoking cessation (74-78). Bupropion was originally marketed as an antidepressant agent but the effect on nicotine addiction appears to be separate from its antidepressant effect. It is an inhibitor of brain dopamine uptake process. In addition, bupropion in low doses can block brain nAChR function (74). The blockade of nAChRs function could decrease positive reinforcement effects in addicted populations (75). This drug is extensively metabolized by liver enzyme ($t_{1/2}$ approximately 21 h). The prolonged absorption of this drug was observed from sustained release and extended release formulations, with T_{max} values of 3.0 and 5.0 h, respectively compared to that of immediate release (T_{max} 1.5 h); however, C_{max} and AUC values found to increase proportionately with dose for all of these formulation (76). It is important to note that the pharmacokinetic profile of this drug is affected by age, sex, smoking, and renal and liver of the consumers. This drug is administered as a sustained-release formulation because of the major adverse effect – generalized seizures, which follow up high peak plasma concentration of that drug. The commonly observed side effect of bupropion is insomnia, but its occurrence can be reduced by taking the medication earlier in the day. Apart from insomnia, the most frequent effects are mouth dryness and nausea. It is contraindicated in patients who are suffering from seizure disorders. The dose is usually 150 mg/day for the first 3 days and then 150 mg twice daily. Bupropion is useful either as a monotherapy or in combination

with NRT. Combination with NRT seems to be safe but there is a lack of studies demonstrating an increased long-term quit rate (3,4). Evidence suggests that bupropion blocks brain dopamine and/or norepinephrine transporters for its antidepressant effect (3). Recently, it was found that bupropion with a very low concentration may act as an antagonist at certain subtype of nicotinic receptors (3,5). Whether this pharmacological property of bupropion may account for smoking cessation effect remains to be confirmed. Although pulmonary delivery of this drug has not been studied yet, this mode of delivery system would be expected to be more efficacious in terms of better pharmacokinetic (PK) and pharmacodynamic (PD) profiles for a better therapeutic outcome and effectiveness in the management of nicotine addiction resulting in enhancing the quit rate.

Varenicline, the latest drug included in the list of non-nicotine medication as a potential drug for the management of smoking cessation. The drug was developed as a cytisine derivative to increase oral bioavailability and improve brain penetration (77). Varenicline is a partial agonist at nAChRs with higher affinity for brain $\alpha 4\beta 2$ compared to other subtypes such as $\alpha 7$ (77). Preclinical and clinical research has shown that varenicline produces less of a response than that of nicotine (30 to 60%) that would counteract the low brain dopamine levels occurred in the absence of nicotine during smoking cessation attempts (78). Thus the drug removes symptoms of craving and withdrawal. Overall, varenicline acts like a functional antagonist, reducing nicotine-induced brain dopaminergic activation (3,4). Moreover, the efficacy of varenicline was found to be higher than that of bupropion in preclinical and clinical studies (4). Several side effects with varenicline, such as nausea, vomiting, and vivid dreams have been reported in addicted populations. There have been reports about depression, suicidal thoughts, suicides, and serious neuropsychiatric symptoms in patients taking varenicline with recommended dose (79). The dose is usually started at a dose of 0.5 mg once daily for the first 3 days, 0.5 mg twice daily for the next four days and then 1 mg twice daily. The half-life of this drug is approximately 17 (\pm 3) h after repeated dose, with T_{max} 4.3 (\pm 2.3) h and C_{max} 4.0 (\pm 0.7) ng/mL (80). Recommended duration of treatment is 12 weeks but in special groups of patients, who have had relapse with shorter duration of treatment, varenicline can be taken even for 24 weeks (4). No pulmonary delivery of this drug or PK of inhaled varenicline has been investigated so far. Despite some objections with reference to its use, varenicline is perceived by many clinicians and researchers as the effective smoking cessation aid. Like NRT and bupropion, lung drug delivery with better formulations of varenicline may be introduced for a better therapeutic outcome and effectiveness in the management of nicotine addiction. It is expected that

the deep lung delivery of this drug would improve the PK/PD profiles for smoking cessation compared to those of existing delivery methods.

The overall justification for the currently available pharmacotherapies for nicotine addiction is to mimic or replace the effects of nicotine by providing an agonist itself or to control the neurobiological mechanisms by NRT. However, these approaches do not show long lasting outcome. It has been reported that under an ideal circumstances the maximum abstinence rates are only 25 to 35% and approximately 80% of patients who used one of the currently available medications returned to smoking within the first year (81). Given the evidence, it is now comprehensible that there is a need to develop more effective therapy compared to those of currently available products for long lasting and effective cessation of tobacco smoking. The pulmonary route seems to be ideal for rapid delivery of nicotine in case of NRT or other medications to the brain, where it has its appropriate therapeutic effects. This route would allow quitters to absorb sufficient amounts of nicotine to diminish their smoking urges. Therefore, it would be excellent to develop such a product that can produce better PK/PD profiles following administration by inhalation.

6. Summary

Tobacco smoking is strongly associated with an increased risk of developing coronary artery disease, chronic obstructive pulmonary disorder, and cancer (82). The odds of successful smoking cessation are improved with pharmacotherapy as reviewed above. These therapies are thought to work primarily by replacing nicotine (*e.g.*, NRT) or modestly stimulating or inhibiting nicotine effects in the brain (*e.g.*, varenicline or bupropion), thereby minimizing withdrawal symptoms experienced during smoking cessation. While the role of effective pharmacotherapy is essential for effective management of nicotine addiction, better formulation with innovative drug delivery might advance therapeutic outcome for various disorders associated with tobacco addiction. It is expected that treatment of nicotine addiction will be improved with least side effects using proposed pulmonary drug delivery method in the coming years. However, insufficient data are available to rank-order the effectiveness of the different cessation agents that are currently on market. Selection of an effective active agent should be individually tailored for each patient. Important factors to consider include patient preference, medication compliance issues, previous experience with cessation agents, and patient characteristics, *e.g.*, contraindications, history of depression, and level of smoking. Finally, pharmacotherapy should be accompanied by appropriate behavioral counseling to enhance long-term cessation rates.

References

- WHO. Smoking statistics. http://www.wpro.who.int/media_centre/fact_sheets/fs_20020528.htm
- U.S. Department of Health and Human Services. The Health Consequences of Smoking: A Report of the Surgeon General. Atlanta, GA: U.S. Department of Health and Human Services, Centers for Disease Control and Prevention, National Center for Chronic Disease Prevention and Health Promotion, Office on Smoking and Health, 2004.
- Henningfield JE, Fant RV, Buchhalter AR, Stitzer ML. Pharmacotherapy for nicotine dependence. *CA Cancer J Clin.* 2005; 55:281-299; quiz 322-323,325.
- Frishman WH. Smoking cessation pharmacotherapy. *Ther Adv Cardiovasc Dis.* 2009; 3:287-308.
- Kenny PJ. Emerging therapeutic targets for the treatment of nicotine addiction. *Expert Rev Clin Pharmacol.* 2009; 2:221-225.
- Stack NM. Smoking cessation: An overview of treatment options with a focus on varenicline. *Pharmacotherapy.* 2007; 27:1550-1557.
- Newman SP, Pavia D, Clarke SW. How should a pressurized beta-adrenergic bronchodilator be inhaled? *Eur J Respir Dis.* 1981; 62:3-21.
- Ikedo A, Nishimura K, Koyama H, Tsukino M, Hajiro T, Mishima M, Izumi T. Comparison of the bronchodilator effects of salbutamol delivered *via* a metered-dose inhaler with spacer, a dry-powder inhaler, and a jet nebulizer in patients with chronic obstructive pulmonary disease. *Respiration.* 1999; 66:119-123.
- Cohen HA, Cohen Z, Pomeranz AS, Czitrion B, Kahan E. Bacterial contamination of spacer devices used by asthmatic children. *J Asthma.* 2005; 42:169-172.
- French DL, Edwards DA, Niven RW. The influence of formulation on emission, deaggregation and deposition of dry powders for inhalation. *J Aerosol Sci.* 1996; 27:769-783.
- Islam N, Stewart P, Larson I, Hartley P. Lactose surface modification by decantation: Are drug-fine lactose Ratios the key to better dispersion of salmeterol xinafoate from lactose-interactive mixtures? *Pharm Res.* 2004; 21:492-499.
- Islam N, Stewart P, Larson I, Hartley P. Effect of carrier size on the dispersion of salmeterol xinafoate from interactive mixtures. *J Pharm Sci.* 2004; 93:1030-1038.
- Newman SP, Clarke SW. Therapeutic aerosols 1 – physical and practical considerations. *Thorax.* 1983; 38:881-886.
- Gonda I. Aerosols for delivery of therapeutic and diagnostic agents to the respiratory tract. *Crit Rev Ther Drug Carrier Syst.* 1990; 6:273-313.
- Byron PR. Prediction of drug residence times in regions of the human respiratory tract following aerosol inhalation. *J Pharm Sci.* 1986; 75:433-438.
- Hickey AJ, Martonen TB. Behavior of hygroscopic pharmaceutical aerosols and the influence of hydrophobic additives. *Pharm Res.* 1993; 10:1-7.
- Suarez S, Hickey AJ. Drug properties affecting aerosol behavior. *Respir Care.* 2000; 45:652-666.
- Gonda I. Targeting by deposition. In: *Pharmaceutical Inhalation Aerosol Therapy* (Hickey AJ, ed.). Marcel Dekker, Inc., New York, 1992; pp. 61-82.
- Brain JD, Blancard JD. Mechanisms of particle deposition and clearance. In: *Aerosols in Medicine, Principles, Diagnosis and Therapy* (Moren F, Dolovich MB, Newhouse MT, Newman SP, eds.). 2nd ed., Elsevier Science Publishers, Amsterdam, 1993; pp. 117-155.
- Bhavna, Ahmad FJ, Mittal G, Jain GK, Malhotra G, Khar RK, Bhatnagar A. Nano-salbutamol dry powder inhalation: A new approach for treating bronchoconstrictive conditions. *Eur J Pharm Biopharm.* 2009; 71:282-291.
- Plumley C, Gorman EM, El-Gendy N, Bybee CR, Munson EJ, Berkland C. Nifedipine nanoparticle agglomeration as a dry powder aerosol formulation strategy. *Int J Pharm.* 2009; 369:136-143.
- Cheow WS, Hadinoto K. Preparations of dry-powder therapeutic nanoparticle aerosols for inhaled drug delivery. *Earozoru Kenkyu.* 2010; 25:155-165.
- Kalantarian P, Najafabadi AR, Haririan I, Vatanara A, Yamini Y, Darabi M, Gilani K. Preparation of 5-fluorouracil nanoparticles by supercritical antisolvents for pulmonary delivery. *Int J Nanomed.* 2010; 5:763-770.
- Zhang Y, Zhu J, Tang Y, Chen X, Yang Y. The preparation and application of pulmonary surfactant nanoparticles as absorption enhancers in insulin dry powder delivery. *Drug Dev Ind Pharm.* 2009; 35:1059-1065.
- Huang M, Ma Z, Khor E, Lim LY. Uptake of FITC-chitosan nanoparticles by A549 Cells. *Pharm Res.* 2002; 19:1488-1494.
- Chono S, Tanino T, Seki T, Morimoto K. Influence of particle size on drug delivery to rat alveolar macrophages following pulmonary administration of ciprofloxacin incorporated into liposomes. *J Drug Target.* 2006; 14:557-566.
- Chan TL, Yu CP. Charge effects on particle deposition in the human tracheobronchial tree. *Ann Occup Hyg.* 1982; 26:65-75.
- Cass LM, Brown J, Pickford M, Fayinka S, Newman SP, Johansson CJ, Bye A. Pharmacoscintigraphic evaluation of lung deposition of inhaled zanamivir in healthy volunteers. *Clin Pharmacokinet.* 1999; 36(Suppl 1):21-31.
- Kuhn RJ. Pharmaceutical considerations in aerosol drug delivery. *Pharmacotherapy.* 2002; 22(3 Pt 2):80S-85S.
- Bosquillon C, Pr at V, Vanbever R. Pulmonary delivery of growth hormone using dry powders and visualization of its local fate in rats. *J Control Release.* 2004; 96:233-244.
- Geller DE, Konstan MW, Smith J, Noonberg SB, Conrad C. Novel tobramycin inhalation powder in cystic fibrosis subjects: Pharmacokinetics and safety. *Pediatr Pulmonol.* 2007; 42:307-313.
- Hickey AJ, Lu D, Ashley ED, Stout J. Inhaled azithromycin therapy. *J Aerosol Med.* 2006; 19:54-60.
- Stoessl J. Potential therapeutic targets for Parkinson's disease. *Expert Opin Ther Targets.* 2008; 12:425-436.
- Xu CX, Jere D, Jin H, Chang SH, Chung YS, Shin JY, Kim JE, Park SJ, Lee YH, Chae CH, Lee KH, Beck GR Jr, Cho CS, Cho MH. Poly(ester amine)-mediated, aerosol-delivered Akt1 small interfering RNA suppresses lung tumorigenesis. *Am J Respir Crit Care Med.* 2008; 178:60-73.
- Li HY, Seville PC, Williamson IJ, Birchall JC. The use of amino acids to enhance the aerosolisation of spray-dried powders for pulmonary gene therapy. *J Gene Med.* 2005; 7:343-353.
- Garcia-Contreras L, Wong YL, Muttill P, Padilla D, Sadoff J, Drouse J, Germishuizen WA, Goonesekera S, Elbert K, Bloom BR, Miller R, Fourie PB, Hickey A, Edwards D. Immunization by a bacterial aerosol. *Proc Natl Acad Sci U S A.* 2008; 105:4656-4660.

37. Wee JL, Scheerlinck JP, Snibson KJ, Edwards S, Pearse M, Quinn C, Sutton P. Pulmonary delivery of ISCOMATRIX influenza vaccine induces both systemic and mucosal immunity with antigen dose sparing. *Mucosal Immunol.* 2008; 1:489-496.
38. Sievers RE. Dry powder aerosol vaccine and antibiotics delivery development to reduce risks of deaths in developing countries. 238th ACS National Meeting, Washington, DC, United States, August 16-20, 2009; PRES-008.
39. Anon. Method of and apparatus for effecting delivery of fine powders. *IP.com Journal.* 2008; 8:13.
40. Sen H, Jayanthi S, Sinha R, Sharma R, Muttill P. Inhalable biodegradable microparticles for target-specific drug delivery in tuberculosis and a process thereof. US patent 2003-685567 2005084455. 2005 20031016.
41. Rawat A, Majumder QH, Ahsan F. Inhalable large porous microspheres of low molecular weight heparin: *In vitro* and *in vivo* evaluation. *J Control Release.* 2008; 128:224-232.
42. Cheatham WW, Leone-Bay A, Grant M, Fog PB, Diamond DC. Pulmonary delivery of inhibitors of phosphodiesterase type 5. WO patent 2005-US30028 2006023944. 2006 20050823.
43. Farr SJ, Otulana BA. Pulmonary delivery of opioids as pain therapeutics. *Adv Drug Deliv Rev.* 2006; 58:1076-1088.
44. Fleischer W, Reimer K, Leyendecker P. Opioids for the treatment of the chronic obstructive pulmonary disease. EP patent 2004-13468 1604666. 2005 20040608.
45. Kleinstreuer C, Zhang Z, Donohue JF. Targeted drug-aerosol delivery in the human respiratory system. *Ann Rev Biomed Eng.* 2008; 10:195-220.
46. Ali R, Jain GK, Iqbal Z, Talegaonkar S, Pandit P, Sule S, Malhotra G, Khar RK, Bhatnagar A, Ahmad FJ. Development and clinical trial of nano-atropine sulfate dry powder inhaler as a novel organophosphorous poisoning antidote. *Nanomedicine.* 2009; 5:55-63.
47. Timothy W, Giles MF, Jonathan MM. Pulmonary inhalation of levodopa containing compositions in the treatment of Parkinson's disease and other central nervous system disorders. GB patent 2007-21856 2454480. 2009 20071107.
48. Onischuk AA, Tolstikova TG, Sorokina IV, Zhukova NA, Baklanov AM, Karasev VV, Borovkova OV, Dultseva GG, Boldyrev VV, Fomin VM. Analgesic effect from ibuprofen nanoparticles inhaled by male mice. *J Aerosol Med Pulm Drug Deliv.* 2009; 22:245-253.
49. Shahiwala A, Misra A. Pulmonary absorption of liposomal levonorgestrel. *AAPS PharmSciTech.* 2004; 5:E13
50. Graham AN, Johnson ES, Persaud NP, Turner P, Wilkinson M. The systemic availability of ergotamine tartrate given by three different routes of administration to healthy volunteers. *Progress in Migraine Research.* 1984; 2:283-292.
51. Bartus RT, Emerich DF. Pulmonary delivery in treating disorders of the central nervous system. WO patent 2001-US29311 2002024158. 2002 20010919.
52. Bartus RT, Emerich D, Snodgrass-Belt P, Fu K, Salzberg-Brenhouse H, Lafreniere D, Novak L, Lo ES, Cooper T, Basile AS. A pulmonary formulation of L-dopa enhances its effectiveness in a rat model of Parkinson's disease. *J Pharmacol Exp Ther.* 2004; 310:828-835.
53. Armer TA, Shrewsbury SB, Newman SP, Pitcairn G, Ramadan N. Aerosol delivery of ergotamine tartrate *via* a breath-synchronized plume-control inhaler in humans. *Curr Med Res Opin.* 2007; 23:3177-3187.
54. Davison S, Thippahawong J, Blanchard J, Liu K, Morishige R, Gonda I, Okikawa J, Adams J, Evans A, Otulana B, Davis S. Pharmacokinetics and acute safety of inhaled testosterone in postmenopausal women. *J Clin Pharmacol.* 2005; 45:177-184.
55. Wolff RK. Safety of inhaled proteins for therapeutic use. *J Aerosol Med.* 1998; 11:197-219.
56. Henningfield JE. Nicotine medications for smoking cessation. *N Engl J Med.* 1995; 333:1196-1203.
57. Benowitz NL. Neurobiology of nicotine addiction: Implications for smoking cessation treatment. *Am J Med.* 2008; 121(4 Suppl 1):S3-S10.
58. Benowitz NL, Jacob P 3rd. Nicotine and cotinine elimination pharmacokinetics in smokers and nonsmokers. *Pharmacol Ther.* 1993; 53:316-323.
59. Benowitz NL, Jacob P 3rd, Denaro C, Jenkins R. Stable isotope studies of nicotine kinetics and bioavailability. *Clin Pharmacol Ther.* 1991; 49:270-277.
60. Fant RV, Henningfield JE, Shiffman S, Strahs KR, Reitberg DP. A pharmacokinetic crossover study to compare the absorption characteristics of three transdermal nicotine patches. *Pharmacol Biochem Behav.* 2000; 67:479-482.
61. Molander L, Lunell E. Pharmacokinetic investigation of a nicotine sublingual tablet. *Eur J Clin Pharmacol.* 2001; 56:813-819.
62. Dempsey D, Tutka P, Jacob P 3rd, Allen F, Schoedel K, Tyndale RF, Benowitz NL. Nicotine metabolite ratio as an index of cytochrome P450 2A6 metabolic activity. *Clin Pharmacol Ther.* 2004; 76:64-72.
63. Sutherland G, Russell MA, Stapleton J, Feyerabend C, Ferno O. Nasal nicotine spray: A rapid nicotine delivery system. *Psychopharmacology (Berl).* 1992; 108:512-518.
64. Shiffman S, Fant RV, Buchhalter AR, Gitchell JG, Henningfield JE. Nicotine delivery systems. *Expert Opin Drug Deliv.* 2005; 2:563-577.
65. Bergström M, Nordberg A, Lunell E, Antoni G, Långström B. Regional deposition of inhaled ¹¹C-nicotine vapor in the human airway as visualized by positron emission tomography. *Clin Pharmacol Ther.* 1995; 57:309-317.
66. Henningfield JE, Shiffman S, Ferguson SG, Gritz ER. Tobacco dependence and withdrawal: Science base, challenges and opportunities for pharmacotherapy. *Pharmacol Ther.* 2009; 123:1-16.
67. Rose JE, Behm F, Turner J. Dry powder delivery system. US patent 95-477562 5687746. 1997 19950607.
68. Andrus PG, Rhem R, Rosenfeld J, Dolovich MB. Nicotine microaerosol inhaler. *Can Respir J.* 1999; 6:509-512.
69. Sumner W 2nd. Estimating the health consequences of replacing cigarettes with nicotine inhalers. *Tob Control.* 2003; 12:124-132.
70. Davies JH. Nicotine inhalation therapies – smoking cessation and other medical uses. WO patent 2007-GB2074 2007141520. 2007 20070606.
71. Caldwell B, Dickson S, Burgess C, Siebers R, Mala S, Parkes A, Crane J. A pilot study of nicotine delivery to smokers from a metered-dose inhaler. *Nicotine Tob Res.* 2009; 11:342-347.
72. Gonda I. Nicotine pulmonary formulation for tobacco use cessation. US patent 2007-931867 2008138398. 2008 20071031.
73. Gonda I, Bruinenberg P, Mudhumba S, Cipolla DC. Smoking cessation approach *via* deep lung delivery of clean nicotine. *Respiratory Drug Delivery Europe* 2009,

- Vol 1, pp. 57-62.
74. Ferry LH. Non-nicotine pharmacotherapy for smoking cessation. *Prim Care*. 1999; 26:653-669.
 75. Lerman C, Niaura R, Collins BN, Wileyto P, Audrain-McGovern J, Pinto A, Hawk L, Epstein LH. Effect of bupropion on depression symptoms in a smoking cessation clinical trial. *Psychol Addict Behav*. 2004; 18:362-366.
 76. Jefferson JW, Pradko JF, Muir KT. Bupropion for major depressive disorder: pharmacokinetic and formulation considerations. *Clin Ther*. 2005; 27:1685-1695.
 77. Tutka P, Zatoński W. Cytisine for the treatment of nicotine addiction: From a molecule to therapeutic efficacy. *Pharmacol Rep*. 2006; 58:777-798.
 78. Coe JW, Brooks PR, Vetelino MG, *et al*. Varenicline: An alpha4beta2 nicotinic receptor partial agonist for smoking cessation. *J Med Chem*. 2005; 48:3474-3477.
 79. Kuehn BM. Studies linking smoking-cessation drug with suicide risk spark concerns. *JAMA*. 2009; 301:1007-1008.
 80. Obach RS, Reed-Hagen AE, Krueger SS, Obach BJ, O'Connell TN, Zandi KS, Miller S, Coe JW. Metabolism and disposition of varenicline, a selective alpha4beta2 acetylcholine receptor partial agonist, *in vivo* and *in vitro*. *Drug Metab Dispos*. 2006; 34:121-130.
 81. Foulds J. The neurobiological basis for partial agonist treatment of nicotine dependence: Varenicline. *Int J Clin Pract*. 2006; 60:571-576.
 82. Botteri E, Iodice S, Bagnardi V, Raimondi S, Lowenfels AB, Maisonneuve P. Smoking and colorectal cancer, a meta-analysis. *JAMA*. 2008; 300:2765-2778.
 83. Lechuga-Ballesteros D, Kuo M-C, Song Y, Bueche B. Aerosol formulation comprising nicotine salts obtained by nicotine base reacted with organic acids. WO patent 2005-US22703 2006004646. 2006 20050628.
 84. Pavkov RM, Armer TA, Mohsen NM. Aerosol formulations for delivery of dihydroergotamine to the systemic circulation *via* pulmonary inhalation. WO patent 2004-US29632 2005025506. 2005 20040910.
 85. Bennett DB, Tyson E, Mah S, de Groot JS, Hegde SG, Terao S, Teitelbaum Z. Sustained delivery of detirelix after pulmonary administration of liposomal formulations. *J Control Release*. 1994; 32:27-35.
 86. Zheng Y, Marsh KC, Bertz RJ, El-Shourbagy T, Adjei AL. Pulmonary delivery of a dopamine D-1 agonist, ABT-431, in dogs and humans. *Int J Pharm*. 1999; 191:131-140.
 87. Okumu FW, Lee RY, Blanchard JD, Queirolo A, Woods CM, Lloyd PM, Okikawa J, Gonda I, Farr SJ, Rubsam R, Adjei AL, Bertz RJ. Evaluation of the AERx pulmonary delivery system for systemic delivery of a poorly soluble selective D-1 agonist, ABT-431. *Pharm Res*. 2002; 19:1009-1012.
 88. Jackson B, Bennett DJ, Bartus RT, Emerich DF. Pulmonary delivery for levodopa. WO patent 2003-US8659 2003079992. 2003 20030319.
 89. Adjei AL, Zheng J, Gupta PK, Marsh KC, Wu V, Lee DY. Formulations for pulmonary delivery of dopamine agonists. US patent 97-822631 6193954. 2001 19970321.
 90. Lunell E, Molander L, Ekberg K, Wahren J. Site of nicotine absorption from a vapor inhaler – comparison with cigarette smoking. *Eur J Clin Pharmacol*. 2000; 55:737-741.
 91. Schneider NG, Olmstead RE, Franzon MA, Lunell E. The nicotine inhaler: Clinical pharmacokinetics and comparison with other nicotine treatments. *Clin Pharmacokinet*. 2001; 40:661-684.
 92. Benowitz NL, Porchet H, Sheiner L, Jacob P 3rd. Nicotine absorption and cardiovascular effects with smokeless tobacco use: Comparison with cigarettes and nicotine gum. *Clin Pharmacol Ther*. 1988; 44:23-28.
 93. Choi JH, Dresler CM, Norton MR, Strahs KR. Pharmacokinetics of a nicotine polacrilex lozenge. *Nicotine Tob Res*. 2003; 5:635-644.
 94. Dalby RN, Hickey AJ, Tiano SL. Medical devices for the delivery of therapeutic aerosols to the lungs. In: *Inhalation Aerosols*. 2nd ed., Informa Health Care, London, UK, 2006; pp. 417-444.

(Received December 12, 2011; Revised May 5, 2012; Accepted May 24, 2012)

Synthesis and anticancer activity of novel 5-(indole-2-yl)-3-substituted 1,2,4-oxadiazoles

Peng Wang, Jianzhen Liu, Hualu Xing, Yang Liu, Wencheng Xie, Guisen Zhao*

Department of Medicinal Chemistry, Key Laboratory of Chemical Biology (Ministry of Education), School of Pharmaceutical Sciences, Shandong University, Ji'nan, Shandong, China.

ABSTRACT: A new series of 5-(indole-2-yl)-3-substituted 1,2,4-oxadiazoles were synthesized and evaluated for their anticancer activities. Structures of the compounds were confirmed by spectroscopic methods. Structural modifications were done to improve the antiproliferative activity of compound 1. The results indicated that a benzyloxy substituent on the C-4 position was better than a methyl substituent on the C-6 position of the indole component. Compounds 10a, 10b, 10g, 10i, 10l, 10n, 10o, and 10p were found to be more active than lead compound 1 in the PC-3 cell line. These compounds may serve as lead candidates in the development of novel chemotherapeutics for cancer treatment.

Keywords: Indole, 1,2,4-oxadiazole, anticancer

1. Introduction

Cancer has become the second largest cause of death in many countries (1). Inhibition of apoptotic pathways is known as an important hallmark for cancer (2,3). In cancer cells, blockage of apoptosis could lead to excessive cell proliferation as well as resistance to cancer treatment. Apoptosis is caused by the activation of intracellular caspases. There are two main pathways triggering activation of caspases, referred to as the intrinsic and extrinsic pathways. Numerous cellular targets of these two pathways have been identified, such as caspases (caspase-2, -3, -6~10, and -12), B-cell lymphoma-2 (Bcl-2) family proteins (Bcl-2, Bcl-XL, Bcl-W, Bcl-B, Mcl-1, and Bfl-1), and tumor necrosis factor (TNF) family death receptors (4,5). It has been recently reported that several anticancer agents exhibited apoptosis-inducing ability, such as imatinib, sorafenib, and lapatinib (6-10). Therefore, the identification of apoptosis

inducers becomes an attractive approach for discovery and development of potential anticancer agents. Pro-apoptotic agents affected more than one target, making optimizations through structure-activity relationships (SAR) studies difficult (2,11,12). For multiple actions of pro-apoptotic agents, screening of these agents was often based on cell line evaluation (11,12).

In recent years, many compounds with diverse structures were identified as pro-apoptotic agents (3,10-21). Compound 1 (Table 1) which might activate caspase-3/7 was reported as a novel 5-(indole-2-yl)-3-substituted 1,2,4-oxadiazole as a pro-apoptotic agent with anticancer activity at micromole concentrations (12). The effects of substitution on the C-6 position of the indole ring system have been studied (12). In order to study the SAR on other positions of the indole ring system, a series of 5-(indole-2-yl)-3-substituted 1,2,4-oxadiazoles were designed and synthesized. Their anticancer activities were tested in this paper.

2. Materials and Methods

2.1. Chemicals

The synthesis of intermediates 5b, 8, and 9 are shown in Scheme 1. Starting with 5-substituted salicylaldehyde (2), 5-substituted-2-benzyloxybenzaldehydes (3) were prepared by benzyl chloride in DMF catalyzed by K₂CO₃ (22,23). Intermediates 4 were prepared by a condensation reaction between 3 and methyl 2-azidoacetate. Heating of intermediates 4 in *p*-xylene to reflux for 1 h generated compounds 5 (22). Compound 6 was easily prepared from 5a by a hydrolysis reaction. Compound 6 reacted with sodium methoxide in DMF/CH₃OH catalyzed by cuprous iodide afforded compound 7. Compound 8 was synthesized by the methylation reaction from 7 using dimethyl sulfate. The preparation of compound 9 was a methylation reaction from 5a.

The synthesis of 5-(indole-2-yl)-3-substituted 1,2,4-oxadiazoles are shown in Scheme 2. The targeting compounds were synthesized using a one-pot reaction between amidoximes (11a~11d) and substituted indoles (5b, 8, 9, 12, and 13) under microwave conditions. Compounds 12 and 13 were commercially available.

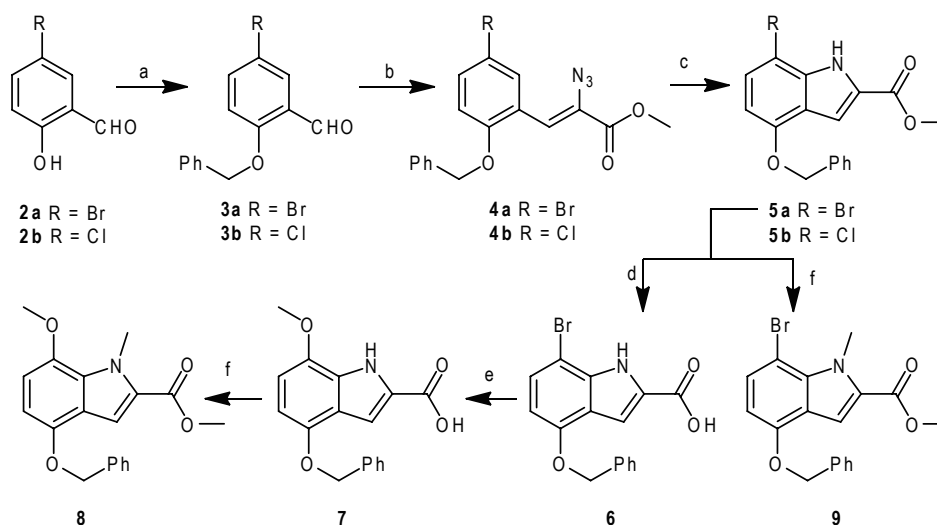
*Address correspondence to:

Dr. Guisen Zhao, School of Pharmaceutical Sciences, Shandong University, Wenhuxi Road No. 44, Ji'nan, Shandong 250012, China.

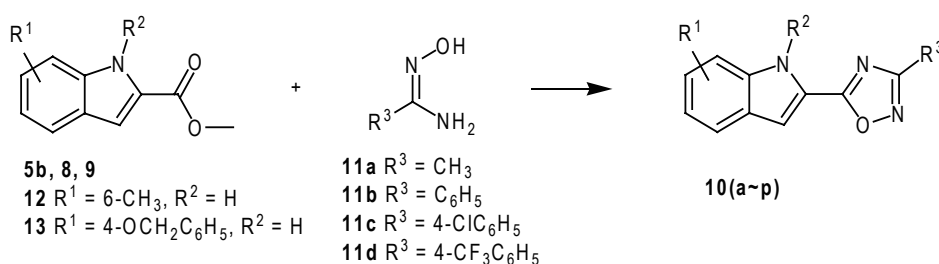
E-mail: guisenzhao@sdu.edu.cn

Table 1. The cells growth inhibitory activities of target compounds

Compounds	R ¹	R ²	R ³	IC ₅₀ (μM)	
				PC-3	MCF-7
1	H	H	CH ₃	60.35	> 80
10a	4-OCH ₂ Ph-7-OCH ₃	CH ₃	CH ₃	14.03	> 80
10b	4-OCH ₂ Ph-7-OCH ₃	CH ₃	Ph	8.96	> 80
10c	4-OCH ₂ Ph-7-OCH ₃	CH ₃	4-Cl-Ph	> 50	> 80
10d	4-OCH ₂ Ph-7-Br	CH ₃	CH ₃	> 80	> 80
10e	4-OCH ₂ Ph-7-Br	CH ₃	Ph	> 80	> 80
10f	4-OCH ₂ Ph-7-Br	CH ₃	4-Cl-Ph	78.65	> 80
10g	4-OCH ₂ Ph-7-Cl	H	CH ₃	16.67	> 80
10h	4-OCH ₂ Ph-7-Cl	H	Ph	> 80	> 80
10i	4-OCH ₂ Ph-7-Cl	H	4-Cl-Ph	42.55	> 80
10j	6-CH ₃	H	CH ₃	> 80	> 80
10k	6-CH ₃	H	Ph	> 80	> 80
10l	6-CH ₃	H	4-Cl-Ph	16.65	> 80
10m	4-OCH ₂ Ph	H	CH ₃	> 80	> 80
10n	4-OCH ₂ Ph	H	Ph	21.41	> 80
10o	4-OCH ₂ Ph	H	4-Cl-Ph	10.52	> 80
10p	6-CH ₃	H	CF ₃	26.58	> 80



Scheme 1. Reagents and conditions. (a) K₂CO₃, DMF, N₂, 50°C, 10 h; (b) methyl 2-azidoacetate, CH₃ONa, 50% THF/CH₃OH, N₂, -17~0°C, 4 h; (c) *p*-xylene, reflux, 1 h; (d) KOH, THF/H₂O, reflux, 4 h; (e) NaH, CH₃OH, DMF, CuI, 120°C, 4 h; (f) (CH₃O)₂SO₂, DMF, NaH, 0°C ~ room temperature.



Scheme 2. Reagents and conditions (DMF, Cs₂CO₃, microwave 800 W, 150°C, 10 min).

2.2. Cell lines

Human prostate cancer cells (PC-3) and human breast adenocarcinoma cells (MCF-7) were maintained in RPMI 1640 medium (HyClone[®], Thermo Fisher Scientific Inc., Waltham, MA, USA). The medium was supplemented with 10% fetal bovine serum (FBS) (Gibco[®], Invitrogen, Carlsbad, CA, USA), 100 µg/mL penicillin and 100 µg/mL streptomycin. Cells were cultured in a humidified atmosphere of 5% CO₂ at 37°C.

2.3. MTT assay

Cells were seeded into 96-well culture plates at a density of 5×10^3 cells per well and cultured for 12 h. Thereafter the cells were treated with various concentrations of tested compounds and incubated for 72 h. Five mg/mL MTT solution was added to each well and the cells were incubated at 37°C for 4 h. The resulting crystals were extracted with dimethyl sulfoxide (DMSO) for 15 min. The optical density (OD) was measured using a plate microreader (Bio-Rad 680, Bio-Rad Co., Hercules, USA).

3. Results and Discussion

The *in vitro* antitumour effect of compounds **10a**~**10p** was assessed against prostate cancer cells (PC-3) and human breast adenocarcinoma cells (MCF-7). Antiproliferative data was compared with the previously reported pro-apoptotic compound **1** as control. All inhibition results are shown in Table 1. The PC-3 cell line was more responsive to 5-(indole-2-yl)-3-substituted 1,2,4-oxadiazoles than the MCF-7 cell line.

First we studied the single substituted indoles (R¹, compounds **10j**~**10p**). When comparing **10n** to **10k**, **10o** to **10l**, we found that compounds (**10n** and **10o**) with a benzyloxyl group on the C-4 position showed more potent inhibitory activities than compounds (**10k** and **10l**) with a methyl group on the C-6 position (IC₅₀ values of 21.41 and 10.52 µM for **10n** and **10o**, > 80 and 16.65 µM for **10k** and **10l**). This result showed that introduction of a benzyloxyl group on the C-4 position of the indole ring was better than a methyl group on the C-6 position.

Keeping the benzyloxyl group on the C-4 position, we introduced different substitutions on the N-1 and/or C-7 position of the indole ring leading to compounds **10a**~**10i**. Compound **10b** showed the highest inhibitory activity among these compounds (IC₅₀ = 8.96 µM), and was up to six times more potent than lead compound **1**. Introduction of a chlorine on the 4-position of benzene ring (R³) in compound **10b** led to compound **10c**, and the activity was decreased dramatically (IC₅₀ > 50 µM). Besides, compounds **10a**, **10g**, **10i**, **10l**, **10n**, **10o**, and **10p** were found to be more active than lead compound **1** in the PC-3 cell line. They showed no activities against the MCF-7 cell line (IC₅₀ > 80 µM).

4. Conclusion

In conclusion, a new series of 5-(indole-2-yl)-3-substituted 1,2,4-oxadiazoles were synthesized with cell inhibitory activities. Several compounds showed more potent activities than lead compound **1**. Compounds with benzyloxyl substituent on the C-4 position had greater antiproliferative activity than those with methyl on the C-6 position of the indole component. Compounds with both C-4 benzyloxyl and C-7 methyloxyl substituents were more efficient than those with C-4 benzyloxyl and C-7 bromine. We successfully identified compound **10b** as the most active compound. Further studies based on this structure will be continued.

Acknowledgements

This work was supported by the National Natural Science Foundation of China (No. 21072115) and Shandong Natural Science Foundation (No. ZR2011HM042).

References

1. Varmus H. The new era in cancer research. *Science*. 2006; 312:1162-1165.
2. Toogood PL. Inhibition of protein-protein association by small molecules: Approaches and progress. *J Med Chem*. 2002; 45:1543-1558.
3. Cai SX, Nguyen B, Jia S, Herich J, Guastella J, Reddy S, Tseng B, Drewe J, Kasibhatla S. Discovery of substituted N-phenyl nicotinamides as potent inducers of apoptosis using a cell- and caspase-based high throughput screening assay. *J Med Chem*. 2003; 46:2474-2481.
4. Reed JC, Pellecchia M. Apoptosis-based therapies for hematologic malignancies. *Blood*. 2005; 106:408-418.
5. Reed JC. Apoptosis-based therapies. *Nat Rev Drug Discov*. 2002; 1:111-121.
6. Cross SA, Lyseng-Williamson KA. Imatinib: In relapsed or refractory philadelphia chromosome-positive acute lymphoblastic leukaemia. *Drugs*. 2007; 67:2645-2654.
7. Baselga J. Targeting tyrosine kinases in cancer: The second wave. *Science*. 2006; 312:1175-1178.
8. Wood LS, Manchen B. Sorafenib: A promising new targeted therapy for renal cell carcinoma. *Clin J Oncol Nurs*. 2007; 11:649-656.
9. Lackey KE. Lessons from the drug discovery of lapatinib, a dual ErbB1/2 tyrosine kinase inhibitor. *Curr Top Med Chem*. 2006; 6:435-460.
10. Rini BI. Sunitinib. *Expert Opin Pharmacother*. 2007; 8:2359-2369.
11. Kemnitzer W, Drewe J, Jiang S, *et al.* Discovery of 4-aryl-4H-chromenes as a new series of apoptosis inducers using a cell- and caspase-based high-throughput screening assay. 1. Structure-activity relationships of the 4-aryl group. *J Med Chem*. 2004; 47:6299-6310.
12. Ziedan NI, Stefanelli F, Fogli S, Westwell AD. Design, synthesis and pro-apoptotic antitumour properties of indole-based 3,5-disubstituted oxadiazoles. *Eur J Med Chem*. 2010; 45:4523-4530.
13. Kemnitzer W, Drewe J, Jiang S, Zhang H, Zhao J, Crogan-

- Grundy C, Xu L, Lamothe S, Gourdeau H, Denis R, Tseng B, Kasibhatla S, Cai SX. Discovery of 4-aryl-4H-chromenes as a new series of apoptosis inducers using a cell- and caspase-based high-throughput screening assay. 3. structure-activity relationships of fused rings at the 7,8-positions. *J Med Chem.* 2007; 50:2858-2864.
14. Kemnitzer W, Jiang S, Wang Y, Kasibhatla S, Crogan-Grundy C, Bubenik M, Labrecque D, Denis R, Lamothe S, Attardo G, Gourdeau H, Tseng B, Drewe J, Cai SX. Discovery of 4-aryl-4H-chromenes as a new series of apoptosis inducers using a cell- and caspase-based HTS assay. Part 5: Modifications of the 2- and 3-positions. *Bioorg Med Chem Lett.* 2008; 18:603-607.
 15. Kemnitzer W, Jiang S, Zhang H, Kasibhatla S, Crogan-Grundy C, Blais C, Attardo G, Denis R, Lamothe S, Gourdeau H, Tseng B, Drewe J, Cai SX. Discovery of 4-aryl-2-oxo-2H-chromenes as a new series of apoptosis inducers using a cell- and caspase-based high-throughput screening assay. *Bioorg Med Chem Lett.* 2008; 18:5571-5575.
 16. Kemnitzer W, Kasibhatla S, Jiang S, *et al.* Discovery of 4-aryl-4H-chromenes as a new series of apoptosis inducers using a cell- and caspase-based high-throughput screening assay. 2. Structure-activity relationships of the 7- and 5-, 6-, 8-positions. *Bioorg Med Chem Lett.* 2005; 15:4745-4751.
 17. Kemnitzer W, Kueimmerle J, Zhang HZ, Kasibhatla S, Tseng B, Drewe J, Cai SX. Discovery of 3-aryl-5-aryl-1,2,4-oxadiazoles as a new series of apoptosis inducers. 2. Identification of more aqueous soluble analogs as potential anticancer agents. *Bioorg Med Chem Lett.* 2009; 19:4410-4415.
 18. Sirisoma N, Kasibhatla S, Pervin A, *et al.* Discovery of 2-chloro-N-(4-methoxyphenyl)-N-methylquinazolin-4-amine (EP128265, MPI-0441138) as a potent inducer of apoptosis with high *in vivo* activity. *J Med Chem.* 2008; 51:4771-4779.
 19. Sirisoma N, Pervin A, Zhang H, Jiang S, Willardsen JA, Anderson MB, Mather G, Pleiman CM, Kasibhatla S, Tseng B, Drewe J, Cai SX. Discovery of N-(4-methoxyphenyl)-N,2-dimethylquinazolin-4-amine, a potent apoptosis inducer and efficacious anticancer agent with high blood brain barrier penetration. *J Med Chem.* 2009; 52:2341-2351.
 20. Zhang HZ, Kasibhatla S, Kueimmerle J, Kemnitzer W, Ollis-Mason K, Qiu L, Crogan-Grundy C, Tseng B, Drewe J, Cai SX. Discovery and structure-activity relationship of 3-aryl-5-aryl-1,2,4-oxadiazoles as a new series of apoptosis inducers and potential anticancer agents. *J Med Chem.* 2005; 48:5215-5223.
 21. Kemnitzer W, Drewe J, Jiang S, Zhang H, Crogan-Grundy C, Labrecque D, Bubenik M, Attardo G, Denis R, Lamothe S, Gourdeau H, Tseng B, Kasibhatla S, Cai SX. Discovery of 4-aryl-4H-chromenes as a new series of apoptosis inducers using a cell- and caspase-based high throughput screening assay. 4. Structure-activity relationships of N-alkyl substituted pyrrole fused at the 7,8-positions. *J Med Chem.* 2008; 51:417-423.
 22. Fresneda PM, Molinap P, Bleda JA. Synthesis of the indole alkaloids meridianins from the tunicate *Aplidium meridianum*. *Tetrahedron.* 2011; 57:2355-2363.
 23. Lin CF, Yang JS, Chang CY, Kuo SC, Lee MR, Huang LJ. Synthesis and anticancer activity of benzyloxybenzaldehyde derivatives against HL-60 cells. *Bioorg Med Chem.* 2005; 13:1537-1544.

(Received May 4, 2012; Revised June 8, 2012; Accepted June 12, 2012)

Appendix

The proton nuclear magnetic resonance ($^1\text{H-NMR}$ and $^{13}\text{C-NMR}$) spectra were recorded with a Bruker Avance DRX600 instrument with tetramethylsilane (TMS) as the internal standard at 600 MHz. The chemical shifts (δ) were reported in parts per million (ppm) and were relative to the central peak of the solvent, which was $\text{DMSO-}d_6$ or CDCl_3 . Mass spectra (MS) were measured with an API 4000 and the high resolution mass spectra data were obtained using an Accela UPLC-LTQ Orbitrap mass spectrometer. All melting points were determined in a Büchi capillary melting point apparatus and are uncorrected. Microwave syntheses were carried out in an XH-100A Xiang Hu instrument with focused microwave heating (microwave power supply 0-1,000 W, open vessel mode). Unless otherwise noted, all materials were obtained from commercial suppliers and used without further purification. Column chromatography was carried out with silica gel using the solvents indicated. Thin-layer chromatography (TLC) was performed on silica gel GF254 plates (layer thickness, 0.2 mm), and compounds were visualized using UV light. Petroleum ether used for TLC and column chromatography had a boiling range of 60-90°C.

Synthesis of compounds 3a and 3b

To a mixture of substituted salicylaldehyde (**2**) (0.1 mol) and K_2CO_3 (20.7 g, 0.15 mol) in DMF (100 mL), benzyl chloride (19.0 g, 0.15 mol) was added dropwise. Then the mixture was heated to 60°C for 8 h. After being allowed to cool to r.t., the mixture was poured into ice-water (1,000 mL). The precipitate was filtered, washed several times with water, and further purified by recrystallization in ethanol to afford **3**.

2-(Benzyloxy)-5-bromobenzaldehyde (3a) Yield 26.8 g (92%); colorless crystal; mp 72.4-73.6°C. $^1\text{H-NMR}$ (600 MHz, $\text{DMSO-}d_6$): δ = 5.30 (s, 2H), 7.32 (d, J = 8.4 Hz, 1H), 7.35 (t, J = 7.2 Hz, 1H), 7.42 (t, J = 7.8 Hz, 2H), 7.52 (d, J = 7.2 Hz, 2H), 7.76 (d, J = 2.4 Hz, 1H), 7.81 (dd, J = 9.0 Hz and J = 3.0 Hz, 1H), 10.33 (s, 1H). MS (ESI): m/z = 291.4 $[\text{M} + \text{H}]^+$.

2-(Benzyloxy)-5-chlorobenzaldehyde (3b) Yield 22.2 g (90%); colorless crystal; mp 81.0-81.9°C. $^1\text{H-NMR}$ (600 MHz, $\text{DMSO-}d_6$): δ = 5.31 (s, 2H), 7.35 (t, J = 7.2 Hz, 1H), 7.38 (d, J = 8.4 Hz, 1H), 7.42 (t, J = 7.2 Hz, 2H), 7.51 (d, J = 7.2 Hz, 2H), 7.65 (d, J = 2.4 Hz, 1H), 7.71 (dd, J = 8.4 Hz and J = 2.4 Hz, 1H), 10.35 (s, 1H). MS (ESI): m/z = 247.4 $[\text{M} + \text{H}]^+$.

Synthesis of compounds 4a and 4b

To a cooled (-20°C) solution of **3** (0.05 mol) and methyl 2-azidoacetate (23.0 g, 0.2 mol) in anhydrous CH_3OH (75 mL) and THF (45 mL) under a N_2 atmosphere, was added a solution of CH_3ONa (10.8 g,

0.2 mol) in anhydrous CH₃OH (30 mL) dropwise over 1 h, maintaining the temperature below -17°C. After 4 h, the mixture was placed in an ice-bath overnight. Cooled CH₃OH (50 mL) was added into the mixture and then the precipitate was filtered, and washed twice with CH₃OH to get compounds **4**.

(*Z*)-Methyl 2-azido-3-(2-(benzyloxy)-5-bromophenyl)acrylate (**4a**) Yellow solid, yield 70%, mp 88.9-90.1°C. ¹H-NMR (600 MHz, DMSO-*d*₆): δ = 8.25 (s, 1H), 7.51 (dd, *J* = 9.0 Hz and *J* = 2.4 Hz, 1H), 7.39-7.43 (m, 4H), 7.33-7.36 (m, 1H), 7.20 (s, 1H), 7.11 (d, *J* = 9.0 Hz, 1H), 5.21 (s, 2H), 3.84 (s, 3H). MS (ESI): *m/z* = 388.2 [M + H]⁺.

(*Z*)-Methyl 2-azido-3-(2-(benzyloxy)-5-chlorophenyl)acrylate (**4b**) Yellow solid, yield 70%, mp 89.2-91.2°C. ¹H-NMR (600 MHz, DMSO-*d*₆): δ = 8.23 (s, 1H), 7.52 (dd, *J* = 9.0 Hz and *J* = 2.4 Hz, 1H), 7.36-7.45 (m, 4H), 7.33-7.36 (m, 1H), 7.22 (s, 1H), 7.15 (d, *J* = 9.0 Hz, 1H), 5.18 (s, 2H), 3.86 (s, 3H). MS (ESI): *m/z* = 344.1 [M + H]⁺.

Synthesis of compounds **5a** and **5b**

Compounds **4** were suspended in *p*-xylene (400 mL). The mixture was heated to 150°C for 4 h. After being allowed to cool to r.t., the crude product precipitated was collected by filtration, and further purified by recrystallization in ethyl acetate/petroleum ether to afford **5**.

Methyl 4-(benzyloxy)-7-bromo-1H-indole-2-carboxylate (**5a**) Yield 68%; colorless crystal; mp 148.7-150.4°C. ¹H-NMR (600 MHz, DMSO-*d*₆): δ = 3.87 (s, 3H), 5.25 (s, 2H), 6.65 (d, *J* = 7.8 Hz, 1H), 7.27 (s, 1H), 7.34 (t, *J* = 7.8 Hz, 1H), 7.38-7.42 (m, 3H), 7.51 (d, *J* = 7.2 Hz, 2H), 11.98 (s, 1H). MS (ESI): *m/z* = 360.3 [M + H]⁺.

Methyl 4-(benzyloxy)-7-chloro-1H-indole-2-carboxylate (**5b**) Yield 65%; colorless crystal; mp 179.9-180.9°C. ¹H-NMR (600 MHz, DMSO-*d*₆): δ = 3.87 (s, 3H), 5.25 (s, 2H), 6.67 (d, *J* = 7.8 Hz, 1H), 7.23-7.26 (m, 2H), 7.34 (t, *J* = 7.8 Hz, 1H), 7.41 (t, *J* = 7.8 Hz, 2H), 7.50 (d, *J* = 7.8 Hz, 2H), 12.21 (s, 1H). MS (ESI): *m/z* = 316.3 [M + H]⁺.

4-(Benzyloxy)-7-bromo-1H-indole-2-carboxylic acid (**6**)

A solution of **5a** (3.6 g, 10 mmol), KOH (2.24 g, 40 mmol) in THF (40 mL) and water (15 mL) was heated to reflux for 4 h. After cooling to r.t., the THF was evaporated under reduced pressure. The mixture was poured into water and acidified with aq HCl (6N) to pH 1-2. The precipitate was filtered, washed several times with water, and further purified by recrystallization in ethyl acetate/petroleum ether to afford **6**. Yield 3.29 g (95%); white powder; mp 248.6-249.8°C. ¹H-NMR (600 MHz, DMSO-*d*₆): δ = 5.25 (s, 2H), 6.63 (d, *J* = 7.8 Hz, 1H), 7.20 (d, *J* = 2.4 Hz, 1H), 7.34 (t, *J* = 7.8 Hz, 1H),

7.36 (d, *J* = 8.4 Hz, 1H), 7.41 (t, *J* = 7.8 Hz, 2H), 7.51 (d, *J* = 7.8 Hz, 2H), 11.75 (s, 1H), 13.05 (br s, 1H). MS (ESI): *m/z* = 346.3 [M + H]⁺.

4-(Benzyloxy)-7-methoxy-1H-indole-2-carboxylic acid (**7**)

A mixture of **6** (3.46 g, 10 mmol), CuI (1.9 g, 10 mmol), CH₃ONa (3.8 g, 70 mmol) in anhydrous CH₃OH (20 mL) and DMF (40 mL) under N₂ atmosphere was heated and refluxed for 5 h. After cooling to r.t., the mixture was poured into water (500 mL) and acidified with aq HCl (6N) to pH 1-2. The precipitate was filtered, washed several times with water, and further purified by recrystallization in ethyl acetate/petroleum ether to afford **7**. Yield 80%, mp 235.2-236.5°C. ¹H-NMR (600 MHz, DMSO-*d*₆): δ = 3.85 (s, 3H), 5.23 (s, 2H), 6.59 (d, *J* = 7.8 Hz, 1H), 7.22 (d, *J* = 2.4 Hz, 1H), 7.34 (t, *J* = 7.8 Hz, 1H), 7.38 (d, *J* = 8.4 Hz, 1H), 7.42 (t, *J* = 7.8 Hz, 2H), 7.50 (d, *J* = 7.8 Hz, 2H), 11.85 (s, 1H), 12.95 (br s, 1H). MS (ESI): *m/z* = 298.4 [M + H]⁺.

Methyl 4-(benzyloxy)-7-methoxy-1-methyl-1H-indole-2-carboxylate (**8**)

Compound **7** was dissolved in anhydrous DMF. NaH (0.36 g, 15 mmol) was added to the solution at 0°C followed by dimethyl sulfate (1.89 g, 15 mmol). The mixture was stirred at r.t. for 4 h, and then was poured into ice-cold water. The precipitate was filtered, washed several times with water, and further purified by recrystallization in ethyl acetate/petroleum ether to afford **8**. Yield 2.09 g (64%); colorless crystal; mp 100.1-101.8°C. ¹H-NMR (600 MHz, DMSO-*d*₆): δ = 3.82 (s, 3H), 3.85 (s, 3H), 4.26 (s, 3H), 5.16 (s, 2H), 6.51 (d, *J* = 7.8 Hz, 1H), 6.69 (d, *J* = 9.0 Hz, 1H), 7.21 (s, 1H), 7.33 (t, *J* = 7.8 Hz, 1H), 7.40 (t, *J* = 7.8 Hz, 2H), 7.49 (d, *J* = 7.2 Hz, 2H). MS (ESI): *m/z* = 326.3 [M + H]⁺.

Methyl 4-(benzyloxy)-7-bromo-1-methyl-1H-indole-2-carboxylate (**9**)

The procedure was the same as compound **7** to **8**. Yield 3.39 g (91%); colorless crystal; mp 108.6-109.9°C. ¹H-NMR (600 MHz, DMSO-*d*₆): δ = 3.84 (s, 3H), 4.35 (s, 3H), 5.24 (s, 2H), 6.65 (d, *J* = 8.4 Hz, 1H), 7.27 (s, 1H), 7.35 (t, *J* = 7.2 Hz, 1H), 7.41 (t, *J* = 7.2 Hz, 2H), 7.44 (d, *J* = 9.0 Hz, 1H), 7.50 (d, *J* = 6.6 Hz, 2H). MS (ESI): *m/z* = 374.3 [M + H]⁺.

General procedure for synthesis of **10a**~**10p** under microwave irradiation

Substituted indole-based carboxylic acid esters (**5b**, **8**, **9**, **12**, and **13**) (1 mmol), amidoximes (2 mmol) and cesium carbonate (0.65 g, 2 mmol) in DMF (5 mL) were placed in a 10 mL flask followed by microwave

irradiation (800 W, 150°C) for the desired time. After cooling to r.t., the mixture was poured into 100 mL cold water, and then extracted with ethyl acetate. The combined organic solvent was dried over Na₂SO₄, filtered, and concentrated in vacuum. The crude product was purified by silica-gel chromatography with petroleum ether-ethyl acetate (15:1) to give the desired compounds **10a**–**10p**.

5-(4-(Benzyloxy)-7-methoxy-1-methyl-1H-indol-2-yl)-3-methyl-1,2,4-oxadiazole (10a) Yield 87%, white powder, mp 145.8-147.6°C. ¹H-NMR (600 MHz, DMSO-*d*₆): δ = 2.44 (s, 3H), 3.87 (s, 3H), 4.38 (s, 3H), 5.20 (s, 2H), 6.56 (d, *J* = 8.4 Hz, 1H), 6.73 (d, *J* = 8.4 Hz, 1H), 7.34 (t, *J* = 7.8 Hz, 1H), 7.38 (s, 1H), 7.41 (t, *J* = 7.8 Hz, 2H), 7.52 (d, *J* = 7.8 Hz, 2H). HRMS-ESI: *m/z* [M + H]⁺ calcd for C₂₀H₂₀N₃O₃: 350.1499; found 350.1504.

5-(4-(Benzyloxy)-7-methoxy-1-methyl-1H-indol-2-yl)-3-phenyl-1,2,4-oxadiazole (10b) Yield 81%, white acicular crystal; mp 179.3-180.7°C. ¹H-NMR (600 MHz, DMSO-*d*₆): δ = 3.89 (s, 3H), 4.48 (s, 3H), 5.22 (s, 2H), 6.59 (d, *J* = 8.4 Hz, 1H), 6.76 (d, *J* = 8.4 Hz, 1H), 7.34 (t, *J* = 7.8 Hz, 1H), 7.42 (t, *J* = 7.8 Hz, 2H), 7.48 (s, 1H), 7.53 (d, *J* = 7.8 Hz, 2H), 7.61~7.65 (m, 3H), 8.13 (d, *J* = 6.6 Hz, 2H). HRMS-ESI: *m/z* [M + H]⁺ calcd for C₂₅H₂₂N₃O₃: 412.1656; found 412.1654.

5-(4-(Benzyloxy)-7-methoxy-1-methyl-1H-indol-2-yl)-3-(4-chlorophenyl)-1,2,4-oxadiazole (10c) Yield 60%; white powder; mp 198.2-199.5°C. ¹H-NMR (600 MHz, CDCl₃): δ = 3.93 (s, 3H), 4.54 (s, 3H), 5.19 (s, 2H), 6.43 (d, *J* = 7.8 Hz, 1H), 7.61 (d, *J* = 7.8 Hz, 1H), 7.36 (t, *J* = 7.8 Hz, 1H), 7.43 (t, *J* = 7.8 Hz, 2H), 7.50~7.54 (m, 4H), 7.64 (s, 1H), 8.13 (d, *J* = 8.4 Hz, 2H). HRMS-ESI: *m/z* [M + H]⁺ calcd for C₂₅H₂₁ClN₃O₃: 446.1266; found 446.1265.

5-(4-(Benzyloxy)-7-bromo-1-methyl-1H-indol-2-yl)-3-methyl-1,2,4-oxadiazole (10d) Yield 80%; white powder; mp 153.8-154.9°C. ¹H-NMR (600 MHz, DMSO-*d*₆): δ = 2.46 (s, 3H), 4.47 (s, 3H), 5.28 (s, 2H), 6.69 (d, *J* = 8.4 Hz, 1H), 7.35 (t, *J* = 7.2 Hz, 1H), 7.42 (t, *J* = 7.8 Hz, 2H), 7.45 (s, 1H), 7.47 (d, *J* = 8.4 Hz, 1H), 7.53 (d, *J* = 7.8 Hz, 2H). HRMS-ESI: *m/z* [M + H]⁺ calcd for C₁₉H₁₇BrN₃O₂: 398.0499; found 398.0496.

5-(4-(Benzyloxy)-7-bromo-1-methyl-1H-indol-2-yl)-3-phenyl-1,2,4-oxadiazole (10e) Yield 79%; white powder; mp 201.2-202.5°C. ¹H-NMR (600 MHz, CDCl₃): δ = 4.68 (s, 3H), 5.23 (s, 2H), 7.38 (t, *J* = 7.2 Hz, 1H), 7.41 (d, *J* = 7.8 Hz, 1H), 7.44 (t, *J* = 7.8 Hz, 2H), 7.50~7.56 (m, 5H), 7.68 (s, 1H), 8.20 (dd, *J* = 7.8 Hz and 1.8 Hz, 2H). HRMS-ESI: *m/z* [M + H]⁺ calcd for C₂₄H₁₉BrN₃O₂: 460.0655; found 460.0651.

5-(4-(Benzyloxy)-7-bromo-1-methyl-1H-indol-2-yl)-3-(4-chlorophenyl)-1,2,4-oxadiazole (10f) Yield 68%; white powder; mp 201.3-202.9°C. ¹H-NMR (600 MHz, DMSO-*d*₆): δ = 4.66 (s, 3H), 5.23 (s, 2H), 6.48 (d, *J* = 8.4 Hz, 1H), 7.37~7.44 (m, 4H), 7.52 (d, *J* = 8.4 Hz, 4H), 7.68 (s, 1H), 8.13 (d, *J* = 8.4 Hz, 2H). HRMS-ESI: *m/z*

[M + H]⁺ calcd for C₂₄H₁₈BrClN₃O₂: 494.0265; found 494.0261.

5-(4-(Benzyloxy)-7-chloro-1H-indol-2-yl)-3-methyl-1,2,4-oxadiazole (10g) Yield 59%; white powder; mp 212.5-214.2°C. ¹H-NMR (600 MHz, DMSO-*d*₆): δ = 2.43 (s, 3H), 5.27 (s, 2H), 6.68 (d, *J* = 7.8 Hz, 1H), 7.25 (d, *J* = 7.8 Hz, 1H), 7.34 (t, *J* = 7.2 Hz, 1H), 7.40~7.42 (m, 3H), 7.52 (d, *J* = 7.2 Hz, 2H), 12.73 (s, 1H). HRMS-ESI: *m/z* [M + H]⁺ calcd for C₁₈H₁₅ClN₃O₂: 340.0847; found 340.0851.

5-(4-(Benzyloxy)-7-chloro-1H-indol-2-yl)-3-phenyl-1,2,4-oxadiazole (10h) Yield 83%; white acicular crystal; mp 195.0-196.4°C. ¹H-NMR (600 MHz, DMSO-*d*₆): δ = 5.30 (s, 2H), 6.74 (d, *J* = 7.8 Hz, 1H), 7.32 (d, *J* = 7.8 Hz, 1H), 7.36 (t, *J* = 7.8 Hz, 1H), 7.43 (t, *J* = 7.8 Hz, 2H), 7.54 (s, 1H), 7.56 (d, *J* = 7.2 Hz, 2H), 7.61~7.65 (m, 3H), 8.13 (dd, *J* = 7.8 Hz and 1.8 Hz, 2H), 12.82 (s, 1H). HRMS-ESI: *m/z* [M + H]⁺ calcd for C₂₃H₁₇ClN₃O₂: 402.1004; found 402.1003.

5-(4-(Benzyloxy)-7-chloro-1H-indol-2-yl)-3-(4-chlorophenyl)-1,2,4-oxadiazole (10i) Yield 60%; white powder; mp 229.4-230.4°C. ¹H-NMR (600 MHz, DMSO-*d*₆): δ = 5.29 (s, 2H), 6.74 (d, *J* = 7.8 Hz, 1H), 7.32 (d, *J* = 8.4 Hz, 1H), 7.36 (t, *J* = 7.8 Hz, 1H), 7.43 (t, *J* = 7.8 Hz, 2H), 7.54~7.56 (m, 3H), 7.70 (d, *J* = 8.4 Hz, 2H), 8.12 (d, *J* = 8.4 Hz, 2H), 12.83 (s, 1H). HRMS-ESI: *m/z* [M + H]⁺ calcd for C₂₃H₁₆Cl₂N₃O₂: 436.0614; found 436.0609.

3-Methyl-5-(6-methyl-1H-indol-2-yl)-1,2,4-oxadiazole (10j) Yield 89%; white acicular crystal; mp 147.5-149.4°C. ¹H-NMR (600 MHz, DMSO-*d*₆): δ = 2.41 (s, 2H), 2.42 (s, 3H), 6.96 (dd, *J* = 8.4 Hz and 1.8 Hz, 1H), 7.26 (s, 1H), 7.30 (d, *J* = 1.8 Hz, 1H), 7.58 (d, *J* = 8.4 Hz, 1H), 12.23 (s, 1H). HRMS-ESI: *m/z* [M + H]⁺ calcd for C₁₂H₁₂N₃O: 214.0975; found 214.0973.

5-(6-Methyl-1H-indol-2-yl)-3-phenyl-1,2,4-oxadiazole (10k) Yield 68%; white powder; mp 215.0-216.8°C. ¹H-NMR (600 MHz, DMSO-*d*₆): δ = 2.43 (s, 3H), 6.98 (dd, *J* = 8.4 Hz and 1.2 Hz, 1H), 7.32 (s, 1H), 7.42 (dd, *J* = 2.4 Hz and 0.6 Hz, 1H), 7.60~7.65 (m, 4H), 8.10~8.12 (m, 2H), 12.33 (s, 1H). HRMS-ESI: *m/z* [M + H]⁺ calcd for C₁₇H₁₄N₃O: 276.1131; found 276.1134.

3-(4-Chlorophenyl)-5-(6-methyl-1H-indol-2-yl)-1,2,4-oxadiazole (10l) Yield 55%; white powder; mp 217.3-218.9°C. ¹H-NMR (600 MHz, DMSO-*d*₆): δ = 2.44 (s, 3H), 6.98 (d, *J* = 8.4 Hz, 1H), 7.31 (s, 1H), 7.42 (d, *J* = 1.8 Hz, 1H), 7.61 (d, *J* = 8.4 Hz, 1H), 7.70 (d, *J* = 8.4 Hz, 2H), 8.11 (d, *J* = 8.4 Hz, 2H), 12.33 (s, 1H). HRMS-ESI: *m/z* [M + H]⁺ calcd for C₁₇H₁₃ClN₃O: 310.0742; found 310.0743.

5-(4-(Benzyloxy)-1H-indol-2-yl)-3-methyl-1,2,4-oxadiazole (10m) Yield 71%; white powder; mp 170.9-172.5°C. ¹H-NMR (600 MHz, DMSO-*d*₆): δ = 2.42 (s, 3H), 5.27 (s, 2H), 6.68 (d, *J* = 7.8 Hz, 1H), 7.07 (d, *J* = 7.8 Hz, 1H), 7.20 (t, *J* = 7.8 Hz, 1H), 7.34 (t, *J* = 7.8 Hz, 2H), 7.41 (t, *J* = 7.8 Hz, 2H), 7.53 (d, *J* = 7.8

Hz, 2H), 12.42 (s, 1H). HRMS-ESI: m/z $[M + H]^+$ calcd for $C_{18}H_{16}N_3O_2$: 306.1237; found 306.1239.

5-(4-(Benzyloxy)-1H-indol-2-yl)-3-phenyl-1,2,4-oxadiazole (10n) Yield 73%; white powder; mp 177.2-179.1°C. 1H -NMR (600 MHz, $DMSO-d_6$): δ = 5.29 (s, 2H), 6.71 (d, J = 7.8 Hz, 1H), 7.12 (d, J = 7.8 Hz, 1H), 7.24 (t, J = 7.8 Hz, 1H), 7.34 (t, J = 7.8 Hz, 1H), 7.43 (t, J = 7.8 Hz, 2H), 7.46 (d, J = 1.8 Hz, 1H), 7.55 (d, J = 7.8 Hz, 2H), 7.60~7.65 (m, 3H), 8.11 (dd, J = 7.8 Hz and 1.8 Hz, 2H), 12.42 (s, 1H). HRMS-ESI: m/z $[M + H]^+$ calcd for $C_{23}H_{18}N_3O_2$: 368.1394; found 368.1395.

5-(4-(Benzyloxy)-1H-indol-2-yl)-3-(4-chlorophenyl)-1,2,4-oxadiazole (10o) Yield 82%; white powder; mp 205.3-207.1°C. 1H -NMR (600 MHz,

$DMSO-d_6$): δ = 5.28 (s, 2H), 6.71 (d, J = 7.8 Hz, 1H), 7.11 (d, J = 8.4 Hz, 1H), 7.24 (t, J = 7.8 Hz, 1H), 7.36 (t, J = 7.8 Hz, 1H), 7.43 (t, J = 7.8 Hz, 2H), 7.46 (d, J = 1.8 Hz, 1H), 7.55 (d, J = 8.4 Hz, 2H), 7.70 (d, J = 8.4 Hz, 2H), 8.11 (d, J = 8.4 Hz, 2H), 12.54 (s, 1H). HRMS-ESI: m/z $[M + H]^+$ calcd for $C_{23}H_{17}ClN_3O_2$: 402.1004; found 402.1001.

5-(6-Methyl-1H-indol-2-yl)-3-(trifluoromethyl)-1,2,4-oxadiazole (10p) Yield 85%; white acicular crystal; mp 158.5-160.4°C. 1H -NMR (600 MHz, $DMSO-d_6$): δ = 2.41 (s, 2H), 2.42 (s, 3H), 6.96 (dd, J = 8.4 Hz and 1.8 Hz, 1H), 7.26 (s, 1H), 7.30 (d, J = 1.8 Hz, 1H), 7.58 (d, J = 8.4 Hz, 1H), 12.23 (s, 1H). HRMS-ESI: m/z $[M + H]^+$ calcd for $C_{12}H_8F_3N_3O$: 267.2066; found 267.2071.

Time and dose-response effects of honokiol on UVB-induced skin cancer development

Ruth F. Guillermo¹, Chandeshwari Chilampalli¹, Xiaoying Zhang², David Zeman³, Hesham Fahmy¹, Chandradhar Dwivedi^{1,*}

¹ Department of Pharmaceutical Sciences, South Dakota State University, Brookings, SD, USA;

² ACEA Biosciences, Inc., Hangzhou, China;

³ Department of Veterinary and Biomedical Sciences, South Dakota State University, Brookings, SD, USA.

ABSTRACT: Honokiol has shown chemopreventive effects in chemically-induced and UVB-induced skin cancer in mice. In this investigation, we assessed the time-effects of a topical low dose of honokiol (30 µg), and then the effects of different honokiol doses (30, 45, and 60 µg) on a UVB-induced skin cancer model to find an optimal dose and time for desirable chemopreventive effects. UVB radiation (30 mJ/cm², 5 days/week for 25 or 27 weeks) was used to induce skin carcinogenesis in SKH-1 mice. For the time-response experiment 30 µg honokiol in acetone was applied topically to the animals before the UVB exposure (30 min, 1 h, and 2 h) and after the UVB exposure (immediately, 30 min, and 1 h). Control groups were treated with acetone. For the dose-response study, animals were treated topically with acetone or honokiol (30, 45, and 60 µg) one hour before the UVB exposure. In the time-response experiment, honokiol inhibited skin tumor multiplicity by 49-58% while reducing tumor volumes by 70-89%. In the dose-response study, honokiol (30, 45, and 60 µg) significantly decreased skin tumor multiplicity by 36-78% in a dose-dependent manner, while tumor area was reduced by 76-94%. Honokiol (60 µg) significantly reduced tumor incidence by 40% as compared to control group. Honokiol applied in very low doses (30 µg) either before or after UVB radiation shows chemopreventive effects. Honokiol (30, 45, and 60 µg) prevents UVB-induced skin cancer in a dose-dependent manner. Honokiol can be an effective chemopreventive agent against skin cancer.

Keywords: Honokiol, nonmelanoma skin cancer, UVB, SKH-1 mice, dose-response, time-response

*Address correspondence to:

Dr. Chandradhar Dwivedi, Department of Pharmaceutical Sciences, College of Pharmacy, South Dakota State University, PO Box 2202C, Brookings, SD 57007, USA. E-mail: Chandradhar.Dwivedi@sdstate.edu

1. Introduction

In recent years the number of skin cancer cases has increased dramatically, accounting for over 3.5 million cases each year in the United States alone. Some scholars propose that there is an unrecognized skin cancer epidemic in the United States (1). American Cancer Society estimates indicated 12,190 deaths from skin cancer in 2012 (2). Ultraviolet (UV) radiation exposure is the major risk factor for most skin cancers (3). Sunlight and tanning lamps are major sources of UV radiation.

UV radiation is composed by UVA, UVB, and UVC rays. UVA and UVB rays damage skin and can cause skin cancer, UVC rays are filtered by the atmosphere and do not reach the Earth's surface. Exposure to UVB rays can induce skin cancer faster than exposure to UVA rays. However, studies have proven that experimentally, UVA rays can cause skin cancer with long term exposure (4). The amount of UV exposure depends on the strength of the rays, the length of time the skin is exposed, and whether the skin is protected with clothing or sunscreen (5). UV rays cause DNA damage to skin cells (6), induction of signal transduction pathways that lead to cell proliferation, and induction of inflammatory responses and immunosuppression. All these effects caused by UV radiation are necessary for tumor development. UV radiation acts as a complete carcinogen on skin causing cancer initiation, promotion and progression (7).

Chemoprevention of skin cancer by natural compounds has gained importance in recent years (8,9). One phytochemical that is being extensively investigated against different models of cancer is honokiol (Figure 1), whose effects are investigated for the prevention of skin cancer in this study. Honokiol (HNK, C₁₈H₁₈O₂, MW 266.33) is a naturally occurring biphenol isolated from the bark and seed cones of *Magnolia officinalis* and other plants of the genus *Magnolia*. The stem bark of *Magnolia officinalis* is known as Houpo in traditional Chinese medicine, and it

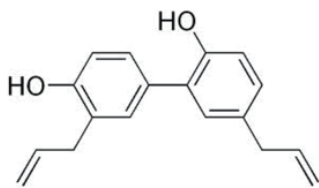


Figure 1. Molecular structure of honokiol.

has been used for relieving neurosis and gastrointestinal complaints (10).

Studies have demonstrated that honokiol has multiple pharmacological properties such as antioxidant (11), anti-inflammatory (12), and central nervous system depressant effects (10,13). It has been reported that honokiol delayed the formation of papillomas in mouse skin initiated by 7,12-dimethylbenz(a)anthracene (DMBA) and promoted by 12-*O*-tetradecanoyl phorbol-13-acetate (TPA) (14). Honokiol has also shown anticancer effects against melanoma (15), pancreatic cancer (16), breast cancer (17), head and neck squamous cell carcinoma (18), and squamous cell skin cancer (19).

Our laboratory and other groups have reported the chemopreventive effects of honokiol on UVB-induced skin cancer development in mice. Honokiol induced apoptosis by both extrinsic and intrinsic pathways, inhibited UVB-induced inflammation and inflammatory mediators, reduced cell survival signals and proliferation markers, up-regulated cell cycle inhibitor proteins, and down regulated cell cycle promoter proteins in skin tumors (20,21). Honokiol also proved to cause apoptosis and cell cycle arrest in A431 squamous carcinoma cell line by increasing the activation of pro-apoptotic proteins and the expression of cell cycle inhibitor proteins p21 and p27. Honokiol decreased the expression of cyclins and CDKs protein promoters of the cell cycle (19).

This study was designed to investigate: *i*) The chemopreventive effects of honokiol when applied topically at low dose (30 μ g) either before or after UVB exposure (time-response) and *ii*) The effects of honokiol on UVB-induced skin carcinogenesis when applied topically at different doses 30, 45, and 60 μ g (dose-response) to find the optimal dose and time for desirable effects.

2. Materials and Methods

2.1. Chemicals and reagents

Honokiol 98% (HPLC) was purchased from Nacalai tesque (Kyoto, Japan). All other reagents were purchased from Fisher Scientific (Pittsburgh, PA, USA).

2.2. Animals

Five to six-week-old female SKH-1 hairless mice were purchased from Charles River Laboratories (Wilmington, MA, USA). Institutional Animal Care and Use Committee (IACUC) approvals were obtained for all experimental protocols. The IACUC oversees animal programs, facilities, and procedures and provides assurance to federal agencies that South Dakota State University is in compliance with federal regulations on the humane care and use of animals in research. Mice were housed in a climate-controlled environment with a 12 h light/dark cycle and were provided with free access to food and water during the experiment.

2.3. UVB light source

Four FS-40-T-12 UVB lamps were used as UVB light source. The dose of UVB exposure was controlled by integrating dosimeters manufactured by Daavlin Corporation (Bryan, OH, USA).

2.4. UVB-induced skin tumor development protocol

Carcinogenesis was initiated and promoted by exposing the backs of six-week-old female SKH-1 mice to a UVB dose of (30 mJ/cm²), 5 days a week (Monday-Friday) for 25 to 27 weeks. The UVB exposure and treatments were performed in the morning throughout the whole experiment, in order to keep consistency. This UVB induced skin cancer protocol has been described in detail elsewhere (21,22), this UVB dose is relevant to the human UVB exposure causing cancer development (23). This skin cancer induction scheme was used for both experiments.

For the time response experiment, six groups of animals ($n = 20$) randomly selected were used for the honokiol treatment: 30 μ g in 200 μ L of acetone. The difference among the groups was the time at which they received the topical honokiol treatment: 30 min, 1 h, or 2 h before UVB exposure (30 mJ/cm²) and immediately, 30 min, or 1 h after UVB exposure. The control groups had 10 animals each, and received an application of 200 μ L acetone either 1 h before or 1 h after UVB exposure. The experiment was carried out for 27 weeks.

For the dose-response experiment, four groups of animals were used. Group 1 served as control and received 200 μ L of acetone, group 2, group 3, and group 4 received topical applications of 30, 45, and 60 μ g of honokiol in 200 μ L of acetone respectively. Treatments were administered one hour before UVB exposure (30 mJ/cm², Monday-Friday). The experiment was carried out for 25 weeks. Earlier reports and our previous studies have indicated that 200 μ L acetone (topical) does not have effects on skin cancer development (24,25).

2.5. Evaluation of tumor development

Over the course of the experiments, the tumors' incidence, multiplicity, and volume were recorded once weekly. Mice's weights and external signs of toxicity also were closely monitored. Vernier caliper was used to determine the length, width, and height of the tumors, these values were then used to determine tumor volume by using the formula: $\text{Volume} = 4\pi r^3/3$ where r is the radius, the diameter is the average of the three dimensional size of each mass (height, length, and width). Tumor areas were quantified as described elsewhere (25) by using images from the mice's backs which were taken at the end of 25 weeks. Tumor boundaries were determined and areas were measured by using Photoshop CS5 (Adobe systems, San Jose, CA, USA). Tumor counts, volume, and body weights were recorded on weekly basis for 25-27 weeks. Results were analyzed for tumor incidence, multiplicity, volume, and area.

2.6. Histopathological analysis of mice tumors

Mice were euthanized by cervical dislocation at the end of the above mentioned protocols. Skin samples randomly collected from five animals per group were fixed by immersion in 10% neutral buffered formalin for 24 h at room temperature. Fixed tissues were processed into paraffin-wax blocks, sectioned, stained with hematoxylin-eosin (HE), and evaluated under a light microscope.

2.7. Statistical analysis

INSTAT software (Graph Pad, San Diego, CA, USA) was used to analyze data. Chi square analysis was used for the data on tumor incidence. Analyses of variance followed by Tukey's test and Krushal-Wallis test (Nonparametric ANOVA) were used for tumor multiplicity and volume. Significance in all experiments was considered at $p < 0.05$. All values were expressed as mean \pm standard error (SE).

3. Results

3.1. Effects of honokiol on weight gain

Treatment of animals with honokiol at all doses and different times did not have any effects on weight gain of mice (data not shown) suggesting safety in the application of honokiol at these doses and times.

3.2. Effects of honokiol on tumor incidence

Tumor incidence reflects the number of animals bearing at least one tumor. In the time response

experiment, by the end of the 27th week, tumor incidence was 100% in the control group meaning that all control animals had at least one tumor. Tumor incidence ranged from 90-100% for all the honokiol (30 μg) pre-treated and post-treated groups. Tumor incidence was not significantly different between control and honokiol (30 μg) applied either before or after UVB exposure. The results for tumor incidence in the time response experiment are presented in Figure 2.

The effects of honokiol pretreatment at different doses on the tumor incidence in SKH-1 mice are shown in Figure 3. By the end of the 25th week, tumor

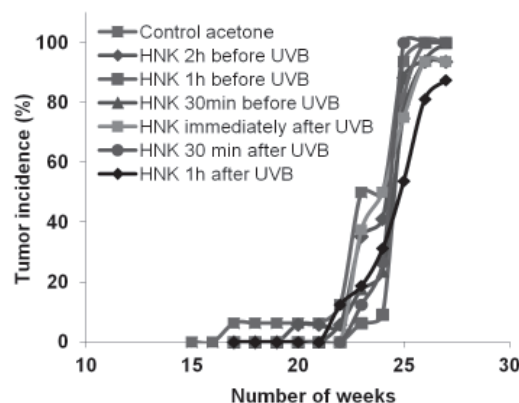


Figure 2. Effects of the topical application of honokiol (HNK) before and after UVB exposure on tumor incidence in SKH-1 hairless mice. Honokiol was applied topically on the mice's skin, either before (30 min-2 h) or after UVB exposure (immediately-1 h). The experiment was carried out for 27 weeks, and tumor counts were monitored weekly. Data represents the percentage of mice with at least one tumor ($n = 20$ per group). Honokiol did not reduce the tumor incidence when applied at 30 $\mu\text{g}/\text{dose}$ either before or after UVB exposure.

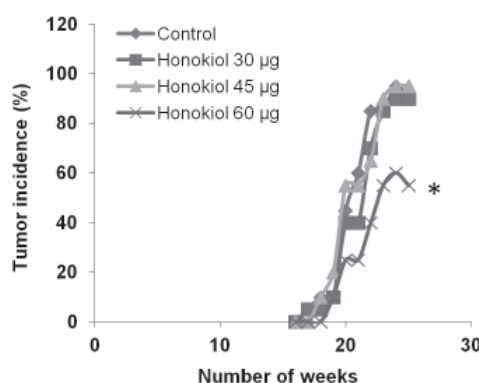


Figure 3. Dose-response effects of honokiol pretreatment on tumor incidence in UVB-induced skin carcinogenesis in SKH-1 hairless mice. From the 20th week to the end of the experiment honokiol 60 μg reduced significantly tumor incidence. At the end of the 25th week the honokiol 60 μg group had a tumor incidence 40% lower than the control group. The groups treated with honokiol 30 μg and 45 μg did not differ significantly from the control group. Each point represents the percentage of animals bearing at least one tumor, values derived from 20 mice per group. * Significant difference ($p < 0.05$).

incidence was 90% in both the control group and honokiol treated groups (30 and 45 μg). The honokiol (60 μg) pretreated group showed delayed appearance of tumors as compared to control, 60 μg application of honokiol resulted in a decrease in tumor incidence by 40% ($p < 0.05$) at the end of the experiment.

3.3. Effects of honokiol on tumor multiplicity

Results of the multiplicity of the time-response experiment are presented in Figure 4. Tumor multiplicity is the total number of tumors on back per mouse, for comparison purposes the number of tumors in the control group was considered as 100%. Topical application of 30 μg of honokiol before or after UVB treatments showed protection against skin tumor development in SKH-1 mice. At the end of the experiment (27th week), we found that Honokiol (30 μg) 30 min, 1 h, and 2 h before UVB treatments resulted in 57.5%, 54%, and 48% decrease in tumor multiplicity, respectively. Honokiol (30 μg) immediately, 30 min, and 1 h after UVB exposure resulted in 55%, 39%, and 48% reduction in tumor multiplicity, respectively. Tumor multiplicity was significantly ($p < 0.05$) lower in the honokiol pretreated groups (30 min and 1 h before UVB exposure) and in the post treated groups (immediately and 1 h after UVB exposure) when compared to the combined control group. Interestingly, honokiol applied 2 h before UVB exposure and 30 min after UVB exposure did reduce the tumor multiplicity but this difference was not statistically significant.

The effects of honokiol dose-response pretreatment on tumor multiplicity are shown in Figure 5. Topical application of 30, 45, and 60 μg of honokiol 1 h before UVB exposure showed protection against skin tumor

development in SKH-1 hairless mice. Average tumor numbers were found to be lower in the honokiol pretreated groups from the 20th week until the end of the experiment (25th week), when compared to the control group treated with acetone ($p < 0.05$). At the end of the experiment, honokiol pretreatment resulted in a 36-78% decrease in tumor multiplicity with 30, 45, and 60 μg of honokiol application, respectively.

3.4. Effects of honokiol on tumor volume

The effects of honokiol (30 μg) before and after UVB treatments on the tumor volume are shown in Figure 6. In the control group, the mean tumor volume per animal was 35.3 mm^3 , in the groups 30 min, 1 h, and 2 h before UVB exposure the average tumor volumes per animal were 3.77, 5.83, and 10.3 mm^3 , respectively. In the post UVB exposure treated groups, the average tumor volumes per animal were 7.69, 5.66, and 6.28 mm^3 for the honokiol (30 μg) immediately, 30 min, and 1 h after UVB exposure, respectively. The control group had a high standard deviation among the animals' tumor volumes. As a consequence, only one group (honokiol treatment 30 min before UVB exposure) had a statistically significant reduction in tumor volume. Results for the tumor volume for the time response experiment are presented in Figure 6.

3.5. Effects of honokiol on tumor area

The effects of honokiol pretreatment on the ratio of total tumor area to total back area are shown in Figure 7. The mean ratio of tumor area to total back area in the control group was 4.0%, in the honokiol pretreated groups (30, 45, and 60 μg) was 0.32%, 0.95%, and

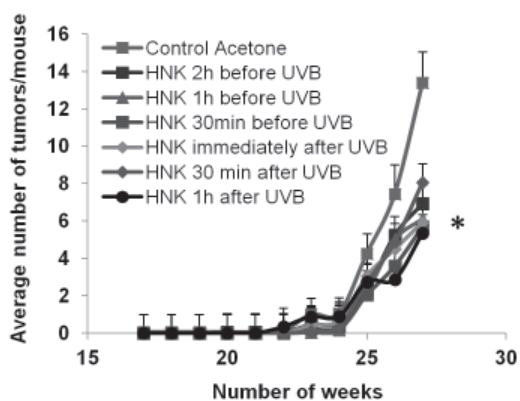


Figure 4. Effects of the topical application of honokiol (HNK) before and after UVB exposure on the tumor multiplicity in SKH-1 hairless mice. Skin carcinogenesis was performed as described in the methods section. Honokiol 30 μg was applied either before or after the UVB radiation. At the end of the experiment (27 weeks) the groups 30 min and 1 h before UVB as well as the groups immediately and 1 h after UVB showed a significant reduction in tumor multiplicity. Each point represents the average number of tumors per animal, $n = 20$, * $p < 0.05$.

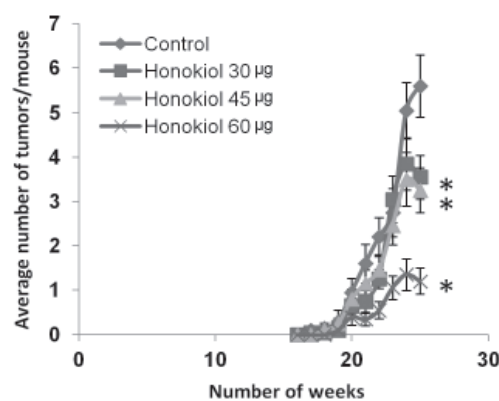


Figure 5. Dose-response effects of honokiol pretreatment on tumor multiplicity. Honokiol 30, 45, and 60 μg pretreatment decreased tumor multiplicities from the 20th to 25th week of UVB induced carcinogenesis. At the end of the experiment, honokiol significantly reduced the tumor multiplicity in 36-78% with 30, 45, and 60 μg applications, respectively. Each point represents mean number of tumors per mouse \pm SE derived from 20 mice. * Significant difference ($p < 0.05$).

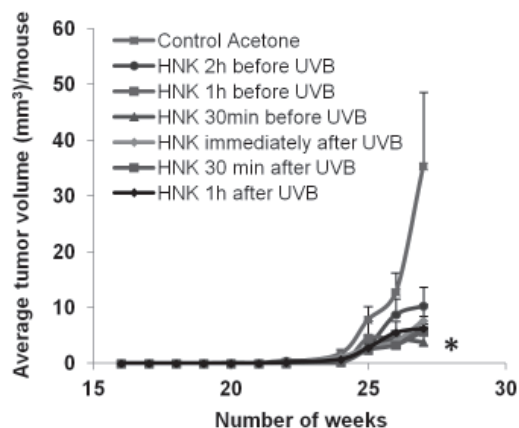


Figure 6. Effects of honokiol (HNK) on tumor volume in SKH-1 hairless mice. Skin carcinogenesis protocol was followed as described in the methods section. Tumors were measured weekly. It was observed an average reduction in tumor volumes in all honokiol treated groups pre and post UVB exposure. Each point represents the average tumor volume per animal, $n = 20$, * $p < 0.05$.

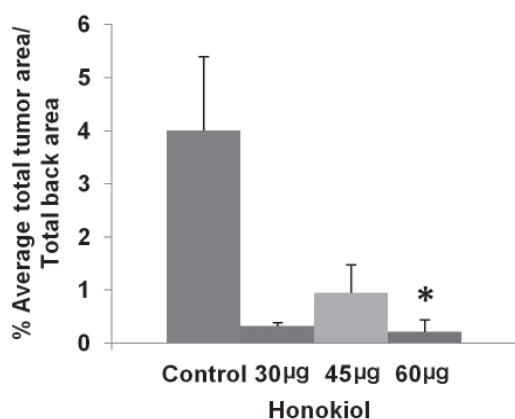


Figure 7. Dose-response effects of honokiol treatment on tumor area in SKH-1 mice. Graph bar represents the average ratio of total tumor area to total back area of the SKH-1 mice. Pictures of the backs of the animals were taken at the end of the 25th week. * Significant difference ($p < 0.05$).

0.22%, respectively. Honokiol pretreatments caused a 76-94.5% reduction in tumor area as compared to control. As in the section 3.4 (tumor volume), the control group had high standard deviation among animal's tumor areas, as consequence only one treatment (honokiol 60 μg) had a statistically significant reduction in tumor area.

3.6. UVB induced squamous cell carcinoma in controls and honokiol treated mice

The histopathological examination of the tumors after 25-27 weeks of treatments indicated that controls and honokiol treated mice in both protocols developed squamous cell carcinoma in the skin (Pictures not shown).

4. Discussion

Honokiol is a small-molecule, hydroxylated biphenolic compound isolated from *Magnolia* genus plants. It has been used in traditional Chinese medicine for thousands of years, and in recent years has been investigated for its effects on cancer and skin carcinogenesis. Previous findings from our laboratory indicated the chemopreventive effects of honokiol when applied topically in doses as low as 30 $\mu\text{g}/\text{dose}$ (21). In this study, we investigated the effects of honokiol in a UVB-induced skin carcinogenesis model with a UVB radiation dose of 30 $\text{mJ}/\text{cm}^2/\text{day}$ which is more translational and relevant to human skin cancer (23) as compared to previous studies that used honokiol as chemopreventive agent and higher doses of UVB radiation (180 mJ/cm^2) (20). We evaluated the effects of a low dose of honokiol (30 μg) applied topically either before or after the UVB exposure. Similar effects in tumor incidence were observed in all groups. Tumor multiplicity was decreased by the honokiol treatment, the average number of tumors per mouse in the control group was 13.38, while in the honokiol treated groups was 5.69, 6.13, and 6.94 for the honokiol pre-treated groups (30 min, 1 h, 2 h); and 5.94, 8.06, and 6.88 for the honokiol post-treated groups (immediately, 30 min, 1 h) respectively. Tumor volume was also decreased by the honokiol treatment, we observed a reduction in tumor volume of 89%, 83.5%, and 70.8% for the honokiol pre-treated groups (30 min, 1 h, 2 h); and 78%, 84%, and 82% for the honokiol post-treated groups (immediately, 30 min, 1 h) respectively. However, because of the high standard deviation in the tumor volumes in the control group, only the 30 min pre-treated group resulted in a statistically significant reduction in tumor volume. Previous studies showed chemopreventive effects when honokiol is applied topically within 30 min before or immediately after UVB exposure (20). In that study, they proved that topical honokiol (1 mg, 3 mg) either before or after UVB exposure (180 mJ/cm^2) prevented skin carcinogenesis. The novelty of our study is that we used very low doses of honokiol (30 μg) and low-chronic UVB exposure (30 mJ/cm^2). With this model we aim to show that honokiol at very low doses prevents skin carcinogenesis by mechanisms that are retained even after the UVB exposure, so it could be included in lotions applied prior to sun exposure (sunscreens) or in products used after sun exposure such as humectants, still retaining preventive effects. This model of low and chronic UVB exposure simulates human behavior of exposing skin to sunlight every day.

In the dose response experiment, we found that honokiol 60 μg markedly reduced the tumor incidence and multiplicity as compared to the control treated with acetone. The results demonstrated that honokiol 60 μg reduced tumor incidence by 40%. Honokiol 30, 45, and 60 μg in 200 μL of acetone showed a protective effect in a dose dependent manner when applied topically. Tumor

multiplicity was reduced by 36-78% while tumor area was reduced by 76-94.5% with treatments of 30, 45, and 60 µg of honokiol respectively as compared to the control.

We used very low doses (in micrograms) of honokiol compared to other chemopreventive agents which use milligrams per applications (8,26,27), thus indicating the higher potency and improved potential of honokiol over other agents. Previous mechanistic studies from our laboratory showed that topical application of honokiol (30 µg) on mice induced apoptosis through the intrinsic and extrinsic pathways, increasing the activation of caspase 8, caspase 9, caspase 3, and PARP. Honokiol 30 µg applied topically also increased the expression of p53 protein in mice skin (21). Additionally, we reported the effects of honokiol on A431 squamous carcinoma cell line. We used this *in vitro* model to gain insight and understanding of signaling mechanisms involved in the honokiol anti-carcinogenic effect. Honokiol overall inhibited cell growth in A431 cells at concentrations 50-75 µM starting at 12 h treatments. Honokiol induced G0/G1 cell cycle arrest and significant apoptosis in A431 cells, down regulated cyclins and cdks protein expressions and up-regulated the expression of cell cycle inhibitors p21 and p27 (19). These cell cycle modulator effects observed *in vitro* were confirmed *in vivo* by Vaid *et al.* (20). They used 1 mg and 3 mg of honokiol per application in SKH-1 mice. They found decreased expression of cyclin D1, D2, E, CDK2, CDK4, and CDK6, as well as increased expression of the cell cycle inhibitors p21 and p27 in the skin of honokiol treated animals. Furthermore, they found that the chemopreventive effects of honokiol at 1 mg and 3 mg involved modulation of PI3K/p-Akt pathway, decrease in inflammation and inflammatory mediators associated with tumorigenesis, and inhibition of UVB-induced cell survival signals in the tumors. Further mechanistic studies on the mice's skin are necessary to confirm if the same mechanisms of action found when honokiol was applied at 1 mg and 3 mg (100 times more) would be responsible for the low dose (30 µg) preventive effects observed in our study.

Our study provided evidence that honokiol pre or post UVB treatment at very low doses (micrograms per applications compared to most other agents which are used in milligrams per application) prevents UVB-induced skin cancer development in SKH-1 mice. Our studies also showed that honokiol exhibited potent chemopreventive effects at doses as low as 30-60 µg when applied topically; the preventive response was dose dependent, being the lowest with 30 µg and highest with 60 µg. Future studies on formulations to increase the retention of low doses of honokiol in skin are warranted, as well as their pharmacokinetic profile.

Honokiol has a great potential to be a safe and potent chemopreventive agent against skin cancer development in human.

Acknowledgements

This study was supported by the Department of Pharmaceutical Sciences Graduate Program and Translational Cancer Research Center funded by the State of South Dakota.

References

1. Rogers HW, Weinstock MA, Harris AR, Hinckley MR, Feldman SR, Fleischer AB, Coldiron BM. Incidence estimate of nonmelanoma skin cancer in the United States, 2006. *Arch Dermatol.* 2010; 146:283-287.
2. Siegel R, Naishadham D, Jemal A. Cancer statistics, 2012. *CA Cancer J Clin.* 2012; 62:10-29.
3. Preston DS, Stern RS. Nonmelanoma cancers of the skin. *N Engl J Med.* 1992; 327:1649-1662.
4. Strickland PT. Photocarcinogenesis by near-ultraviolet (UVA) radiation in Sencar mice. *J Invest Dermatol.* 1986; 87:272-275.
5. Wright CY, Reeder AI. Youth solar ultraviolet radiation exposure, concurrent activities and sun-protective practices: A review. *Photochem Photobiol.* 2005; 81:1331-1342.
6. Alcalay J, Freeman SE, Goldberg LH, Wolf JE. Excision repair of pyrimidine dimers induced by simulated solar radiation in the skin of patients with basal cell carcinoma. *J Invest Dermatol.* 1990; 95:506-509.
7. Matsumura Y, Ananthaswamy HN. Toxic effects of ultraviolet radiation on the skin. *Toxicol Appl Pharmacol.* 2004; 195:298-308.
8. Zhang X, Dwivedi C. Skin cancer chemoprevention by alpha-santalol. *Front Biosci (Schol Ed).* 2011; 3:777-787.
9. Nichols JA, Katiyar SK. Skin photoprotection by natural polyphenols: Anti-inflammatory, antioxidant and DNA repair mechanisms. *Arch Dermatol Res.* 2010; 302:71-83.
10. Watanabe K, Watanabe H, Goto Y, Yamaguchi M, Yamamoto N, Hagino K. Pharmacological properties of magnolol and honokiol extracted from *Magnolia officinalis*: Central depressant effects. *Planta Med.* 1983; 49:103-108.
11. Dikalov S, Losik T, Arbiser JL. Honokiol is a potent scavenger of superoxide and peroxy radicals. *Biochem Pharmacol.* 2008; 76:589-596.
12. Chao LK, Liao PC, Ho CL, Wang EI, Chuang CC, Chiu HW, Hung LB, Hua KF. Anti-inflammatory bioactivities of honokiol through inhibition of protein kinase C, mitogen-activated protein kinase, and the NF-kappaB pathway to reduce LPS-induced TNFalpha and NO expression. *J Agric Food Chem.* 2010; 58:3472-3478.
13. Kuribara H, Stavinoha WB, Maruyama Y. Behavioural pharmacological characteristics of honokiol, an anxiolytic agent present in extracts of *Magnolia* bark, evaluated by an elevated plus-maze test in mice. *J Pharm Pharmacol.* 1998; 50:819-826.
14. Konoshima T, Kozuka M, Tokuda H, Nishino H, Iwashima A, Haruna M, Ito K, Tanabe M. Studies on inhibitors of skin tumor promotion. IX. Neolignans from *Magnolia officinalis*. *J Nat Prod.* 1991; 54:816-822.
15. Mannal PW, Schneider J, Tangada A, McDonald D, McFadden DW. Honokiol produces anti-neoplastic effects on melanoma cells *in vitro*. *J Surg Oncol.* 2011; 104:260-264.

16. Arora S, Bhardwaj A, Srivastava SK, Singh S, McClellan S, Wang B, Singh AP. Honokiol arrests cell cycle, induces apoptosis, and potentiates the cytotoxic effect of gemcitabine in human pancreatic cancer cells. *PLoS One*. 2011; 6:e21573.
17. Liu H, Zang C, Emde A, Planas-Silva MD, Rosche M, Kuhl A, Schulz CO, Elstner E, Possinger K, Eucker J. Anti-tumor effect of honokiol alone and in combination with other anti-cancer agents in breast cancer. *Eur J Pharmacol*. 2008; 591:43-51.
18. Leeman-Neill RJ, Cai Q, Joyce SC, Thomas SM, Bhola NE, Neill DB, Arbiser JL, Grandis JR. Honokiol inhibits epidermal growth factor receptor signaling and enhances the antitumor effects of epidermal growth factor receptor inhibitors. *Clin Cancer Res*. 2010; 16:2571-2579.
19. Chilampalli C, Guillermo R, Kaushik RS, Young A, Chandrasekher G, Fahmy H, Dwivedi C. Honokiol, a chemopreventive agent against skin cancer, induces cell cycle arrest and apoptosis in human epidermoid A431 cells. *Exp Biol Med (Maywood)*. 2011; 236:1351-1359.
20. Vaid M, Sharma SD, Katiyar SK. Honokiol, a phytochemical from the *Magnolia* plant, inhibits photocarcinogenesis by targeting UVB-induced inflammatory mediators and cell cycle regulators: Development of topical formulation. *Carcinogenesis*. 2010; 31:2004-2011.
21. Chilampalli S, Zhang X, Fahmy H, Kaushik RS, Zeman D, Hildreth MB, Dwivedi C. Chemopreventive effects of honokiol on UVB-induced skin cancer development. *Anticancer Res*. 2010; 30:777-783.
22. Chilampalli C, Guillermo R, Zhang X, Kaushik RS, Young A, Zeman D, Hildreth MB, Fahmy H, Dwivedi C. Effects of magnolol on UVB-induced skin cancer development in mice and its possible mechanism of action. *BMC Cancer*. 2011; 11:456.
23. Lu YP, Lou YR, Xie JG, Peng QY, Liao J, Yang CS, Huang MT, Conney AH. Topical applications of caffeine or (-)-epigallocatechin gallate (EGCG) inhibits carcinogenesis and selectively increase apoptosis in UV B-induced skin tumors in mice. *Proc Natl Acad Sci U S A* 2002; 99:12455-12460.
24. Lowe NJ, Connor MJ, Breeding J, Chalet M. Inhibition of ultraviolet-B epidermal ornithine decarboxylase induction and skin carcinogenesis in hairless mice by topical indomethacin and triamcinolone acetonide. *Cancer Res*. 1982; 42:3941-3943.
25. Zhang X, Bommarreddy A, Chen W, Hildreth MB, Kaushik RS, Zeman D, Khalifa S, Fahmy H, Dwivedi C. Chemopreventive effects of sarcophine-diol on ultraviolet B-induced skin tumor development in SKH-1 hairless mice. *Mar Drugs*. 2009; 7:153-165.
26. Gu M, Singh RP, Dhanalakshmi S, Agarwal C, Agarwal R. Silibinin inhibits inflammatory and angiogenic attributes in photocarcinogenesis in SKH-1 hairless mice. *Cancer Res*. 2007; 67:3483-3491.
27. Katiyar SK, Korman NJ, Mukhtar H, Agarwal R. Protective effects of silymarin against photocarcinogenesis in a mouse skin model. *J Natl Cancer Inst*. 1997; 89:556-566.

(Received May 30, 2012; Revised June 13, 2012; Accepted June 14, 2012)

Ameliorating effect of DL- α -lipoic acid against cisplatin-induced nephrotoxicity and cardiotoxicity in experimental animals

Asmma Hussein¹, Amany A. E. Ahmed^{2,*}, Samia A. Shouman³, Sabry Sharawy³

¹ Department of Pharmacology and Toxicology, Faculty of Pharmacy, Omar Al-Mukhtar University, Al-Bayda, Libya;

² Department of Pharmacology and Toxicology, Faculty of Pharmacy, Helwan University, Cairo, Egypt;

³ Department of Cancer Biology, National Cancer Institute, Cairo University, Cairo, Egypt.

ABSTRACT: Cisplatin is a potent chemotherapeutic agent with a wide range of activities. Nephrotoxicity and cardiotoxicity represent its major complication upon clinical use. The present study was carried out to evaluate the possible protective effect of DL- α -lipoic acid (LA) against cisplatin-induced nephrotoxicity and cardiotoxicity. Different groups of rats ($n = 10$) were administered either saline (control), cisplatin (10 mg/kg, *i.p.*), LA (100 mg/kg, *i.p.*) or their combination (LA 30 min prior to cisplatin administration). Twenty-four hours later all animals were decapitated and sera were used for estimation of activities of urea (BUN), creatinine (Cr), lactate dehydrogenase (LDH), and creatine kinase (CK). Homogenates of the kidney and heart were used for estimation of oxidative stress markers (reduced glutathione (GSH), malondialdehyde (MDA), superoxide dismutase (SOD), and nitric oxide (NO)). Additionally, caspase-3 activities and DNA-fragmentation were investigated in renal tissues. The results showed that cisplatin produced significant elevation in serum activities of LDH, CK, BUN, and Cr and also induced significant elevation in the oxidative stress makers (MDA and NO) accompanied by significant reduction in GSH and SOD in both kidney and heart. The integrity of DNA was heavily damaged and caspase-3 was activated in renal tissues. The results emphasized nephrotoxicity and cardiotoxicity of cisplatin. On the other hand, prior administration of LA significantly attenuated the cisplatin-evoked disturbances in the above mentioned parameters and protected both kidney and heart tissues. The histopathological examination emphasized the obtained results. In conclusion, LA is suggested to be a potential candidate to ameliorate cisplatin-induced nephrotoxicity and cardiotoxicity without altering the antitumor efficacy of cisplatin.

Keywords: Cisplatin, DL- α -lipoic acid, oxidative stress, nephrotoxicity, cardiotoxicity

1. Introduction

Cisplatin is a potent chemotherapeutic agent that has wide range of activity against different tumors such as testicular, head and neck, ovarian, and non-small cell lung cancers as well as hematological malignancies (1). Despite its usefulness, major side effects such as nephrotoxicity, cardiotoxicity, neurotoxicity, emetogenesis, and ototoxicity have limited its use in clinical treatment (2). Several studies have documented the involvement of generation of reactive oxygen species, such as superoxide anion and hydroxyl radical in its mechanism of toxicity (1,3) with reduction of various antioxidants in patient plasma (4). Failure of the antioxidant defense mechanism against free radical-mediated organ damage after cisplatin administration was also recorded (5). All these mechanisms greatly encourage the using of free radical scavengers and antioxidants to counteract cisplatin-induced toxicities (6,7).

DL- α -Lipoic acid (LA), a dithiol compound, is found naturally in the mitochondria and acts as an essential cofactor for mitochondrial respiratory enzymes pyruvate dehydrogenase and α -ketoglutarate dehydrogenase. It displays antioxidant effects by scavenging reactive oxygen species and stimulates the synthesis of other antioxidants, such as glutathione (8). Several studies have shown that LA exerts multiple pharmacological actions in different models of diseases characterized by increase in oxidative stress markers (9-11). Additionally, the cardioprotective effects of LA against adriamycin and cyclophosphamide induced-toxicities are well documented (12,13). Moreover, LA exerts anti-inflammatory actions by inhibiting nuclear factor- κ B (NF- κ B) activation and by decreasing adhesion molecule expression in endothelial cells (14). Accordingly, in the present investigation, LA was suggested to be a good candidate for protection against cardiotoxicity and nephrotoxicity induced by cisplatin.

*Address correspondence to:

Dr. Amany A. E. Ahmed, Department of Pharmacology and Toxicology, Faculty of Pharmacy, Helwan University, Ain Helwan, P.O. Box, 11795, Cairo, Egypt.
E-mail: amresearch2009@yahoo.com

The aim of the present study was to evaluate the possible efficacy of LA as a protective agent against cisplatin-induced nephrotoxicity and cardiotoxicity in rats and to investigate whether this protection may affect the antitumor activity of cisplatin.

2. Materials and Methods

2.1. Chemicals and drugs

Cisplatin vials (Bristol Myers Squibb Co., USA) were used. DL- α -lipoic acid was purchased from Sigma-Aldrich Chemie, Germany. All other chemicals and reagents used were of the highest purity grade available and were purchased from Sigma-Aldrich Chemie, Germany.

2.2. Animals

Adult male Wistar albino rats weighing 180-200 g purchased from the Egyptian Organization for Biological Products and Vaccines (VACSERA, Giza, Egypt) and Female Swiss albino mice weighing 22-25 g obtained from animal house facility, Pharmacology Unit, National Cancer Institute (NCI), Cairo University, Egypt, were used in this study. Animals were kept under standardized conditions (temperature $22 \pm 1^\circ\text{C}$, relative humidity $55 \pm 15\%$ with a 12-h light and dark cycle and were allowed food and tap water *ad libitum*). The animal's treatment protocol has been approved by the animal care committee of the National Cancer Institute, Cairo University, Egypt. The protocol is in accordance with the international guidelines of handling the experimental animals.

2.3. Experimental design

The doses of cisplatin and LA were chosen according to a pilot study and were matched with that in the literature (15). The current study includes two parts: *i*) estimation of the effect of LA on the cisplatin producing reduction in tumor volume in mice bearing solid Ehrlich carcinoma (SEC); *ii*) evaluation of the protective effect of LA against cisplatin-induced toxicities in kidney and heart of rats.

In the first part, solid tumor was transplanted subcutaneously in the right thigh of the lower limb of each mouse. Mice with a palpable tumor mass (100 mm^3) that developed within 7 days after implantation were divided into 4 groups ($n = 10$) and followed the same treatment in previous experimental design. The change in tumor volume was measured three times weekly using a vernier caliper and calculated by the following formulas previously described (16).

Tumor volume (mm^3) = $[4\pi (A/2)^2 \times (B/2)]/3 = 0.52 \times A^2 \times B$, where A and B denoted the minor and major tumor axis, respectively.

In the second part, rats were divided into four groups ($n = 10$). In one group, rats were injected with 0.2 mL saline

solution and served as control group. In the second group rats were injected with single dose of cisplatin (10 mg/kg, *i.p.*). In the third group, rats were administered LA (100 mg/kg, *i.p.*). In the fourth group, rats were administered LA (100 mg/kg, *i.p.*) followed by cisplatin (10 mg/kg, *i.p.*) 30 min later. Twenty-four hours after the last dose of the specific treatment, all animals were sacrificed by decapitation under light ether anesthesia. Blood samples were collected from heart puncture and serum samples were separated for measurement of renal function tests and serum cardiac enzymes. The kidney and heart were excised, immediately washed in ice-cold isotonic saline, blotted between two filter papers and used for preparing homogenates (20%, w/v) with normal saline, and were kept at -20°C till estimation of oxidative stress markers. Parts of the kidney homogenate were used for evaluation of DNA fragmentation and caspase-3 activation. Samples of the intact tissue of heart and kidney were washed with saline and fixed in 10% neutral buffered formalin solution for histopathological examination.

2.4. Determination of biochemical parameters

2.4.1. Cardiac biomarkers

Serum cardiac enzymes lactate dehydrogenase (LDH) and creatine kinase (CK) were determined using standard commercial kits (Spectrum diagnostics, Cairo, Egypt) according to the methods previously described by Bais and Philcox (17), and Wu and Bowers (18), respectively. The values were expressed as U/L and were presented as percent of control values.

2.4.2. Renal biomarkers

Serum levels of urea (BUN) and creatinine (Cr) were determined using standard commercial kits (Spectrum diagnostics, Cairo, Egypt) and according to the methods described by Tabacco *et al.* (19), and Bowers and Wong (20), respectively. The values were expressed as mg/dL and were presented as percent of control values.

2.5. Determination of oxidative stress markers

2.5.1. Estimation of tissue lipid peroxidation contents

MDA is formed from the breakdown of polyunsaturated fatty acids, and serves as a convenient index for determining the extent of the peroxidation reaction. MDA was measured according to the method of Buege and Aust (21). The results were expressed as nmol/g tissue.

2.5.2. Measurement of tissue glutathione (GSH) contents

Reduced GSH was measured spectrophotometrically at 412 nm according to the method of Ellman (22). The amount of GSH was expressed as $\mu\text{mol/g}$ tissue.

2.5.3. Determination of tissue superoxide dismutase (SOD) activity

SOD activity was determined spectrophotometrically at 540 nm following the inhibition of pyrogallol autooxidation as described previously by Minami and Yoshikawa (23). The rate of inhibition of pyrogallol autooxidation is directly proportional to the activity of SOD in the tissues. The values of SOD were expressed as $\mu\text{mol}/\text{mg}$ tissue.

2.5.4. Assessment of tissue total nitrate/nitrite (NO) concentration

Total NO was measured chemically according to the method of Miranda *et al.* (24). The levels of NO were expressed as $\mu\text{mol}/\text{g}$ tissue in homogenate.

2.6. Evaluation of DNA fragmentation in the kidney tissues

DNA fragmentation in the kidney was evaluated according to the method described by Katoh *et al.* (25) using agarose gel electrophoresis. The kidney tissues were homogenized and lysed in a cold lysis buffer (10 mM Tris-HCl, 5 mM disodium EDTA, and 0.5% Triton X-100, pH 8.0) for 10 min at 4°C. The DNA was sequentially extracted twice using half volumes of phenol/chloroform and incubated at 55°C for 10 min. After centrifugation at 3,000 rpm for 20 min, the upper layer was incubated with proteinase at 37°C for 60 min followed by incubation with ribonuclease at 37°C for 60 min. The DNA was precipitated by adding 10 M ammonium acetate and 100% ethanol and maintained at -20°C overnight. DNA was collected by centrifugation at $15,000 \times g$ for 20 min, air-dried, and resuspended in TE buffer (10 mM Tris-HCl, 5 mM EDTA, pH 7.4). The resulting DNA preparations were electrophoresed through a 1.4% agarose gel containing ethidium bromide using TBE buffer (Tris-boric acid-EDTA buffer, pH 8.3) at 40 V for 5 h. Equal quantities of DNA (based on optical density measurements at 260 nm) were loaded in each lane, and a molecular DNA marker was used as a molecular mass standard (26). DNA fragmentation was visualized and photographed under ultraviolet illumination for testing the degree of fragmentation.

2.7. Evaluation of caspase-3 activities in the kidney tissues

The kidney tissues were homogenized followed by centrifugation at 11,000 rpm, 4°C for 15 min. Protein content in the resulting supernatant was determined using Bradford reagent (Thermo scientific, USA). Equal volume of supernatant was mixed with $1 \times$ loading buffer and 5 μL of β -mercaptoethanol and boiled for 5 min. Proteins were separated by SDS-polyacrylamide gel electrophoresis and then electrotransferred onto PVDF membrane using semidry transfer apparatus. The membrane was blocked according to manufacture instruction of chromogenic

western max detection kit (Ameresco, USA). After blocking with dilution buffer DBT (DB plus 1% Tween-20) plus 1% bovine serum albumin (BSA), the membrane blots was incubated within dicated primary antibody at 4°C over night then washed, and incubated with horseradish peroxidase-conjugated secondary antibody for 4 h at room temperature. After washing, the protein bands were visualized by 3,3-diaminobenzidine (DAB) chromogen which gives brown precipitate at the reaction site, specific protein bands on these transferred membranes were detected using antibodies (purified anti- β -actin antibody obtained from (Biolegend, USA) and anti-mouse caspase 3 monoclonal antibody obtained from (Bioscience, USA)). Relative expression of proteins was evaluated by normalizing the expression of proteins with quantitative housekeeping protein β -actin (27).

2.8. Histopathological examination

Heart and kidney samples were kept in 10% neutral buffered formalin and were dehydrated through alcohols, cleared in xylene and then embedded in paraffin wax. Sections (5 mm thick) were stained with haematoxylin and eosin. The magnification power of 400 was used to elucidate the histopathological changes using light microscopy.

2.9. Statistical analysis

The results were expressed as (mean \pm SEM). The comparison between means of the groups ($n = 10$) were carried out using one way analysis of variance (ANOVA) followed by the Tukey multiple comparison test. p value of 0.05 or less was taken as a criterion for a statistically significant difference.

3. Results

3.1. Effect of cisplatin, DL- α -lipoic acid and their combination on tumor volume

As shown in Table 1, administration of a single dose of cisplatin resulted in a significant decrease in the tumor volume ($95.57 \pm 16.44 \text{ mm}^3$) as compared to the control group. Treatment with LA (100 mg/kg) alone

Table 1. Effect of administration of cisplatin (10 mg/kg, *i.p.*), DL- α -lipoic acid (100 mg/kg, *i.p.*) and their combination on the tumor volume of solid Ehrlich carcinoma in mice

Groups	Tumor volume (mm^3)
Control	273.00 ± 104.05
Cisplatin	95.57 ± 16.44^a
DL- α -lipoic acid	268.65 ± 103.34^b
DL- α -lipoic acid + cisplatin	98.25 ± 14.39^a

Values are expressed as means \pm SEM ($n = 10$ rats). One-way ANOVA followed by Tukey's test was used for comparing the results. ^a $p < 0.05$ vs. control, ^b $p < 0.05$ vs. cisplatin.

did not produce any significant change in the tumor volume ($268.65 \pm 103.34 \text{ mm}^3$) as compared to control. Administration of LA (100 mg/kg) 30 min prior to cisplatin produced a significant decrease in the tumor volume ($98.25 \pm 14.39 \text{ mm}^3$) as compared to control. However this effect was not significant from cisplatin group.

3.2. Biomarkers of cardiotoxicity

Results of the current study revealed that administration of cisplatin (10 mg/kg) resulted in a significant increase in serum LDH and CK levels to 33% and 140% compared to the control group, respectively. This indicates the marked heart injury. In contrast, co-administration of LA with cisplatin induced a significant reduction in serum LDH and CK compared to cisplatin group (Figures 1A and 1B).

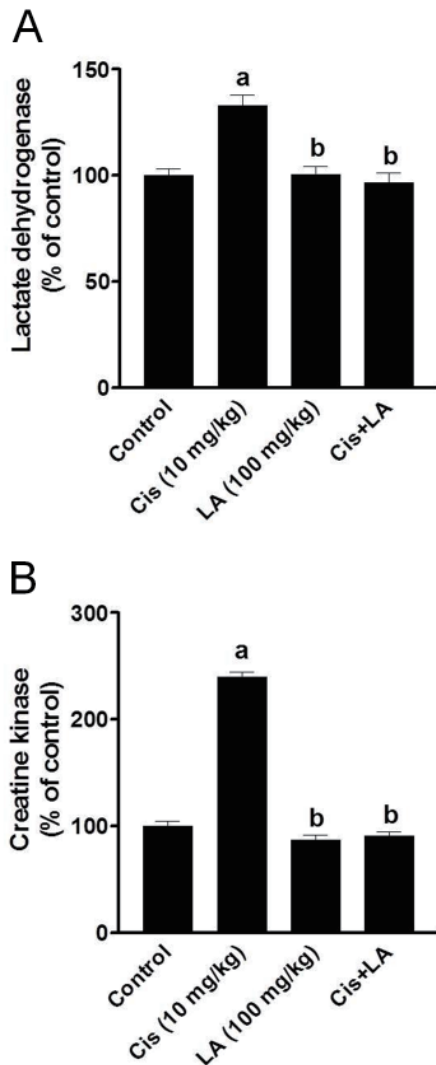


Figure 1. Effect of cisplatin (Cis), DL- α -lipoic acid (LA), and their combination (LA + Cis) on serum lactate dehydrogenase activity (A) and creatine kinase activity (B) in rats. Values represent the mean \pm SEM of ($n = 10$ rats). One-way ANOVA followed by Tukey's multiple comparison test. ^a $p < 0.05$ vs. control, ^b $p < 0.05$ vs. cisplatin.

3.3. Biomarkers of nephrotoxicity

As shown in Figures 2A and 2B, treatment with a single dose of cisplatin (10 mg/kg) resulted in a significant increase in BUN (155%) and the Cr (219%) compared to the control. Administration of LA (100 mg/kg) resulted in a non significant change in BUN or Cr levels, compared to the control group. Meanwhile, co-administration of LA (100 mg/kg) 30 min before cisplatin (10 mg/kg) resulted in a complete reversal of cisplatin-induced increase in BUN or Cr levels compared to the cisplatin values.

3.4. Biochemical markers of oxidative stress

3.4.1. Effect on lipid peroxidation level

Results in Tables 2 and 3 showed that, cisplatin administration to rats significantly increased the MDA

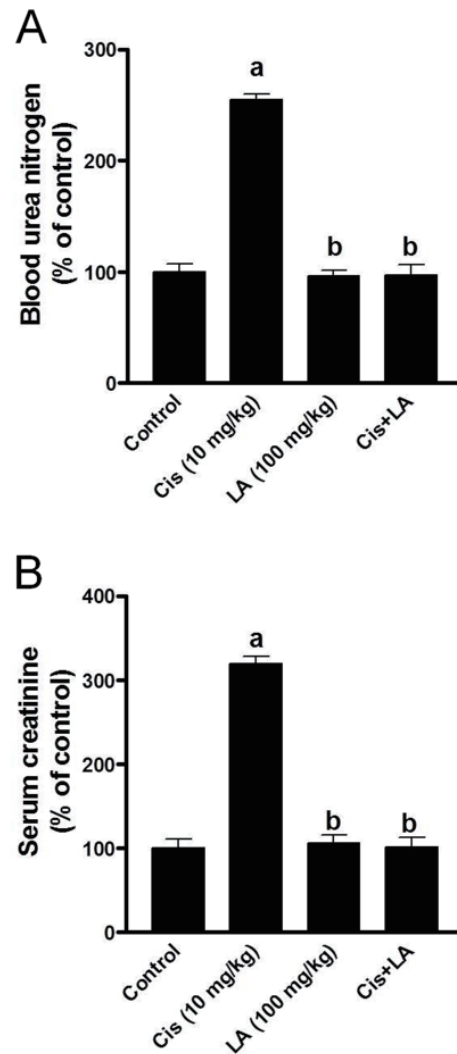


Figure 2. Effect of cisplatin (Cis), DL- α -lipoic acid (LA), and their combination (LA + Cis) on serum urea (A) and creatinine (B) level in rats. Values represent the mean \pm SEM of ($n = 10$ rats). One-way ANOVA followed by Tukey's multiple comparison test. ^a $p < 0.05$ vs. control, ^b $p < 0.05$ vs. cisplatin.

Table 2. Effect of administration of cisplatin (10 mg/kg, i.p.), DL- α -lipoic acid (100 mg/kg, i.p.) and their combination on MDA, GSH, NO, and SOD activities in the heart tissues of rats

Groups	MDA (nmol/g)	GSH (μ mol/g)	NO (μ mol/g)	SOD (μ mol/mg)
Control	1,213.66 \pm 18.72	0.59 \pm 0.031	38.81 \pm 1.55	83.09 \pm 1.64
Cisplatin	1,962.66 \pm 10.78 ^a	0.32 \pm 0.048 ^a	62.99 \pm 1.58 ^a	45.62 \pm 2.17 ^a
DL- α -lipoic	351.13 \pm 3.16 ^{ab}	0.75 \pm 0.039 ^{ab}	22.96 \pm 1.28 ^{ab}	89.88 \pm 2.02 ^b
DL- α -lipoic acid + cisplatin	854.72 \pm 8.09 ^{ab}	0.64 \pm 0.043 ^{ab}	22.22 \pm 0.82 ^{ab}	79.94 \pm 2.05 ^b

Values are expressed as means \pm SEM ($n = 10$ rats). One-way ANOVA followed by Tukey's test was used for comparing the results. ^a $p < 0.05$ vs. control, ^b $p < 0.05$ vs. cisplatin.

Table 3. Effect of administration of cisplatin (10 mg/kg, i.p.), DL- α -lipoic acid (100 mg/kg, i.p.) and their combination on MDA, GSH, NO, and SOD activities in the kidney tissues of rats

Groups	MDA (nmol/g)	GSH (μ mol/g)	NO (μ mol/g)	SOD (μ mol/mg)
Control	164.97 \pm 1.97	0.80 \pm 0.01	26.32 \pm 1.13	75.77 \pm 2.55
Cisplatin	313.42 \pm 3.96 ^a	0.31 \pm 0.015 ^a	38.47 \pm 1.88 ^a	58.15 \pm 1.42 ^a
DL- α -lipoic	145.35 \pm 2.11 ^{ab}	1.49 \pm 0.047 ^{ab}	15.23 \pm 1.16 ^{ab}	78.92 \pm 1.36 ^b
DL- α -lipoic acid + cisplatin	108.69 \pm 2.64 ^{ab}	1.19 \pm 0.049 ^{ab}	15.25 \pm 1.18 ^{ab}	71.11 \pm 2.36 ^b

Values are expressed as means \pm SEM ($n = 10$ rats). One-way ANOVA followed by Tukey's test was used for comparing the results. ^a $p < 0.05$ vs. control, ^b $p < 0.05$ vs. cisplatin.

levels in both heart and kidney tissues, by 62% and 90%, respectively, compared to the control group. Administration of LA with cisplatin diminished the cisplatin-induced increase in MDA levels in both tissues. Moreover, LA normalized the MDA in these tissues.

3.4.2. Effect on reduced GSH content

LA produced a significant elevation in the levels of reduced GSH in the heart and kidney tissues. On the other hand, cisplatin administration, significantly decreased the GSH levels in the heart and kidney tissues by 46% and 61%, respectively, compared to the control (Tables 2 and 3). Administration of LA (100 mg/kg) 30 min prior to cisplatin (10 mg/kg) treatment resulted in significant increase in the content of reduced glutathione in the heart and kidney tissues by 100% and 284% respectively, as compared to cisplatin-treated group.

3.4.3. Effect on SOD activity

The current study showed that, treatment with LA slightly elevated the SOD activity. In contrast, SOD activity was significantly attenuated in cisplatin-treated rats (45% in heart and 23% in kidney tissues compared to control). However, a marked increase in SOD activity was observed upon administration of LA with cisplatin (75% in heart and 22% in kidney tissues compared to cisplatin group). Interestingly LA could elevate activity of SOD compared with cisplatin group (Tables 2 and 3).

3.4.4. Effect on nitric oxide contents

Results of the present investigation showed that LA produced a significant decrease in levels of nitric oxide in the heart and kidney tissues. On the other hand,

cisplatin administration significantly increased the level of nitric oxide in heart and kidney tissues, by 62% and 46%, respectively, compared to the control (Tables 2 and 3). Administration of LA (100 mg/kg) 30 min before cisplatin (10 mg/kg) resulted in a significant decrease in heart tissues content of nitric oxide (43%) as compared to the control, and a significant decrease (65%) as compared to cisplatin group. Co-administration of LA (100 mg/kg) with cisplatin (10 mg/kg) resulted in a significant decrease in kidney tissues content of nitric oxide (42%) as compared to the control, and a significant decrease (60%) as compared to cisplatin group.

3.5. Evaluation of DNA fragmentation in the kidney tissue

As illustrated in Figure 3, no appreciable fragmentation of DNA was observed in the kidney tissues of control rats, LA, and the combination group. Whereas, cisplatin exposure resulted in a marked damage of DNA in the kidney tissues.

3.6. Evaluation of caspase-3 activities in the kidney tissue

The results in Figure 4 revealed that, administration of cisplatin induced a significant increase in cleaved caspase-3 in the kidney tissues. Treatment with LA 30 min before cisplatin administration showed a significant decrease in cleaved caspase-3 in the kidney compared with the cisplatin-treated group.

3.7. Histopathological examination

Figures 5A and 5B indicated that, LA prevented cisplatin-induced kidney and heart damage. Where

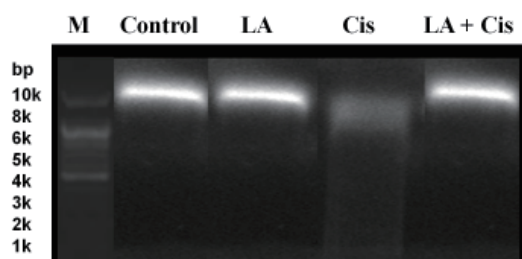


Figure 3. Effect of cisplatin (10 mg/kg), DL- α -lipoic acid (100 mg/kg) and their combination on DNA extracted from the kidney tissues of rats. Agarose gel electrophoresis of DNA fragments in rat kidney. Lane M: 10 kbp DNA ladder; lane Control: intact DNA of normal control; lane LA, lane Cis, and lane LA + Cis: DNA samples isolated from rats treated with DL- α -lipoic acid (LA), cisplatin (Cis), and their combination (LA + Cis), respectively. Cisplatin exposure resulted in a marked damage of DNA in the kidney tissues. No appreciable fragmentation of DNA was observed in the kidney tissues of control rats, LA, and the combination group.

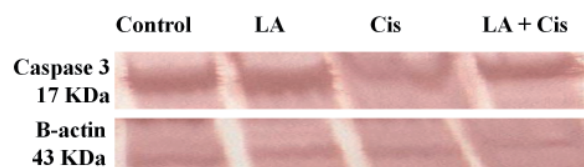


Figure 4. Effect of cisplatin (10 mg/kg) (Cis), DL- α -lipoic acid (100 mg/kg) (LA), and their combination (LA + Cis) on caspase-3 expression in renal tissues of rats using western blot analysis. The combination group showed a significant decrease in cleaved caspase-3 in the kidney compared with the cisplatin-treated group.

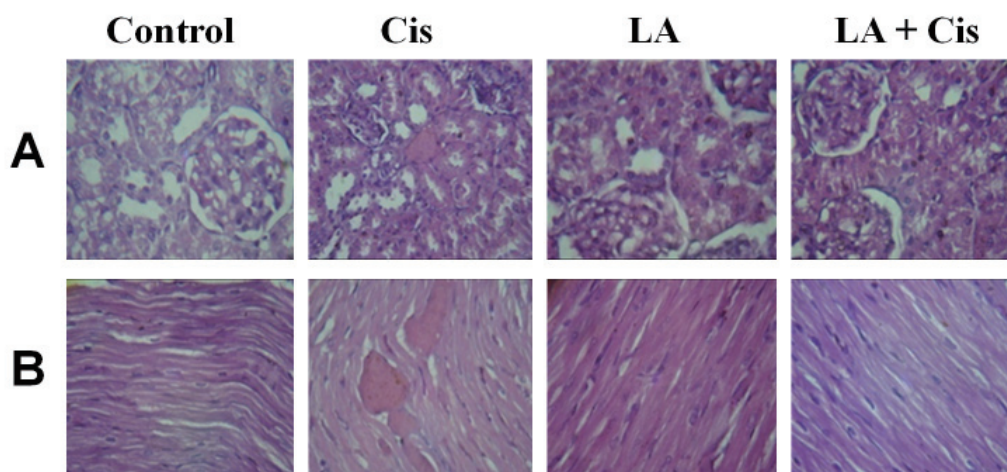


Figure 5. Effect of cisplatin (10 mg/kg), DL- α -lipoic acid (100 mg/kg), and their combination on kidney (A) and cardiac (B) tissues of rats. (A): Histopathologic sections from control and DL- α -lipoic acid (LA) alone or with cisplatin (Cis + LA) showed near normal glomeruli and tubules. Whereas, sections from cisplatin group (Cis) showed extensive renal tubular injury such as tubular cell necrosis, cast formation, loss of brush border, dilatation of tubules, and inflammatory cell infiltration. (H&E, $\times 400$). (B): Histologic sections from control or DL- α -lipoic acid (LA) alone showed near normal appearance of the cardiac muscle fibers. Whereas, sections from cisplatin group (Cis) showed extensive degenerated and fragmented in some cardiac muscle fibers and separated cardiac muscles with interruption of myofibrils and sever interstitial hemorrhages. These changes were less pronounced in rat treated with combined therapy (LA + Cis). (H&E, $\times 400$).

24 h after cisplatin treatment, extensive renal tubular injury were observed, which included tubular cell necrosis, extensive degeneration, and sever damage in some proximal and distal tubules with loss of normal architecture of cells. Moreover, interstitial hemorrhage between the kidney tubules was also observed (Figure 5A). The heart section of cisplatin treatment showed separated cardiac muscles with interruption of myofibrils and severs interstitial hemorrhages (Figure 5B). Cisplatin administration significantly increased kidney and heart injury compared with the control group. Treatment with LA significantly reduced the cisplatin-induced kidney and heart damage. Treatment with LA alone caused no significant morphologic alterations in both tissues.

4. Discussion

In the current study, administration of cisplatin produced a significant decrease in the tumor volume as compared to control group indicating its powerful chemotherapeutic activity. LA alone showed no effect on tumor volume indicating that it has no antitumor activity. Additionally, co-administration of LA with cisplatin produced a non-significant change in the antitumor activity of the latter, indicating no change in the efficacy of cisplatin upon combination with LA.

In the present study, cisplatin significantly increased cardiac enzymes (CK, LDH) activities. A significant increase was also observed in kidney

function tests (BUN, Cr) compared with control group. Previous studies reported similar elevation in CK and LDH after cisplatin administration (15,28,29). The elevation in activities of these enzymes in serum is diagnostic marker for cardiac injury. Cisplatin has the ability to generate reactive oxygen species, such as superoxide anion and hydroxyl radical (5), that results in irreversible modification of myocardial membrane structures, functions and integrity with the consequent leakage of cardiac enzymes (13,15).

Nephrotoxicity is one of the most common side effects of cisplatin encountered in cancer patients. More than 25% of patients developed acute renal failure after receiving an initial dose of cisplatin due to its preferential accumulation within the proximal tubular epithelial cells (30-32). Nephrotoxicity was manifested by significant increase in urea and creatinine resulted from reduction of glomerular filtration rate (30-33). Several factors including inflammation, genotoxic damage, and cell cycle arrest have been incriminated in the pathogenesis of cisplatin nephrotoxicity (34,35).

The marked oxidative stress, as evidenced by increased lipid peroxidation and decreased antioxidant capacity in heart and kidney tissues, observed in the current study after cisplatin treatment is in accordance with previous reports (15,34,35). This decline in antioxidants further aggravates the levels of free radicals in heart and kidney and prevents organ protection against cisplatin toxicity (3,15,36,37). In one study, the low cardiac glutathione level was a risk factor for developing cyclophosphamide-induced congestive heart failure (38). The heart and kidney have a variety of endogenous enzymatic and non-enzymatic antioxidants that act in coordination to provide cellular defense against reactive oxygen species.

In the present work, nitric oxide levels in the heart and kidney were significantly elevated following cisplatin administration. Overproduction of nitric oxide was directly linked to heart damage in other models of chemotherapeutic agents-induced cardiotoxicity, as in cyclophosphamide (13), and doxorubicin (39). Negative inotropic effects with deterioration of myocardial performance and the induction of myocardial damage (40) were attributed to overproduction of NO. In addition, it has been demonstrated that NO may enhance cellular injury by decreasing intracellular GSH levels (41). Nitric oxide promotes oxidative stress-induced cell injury by formation of peroxynitrite anion, a potent prooxidant and cytotoxic intermediate, that causes protein nitration and tissue injury (42,43).

Another possible explanation may be attributed to the fact that cisplatin induces a cascade of inflammatory reactions, which play an important pathogenic role in cisplatin-induced tissues injury (2).

The activation in caspase-3 accompanied with DNA fragmentation in kidney tissues of cisplatin treated rats observed in the present study can be explained on the bases that, the reactive oxygen species generated by cisplatin may trigger the opening of the mitochondrial permeability transition pores and permits the release of cytochrome *c* from mitochondria to cytosol and hence activates the mitochondria dependent pathway leading to apoptosis (44). Caspase activation is thought to be important in the genesis of apoptosis, in particular, caspase-3, the execution caspase, which is instrumental in the apoptotic process, and it cleaves and activates poly (ADP-ribose) polymerase and the inhibitor of caspase activator domain protein, leading to DNA fragmentation (45,46).

In the present study, administration of LA alone, increased the level of GSH, compared to the control group, a finding which is in agreement with that of Melhem *et al.* (47). This may be explained on the bases that LA and their reduced form (dihydropolipoic acid) may act as extra- and intracellular redox couples and powerful lipophilic free radical scavenger (48). It is well documented that, LA is a powerful free radicals scavenger and capable of increasing concentration of GSH in tissues (49). Additionally, LA is involved in recycling of antioxidant vitamins C and E and in modulating the activities of SOD (50). There is mounting evidence that LA increases or maintains cellular GSH levels by acting as a transcriptional inducer of genes governing GSH synthesis (51).

In the present study the beneficial effects of LA were manifested by significant decrease in serum levels of cardiac enzymes (LDH and CK) and in kidney biomarker enzymes (BUN and Cr). Additionally, MDA levels in heart and kidney tissues were significantly diminished and the antioxidants GSH level and SOD activity were restored. Similar decrease in cardiac enzymes activities by LA in rats treated with doxorubicin (52) as well as in rats treated with cisplatin (15) was previously reported. Moreover, LA was effective in normalizing the antioxidant levels, as well as levels of creatinine and blood urea nitrogen in acetaminophen-induced renal damage in rats (36). In another study, LA attenuated the elevation in creatinine and blood urea nitrogen induced by cisplatin in mice (2). Additionally, comparable effects of LA on the antioxidant defense system and prevention of the increase in lipid peroxidation were previously reported in renal tissues (53) and in cochlear tissues (54) of rats treated with cisplatin. LA has strong ability to chelate metals and to scavenge free radicals such as hydroxyl radical (15,55). In addition, LA is easily absorbed and transported across cell membranes, thus, free radical protection occurs both inside and outside of cells (56). LA not only exerts potent antioxidant activities but also has anti-inflammatory effects against different inflammatory conditions (2,11,57).

There is an ample of evidence indicating that inhibition of nitric oxide overproduction by LA can protect against the heart and kidney injury induced by other chemicals or drugs (39,41). The ability of LA to modify nitric oxide production by preventing the up-regulation of nitric oxide synthase was previously documented, where LA inhibits lipopolysaccharide-induced NO production in isolated rat Kupffer's cells and in murine macrophages (58). Furthermore, pre-treatment with LA may protect against cisplatin-induced kidney and heart injury through prevention of NO overproduction (36,59). Another possible explanation is the direct scavenging effect of NO by the sulphhydryl group of LA (60).

In the current investigation, the significant decrease in cleaved caspase-3 and DNA fragmentation induced by cisplatin observed after LA treatment can be explained by the protective and the anti-apoptotic properties of LA. This protective effect may be attributed to its antioxidant action exerted against the pro-oxidant effects of cisplatin. LA is a hydroxyl radical scavenging agent. It prevents hydroxylation of deoxyguanosine and thus the associated DNA damage (61). Furthermore, LA inhibited the site-specific degradation of deoxyribose by prooxidants due to its iron chelating ability (62).

In histopathological examination, the observed abnormalities in kidney tissues observed after cisplatin treatment are in accordance with the previous studies (31,63,64). As cisplatin-induced nephrotoxicity exhibits histological alterations including swelling and vacuolation of the lining endothelium of the glomerulus tuft as well as tubular degeneration of the renal tubular cells. These changes are associated with the loss of renal functions as revealed by the observed abnormalities in renal enzymes. On the other hand, the concurrent administration of LA with cisplatin, almost prevents the histopathology changes of the heart and kidney, especially necrosis and sever interstitial hemorrhages (2).

5. Conclusion

It could be concluded that, cisplatin administration results in pronounced oxidative stress which is revealed by cellular damage to the heart and kidney of the rats. Coadministration of DL- α -lipoic acid was found to be effective candidate in protecting the heart and kidney tissues from cisplatin-induced nephrotoxicity and cardiotoxicity without interfering with antitumor activity of cisplatin. It is greatly recommended to co-administer DL- α -lipoic acid with cisplatin to minimize the nephrotoxicity and cardiotoxicity of the latter. Further clinical studies are encouraged to approve the validity of these results in human.

References

1. Pabla N, Dong Z. Cisplatin nephrotoxicity: Mechanisms and renoprotective strategies. *Kidney Int.* 2008; 73:994-1007.
2. Kang KP, Kim DH, Jung YJ, Lee AS, Lee S, Lee SY, Jang KY, Sung MJ, Park SK, Kim W. Alpha-lipoic acid attenuates cisplatin-induced acute kidney injury in mice by suppressing renal inflammation. *Nephrol Dial Transplant.* 2009; 24:3012-3020.
3. Chirino YI, Pedraza-Chaverri J. Role of oxidative and nitrosative stress in cisplatin-induced nephrotoxicity. *Exp Toxicol Pathol.* 2009; 61:223-242.
4. Weijl NI, Hopman GD, Wipkink-Bakker A, Lentjes EG, Berger HM, Cleton FJ, Osanto S. Cisplatin combination chemotherapy induces a fall in plasma antioxidants of cancer patients. *Ann Oncol.* 1998; 9:1331-1337.
5. Wozniak K, Czechowska A, Blasiak J. Cisplatin-evoked DNA fragmentation in normal and cancer cells and its modulation by free radical scavengers and the tyrosine kinase inhibitor STI571. *Chem Biol Interact.* 2004; 147:309-318.
6. Dickey DT, Wu YJ, Muldoon LL, Neuwelt EA. Protection against cisplatin induced toxicities by N-acetylcysteine and sodium thiosulfate as assessed at the molecular, cellular and *in vivo* levels. *J Pharmacol Exp Ther.* 2005; 314:1052-1058.
7. Tsuruya K, Tokumoto M, Ninomiya T, Hirakawa M, Masutani K, Taniguchi M, Fukuda K, Kanai H, Hirakata H, Iida M. Antioxidant ameliorates cisplatin-induced renal tubular cell death through inhibition of death receptor mediated pathways. *Am J Physiol Renal Physiol.* 2003; 285:F208-F218.
8. Bilska A, Kryczyk A, Wlodek L. The different aspects of the biological role of glutathione. *Postepy Hig Med Dosw (Online).* 2007; 61:438-453.
9. Bharat S, Cochran BC, Hsu M, Liu J, Ames BN, Andersen JK. Pre-treatment with R-lipoic acid alleviates the effects of GSH depletion in PC12 cells: Implications for Parkinson's disease therapy. *Neurotoxicology.* 2002; 23:479-486.
10. Henriksen EJ. Exercise training and the antioxidant alpha-lipoic acid in the treatment of insulin resistance and type 2 diabetes. *Free Radic Biol Med.* 2006; 40:3-12.
11. Ahmed HH. Modulatory effects of vitamin E, acetyl-L-carnitine and α -lipoic acid on new potential biomarkers for Alzheimer's disease in rat model. *Exp Toxicol Pathol.* 2010. In press. doi:10.1016/j.etp.2010.11.012
12. Balachandar AV, Malarkodi KP, Varalakshmi P. Protective role of DL- α -lipoic acid against adriamycin induced cardiac lipid peroxidation. *Hum Exp Toxicol.* 2003; 22:249-254.
13. Mythili Y, Sudharsan PT, Selvakumar E, Varalakshmi P. Protective effect of DL-lipoic acid on cyclophosphamide induced oxidative cardiac injury. *Chem Biol Interact.* 2004; 151:13-19.
14. Zhang WJ, Frei B. Alpha-lipoic acid inhibits TNF- α -induced NF κ B activation and adhesion molecule expression in human aortic endothelial cells. *FASEB J.* 2001; 15:2423-2432.
15. El-Awady el-SE, Moustafa YM, Abo-Elmatty DM, Radwan A. Cisplatin-induced cardiotoxicity: Mechanisms and cardioprotective strategies. *Eur J Pharmacol.* 2011; 650:335-341.
16. Osman A el-M, Ahmed MM, Khayyal MT, el-Merzabani MM. Hyperthermic potentiation of cisplatin on solid

- Ehrlich carcinoma. *Tumori*. 1993; 79:268-272.
17. Bais R, Philcox M. Approved recommendation on IFCC methods for the measurement of catalytic concentration of enzymes. Part 8. IFCC method for LDH (L-Lactate: NAD+Oxidoreductase, EC1.1.1.27). International Federation of Clinical Chemistry (IFCC). *Eur J Clin Chem Clin Biochem*. 1994; 32:639-655.
 18. Wu AH, Bowers GN Jr. Evaluation and comparison of immunoinhibition and immunoprecipitation methods for differentiating MB and BB from macro forms of creatine kinase isoenzymes in patients and health individuals. *Clin Chem*. 1982; 28:2017-2021.
 19. Tabacco A, Meiattini F, Moda E, Tarli P. Simplified enzymic/colorimetric serum urea nitrogen determination. *Clin Chem*. 1979; 25:336-337.
 20. Bowers LD, Wong ET. Kinetic serum creatinine assays. A critical evaluation and review. *Clin Chem*. 1980; 26:555-561.
 21. Buege JA, Aust SD. Microsomal lipid peroxidation. *Methods Enzymol*. 1978; 52:302-310.
 22. Ellman GL. Tissue sulfhydryl groups. *Arch Biochem Biophys*. 1959; 82:70-77.
 23. Minami M, Yoshikawa H. Simplified assay method of superoxide dismutase activity for clinical use. *Clin Chim Acta*. 1979; 92:337-342.
 24. Miranda KM, Espey MG, Wink DA. A rapid, simple spectrophotometric method for simultaneous detection of nitrate and nitrite. *Nitric Oxide*. 2001; 5:62-71.
 25. Katoh K, Ikata T, Katoh S, Hamada Y, Nakauchi K, Sano T, Niwa M. Induction and its spread of apoptosis in rat spinal cord mechanical trauma. *Neurosci Lett*. 1996; 216:9-12.
 26. Yokozawa T, Dong E. Role of ginsenoside-Rd in cisplatin-induced renal injury: Special reference to DNA fragmentation. *Nephron*. 2001; 89:433-438.
 27. Salami S, Karami-Tehrani F. Biochemical studies of apoptosis induced by tamoxifen in estrogen receptor positive and negative breast cancer cell lines. *Clin Biochem*. 2003; 36:247-253.
 28. Pai VB, Nahata MC. Cardiotoxicity of chemotherapeutic agents: Incidence, treatment and prevention. *Drug Saf*. 2000; 22:263-302.
 29. Al-Majed AA, Sayed-Ahmed MM, Al-Yahya AA, Aleisa AM, Al-Rejaie SS, Al-Shabanah OA. Propionyl-L-carnitine prevents the progression of cisplatin-induced cardiomyopathy in a carnitine-depleted rat model. *Pharmacol Res*. 2006; 53:278-286.
 30. Gonzalez R, Borrego A, Zamora Z, Romay C, Hernandez F, Menendez S, Montero T, Rojas E. Reversion by ozone treatment of acute nephrotoxicity induced by cisplatin in rats. *Mediators Inflamm*. 2004; 13:307-312.
 31. Kang DG, Lee AS, Mun YJ, Woo WH, Kim YC, Sohn EJ, Moon MK, Lee HS. Butein ameliorates renal concentrating ability in cisplatin-induced acute renal failure in rats. *Biol Pharm Bull*. 2004; 27:366-370.
 32. Saleh S, El-Demerdash E. Protective effects of L-arginine against cisplatin induced renal oxidative stress and toxicity: Role of nitric oxide. *Basic Clin Pharmacol Toxicol*. 2005; 97:91-97.
 33. Noori S, Mahboob T. Antioxidant effect of carnosine pretreatment on cisplatin induced renal oxidative stress in rats. *Indian J Clin Biochem*. 2010; 25:86-91.
 34. Ramesh G, Reeves WB. Salicylate reduces cisplatin nephrotoxicity by inhibition of tumor necrosis factor- α . *Kidney Int*. 2004; 65:490-499.
 35. Price PM, Safirstein RL, Megyesi J. Protection of renal cells from cisplatin toxicity by cell cycle inhibitors. *Am J Physiol Renal Physiol*. 2004; 286:F378-F384.
 36. Abdel-Zaher AO, Abdel-Hady RH, Mahmoud MM, Farrag MM. The potential protective role of alpha-lipoic acid against acetaminophen-induced hepatic and renal damage. *Toxicology*. 2008; 243:261-270.
 37. Karthikeyan K, Bai BR, Devaraj SN. Cardioprotective effect of grape seed proanthocyanidins on isoproterenol-induced myocardial injury in rats. *Int J Cardiol*. 2007; 115:326-333.
 38. Dorr RT, Lagel K. Effect of sulphhydryl compounds and glutathione depletion on rat heart myocyte toxicity induced by 4 hydroxy cyclophosphamide and acrolein *in vitro*. *Chem Biol Interact*. 1994; 93:117-128.
 39. Ghibu S, Delemasure S, Richard C, Guillaud JC, Martin L, Gambert S, Rochette L, Vergely C. General oxidative stress during doxorubicin-induced cardiotoxicity in rats: Absence of cardioprotection and low antioxidant efficiency of alpha-lipoic acid. *Biochimie*. 2012; 94:932-939.
 40. Massion PB, Feron O, Dessy C, Balligand JL. Nitric oxide and cardiac function: Ten years after, and continuing. *Circ Res*. 2003; 93:388-398.
 41. Zhang C, Walker LM, Mayeux PR. Role of nitric oxide in lipopolysaccharide-induced oxidant stress in the rat kidney. *Biochem Pharmacol*. 2000; 59:203-209.
 42. Gardner CR, Laskin JD, Dambach DM, Sacco M, Durham SK, Bruno MK, Cohen SD, Gordon MK, Gerecke DR, Zhou P, Laskin DL. Reduced hepatotoxicity of acetaminophen in mice lacking inducible nitric oxide synthase: Potential role of tumor necrosis factor- α and interleukin-10. *Toxicol Appl Pharmacol*. 2002; 184:27-36.
 43. Harstad EB, Klaassen CD. INOS-null mice are not resistant to cadmium chloride-induced hepatotoxicity. *Toxicology*. 2002; 175:83-90.
 44. Kim JS, He L, Lemasters JJ. Mitochondrial permeability transition: A common pathway to necrosis and apoptosis. *Biochem Biophys Res Commun*. 2003; 304:463-470.
 45. Lau AH. Apoptosis induced by cisplatin nephrotoxic injury. *Kidney Int*. 1999; 56:1295-1298.
 46. Lieberthal W, Triaca V, Levine J. Mechanisms of death induced by cisplatin in proximal tubular epithelial cells: Apoptosis vs. necrosis. *Am J Physiol*. 1996; 270: F700-F708.
 47. Melhem MF, Craven PA, Liachenko J, DeRubertis FR. Alpha-lipoic acid attenuates hyperglycemia and prevents glomerular mesangial matrix expansion in diabetes. *J Am Soc Nephrol*. 2002; 13:108-116.
 48. Aly HA, Lightfoot DA, El-Shemy HA. Modulatory role of lipoic acid on lipopolysaccharide-induced oxidative stress in adult rat Sertoli cells *in vitro*. *Chem Biol Interact*. 2009; 182:112-118.
 49. Packer L, Tritschler HJ, Wessel K. Neuroprotection by the metabolic antioxidant alpha-lipoic acid. *Free Radic Biol Med*. 1997; 22:359-378.
 50. Petersen Shay K, Moreau RF, Smith EJ, Hagen TM. Is α -lipoic acid a scavenger of reactive oxygen species *in vivo*? Evidence for its initiation of stress signaling pathways that promote endogenous antioxidant capacity. *IUBMB Life*. 2008; 60:362-367.
 51. Zhang DD, Lo SC, Cross JV, Templeton DJ, Hannink M. Keap1 is a redox-regulated substrate adaptor protein for a Cul3-dependent ubiquitin ligase complex. *Mol Cell Biol*. 2004; 24:10941-10953.
 52. Ramadan W. The protective effect of α -lipoic acid in doxorubicin induced cardiotoxicity in rats. Department of

- Biology, Baylor University. 2008; p.74.
53. Somani SM, Husain K, Whitworth C, Trammell GL, Malafa M, Rybak LP. Dose-dependent protection by lipoic acid against cisplatin-induced nephrotoxicity in rats: Antioxidant defense system. *Pharmacol Toxicol.* 2000; 86:234-241.
 54. Rybak LP, Husain K, Whitworth C, Somani SM. Dose dependent protection by lipoic acid against cisplatin-induced ototoxicity in rats: Antioxidant defense system. *Toxicol Sci.* 1999; 47:195-202.
 55. Matsugo S, Yan LJ, Han D, Trischler HJ, Packer L. Elucidation of antioxidant activity of alpha-lipoic acid toward hydroxyl radical. *Biochem Biophys Res Commun.* 1995; 208:161-167.
 56. Packer L, Witt EH, Trischler HJ. Alpha-lipoic acid as a biological antioxidant. *Free Radic Biol Med.* 1995; 19:227-250.
 57. Sung MJ, Kim W, Ahn SY, Cho CH, Koh GY, Moon SO, Kim DH, Lee S, Kang KP, Jang KY, Park SK. Protective effect of alpha-lipoic acid in lipopolysaccharide-induced endothelial fractalkine expression. *Circ Res.* 2005; 97:880-890.
 58. Demarco VG, Scumpia PO, Bosanquet JP, Skimming JW. Alpha-lipoic acid inhibits endotoxin-stimulated expression of iNOS and nitric oxide independent of the heat shock response in RAW264.7 cells. *Free Radic Res.* 2004; 38:675-682.
 59. El-Beshbishy HA, Bahashwan SA, Aly HA, Fakher HA. Abrogation of cisplatin-induced nephrotoxicity in mice by alpha lipoic acid through ameliorating oxidative stress and enhancing gene expression of antioxidant enzymes. *Eur J Pharmacol.* 2011; 668:278-284.
 60. Biewenga GP, Haenen GR, Bast A. The pharmacology of the antioxidant lipoic acid. *Gen Pharmacol.* 1997; 29:315-331.
 61. Scarpulla RC. Nuclear activators and coactivators in mammalian mitochondrial biogenesis. *Biochim Biophys Acta.* 2002; 1576:1-14.
 62. Devasagayam TP, Subramanian M, Pradhan DS, Sies H. Prevention of singlet oxygen-induced DNA damage by lipoate. *Chem Biol Interact.* 1993; 86:79-92.
 63. Evenepoel P. Acute toxic renal failure. *Best Pract Res Clin Anaesthesiol.* 2004; 18:37-52.
 64. Lameire N, Van Biesen W, Vanholder R. Acute renal failure. *Lancet.* 2005; 365:417-430.

(Received May 29, 2012; Revised June 18, 2012; Accepted June 20, 2012)

Evaluation of skin surface hydration state and barrier function of stratum corneum of dorsa of hands and heels treated with PROTECT X2 skin protective cream

Takahiro Kubota

Pharmaceutical Department of Scientific Research, Graduate School of Pharmaceutical Sciences, Chiba Institute of Science, Chiba, Japan.

ABSTRACT: Skin roughness is a term commonly used in Japan to describe a poor skin condition related to a rough and dry skin surface that develops as a result of various damaging effects from the environment or skin inflammation. Recovery from skin roughness requires skin care for a long period, thus it is important to prevent development of such skin changes. PROTECT X2 contains agents used for a protective covering of the skin from frequent hand washing or use of alcohol-based disinfectants. These unique components are also thought to be effective to treat skin roughness of the dorsa of the hands and heels. In the present study, we evaluated the effectiveness of PROTECT X2 to increase skin surface hydration state, as well as enhance the barrier function of the stratum corneum of the dorsa of the hands and heels in elderly individuals. A total of 8 elderly subjects and their caretakers without any skin diseases participated in the study. They applied PROTECT X2 by themselves to the dorsum area of 1 hand and heel 3 to 5 times daily for 1 month, while the opposite sides were left untreated. We measured stratum corneum (SC) hydration and transepidermal water loss (TEWL) before beginning treatment, then 1 week and 1 month after the start of treatment to compare between the treated and untreated skin. SC hydration state after applications of PROTECT X2 was 1.5- to 3.0-fold higher than that of the untreated skin in the dorsa of both hands and heels, indicating that the moisturizing ingredients accompanied by water were replenished in those areas where the cream was applied. Also, TEWL in the dorsum of the hands was 17.0-27.9% lower on the treated side, indicating improvement in SC barrier function. On the basis of these findings,

we concluded that PROTECT X2 enhances water-holding in the SC and aids the barrier function of the skin in the dorsum of the hands. In addition, we consider that this formulation is useful for not only protecting the hands from the effects of such agents as detergents and alcohol-based disinfectants, but also for protecting heel skin covered by a thick SC from dry and cold conditions such as those encountered in winter. However, since the SC in that area is much thicker than that of the hands, the barrier function was not significantly improved within 1 month of daily treatments.

Keywords: Stratum corneum, skin protective cream, transepidermal water loss, water content

1. Introduction

"Skin roughness" is a commonly utilized term in Japan for disturbed skin surface, which develops from synergistic interactions of various factors such as dryness and inflammation. The skin is composed from external to internal of the stratum corneum (SC), epidermis, dermis, and subcutaneous tissue. The SC covers the skin surface as an extremely thin membranous barrier and has an important protective role against the external environment (1). Approximately 30% of the content of the SC is water, which functions to maintain smoothness and softness of the skin surface even under dry external environmental conditions (2). Thus, the SC has an important barrier function to prevent the infiltration of harmful substances from outside of the body and also prevents water loss from the living tissues that it covers (1).

Various substances in the SC play a role to maintain hydration of the SC. They consist of sebum secreted from the sebaceous glands to cover the skin surface, except for the palms and soles, low-molecular weight substances termed natural moisturizing factor (NMF), which are chiefly composed of highly hygroscopic amino acids present in corneocytes (3), and intercellular lipids that spread between the corneocytes, such as ceramides,

*Address correspondence to:

Dr. Takahiro Kubota, Pharmaceutical Department of Scientific Research, Graduate School of Pharmaceutical Sciences, Chiba Institute of Science, 15-8 Shiomi-cho, Choshi-city, Chiba 288-0025, Japan.
E-mail: tkubota-tky@umin.net

cholesterol, and fatty acids, which inhibit water loss from the tissues and prevent NMF effusion to the outside of the cells (4). The SC is produced by proliferation and differentiation of keratinocytes composing the epidermis as a result of epidermal turnover, which normally occurs over a period of 28 days in most parts of the body, such as the trunk and limbs. However, once inflammation involves the epidermis, the cell cycle shortens to induce increased keratinocyte proliferation, which causes reductions in the amounts of intercellular lipids and NMF, leading to a decrease in water content in the SC. Under such conditions, so-called dry skin develops, in which the skin surface texture is disturbed to induce exfoliation of the corneocytes as a mass, namely scaling. Thus, it is inevitable that a decrease in SC barrier function protecting the body from desiccation occurs due to a dry external environment (5).

For objective and non-invasive evaluations of skin surface conditions, measurements of high-frequency conductance and transepidermal water loss (TEWL) are widely used (6-8). With the former, it is possible to determine the hydration state of the skin surface, *i.e.*, water content in the superficial portion of the SC that faces the environment. Thus, it can also be used to determine the efficacy of a cosmetic base on water content in the SC when measured under constant temperature and moisture conditions (6,7). In contrast, TEWL measurement assesses the barrier function of the SC by determining the amount of water that evaporates from the skin surface and is lost from water-saturated skin tissues (8). It has been reported that such measurements should be made without the influence of perspiration or airflow, at around 20°C (9). Since the water content of the superficial portion and barrier function constitute the vital functional characteristics of the SC that covers the skin surface, these measurements are generally performed in combination. Recently, for evaluating skin surface morphology, or skin texture, imaging analysis using replicas has also been utilized (10).

When skin roughness is left untreated, an increase in the risk of inflammation or infection can develop due to the formation of cracks in the SC. Thus, it is considered that the fundamental issue for maintaining healthy skin is moisturizing to keep the skin surface smooth and soft, and prevent development of cracking. Cosmetic products produced for improving skin roughness are generally composed of water, oil, and moisturizing agents, which are suitable for maintaining the balance of water, NMF, and lipids on the skin surface. These are broadly interpreted as preparations that maintain homeostasis of the skin, thus cosmetic products and quasi-drugs used for maintaining, restoring, and improving the function of epidermal tissue have been actively developed. An agent that improves rough skin is sometimes used alone, but mostly in combination with multiple moisturizing agents such as highly concentrated glycerin and propylene glycol, and anti-inflammatory agents such as

glycyrrhizinate and lysozyme chloride for suppressing minor inflammation.

In elderly individuals, a relatively thick SC is formed in the skin surface as epidermal proliferation reduces and differentiation slows with poor production of the NMF in the epidermis with aging, resulting in accumulation of dry corneocytes in the superficial portion of the SC. Accordingly, corneocytes with low NMF content tend to remain on the skin surface of elderly subjects due to reduced activity of the proteolytic enzymes to facilitate to reduce their adhesion to each other (11). Moreover, sebum secretion begins to decline in the fifth decade of life, and skin changes termed senile xerosis begin to develop in the dry and cold conditions of winter. In most affected individuals, the skin surface of the back, hips, and legs becomes dry and cracked, inducing itchiness (11). Furthermore, in bedridden or wheelchair-bound elderly individuals, the incidence of pressure sores, so-called bedsores, also increases. Pressure sores is a condition in which blood flow in the skin deteriorates due to compression for long periods of time while sitting in a chair or lying on a bed, causing cracking of the SC, which then spreads from the skin surface to subcutaneous tissue and maintained in the presence of poor blood circulation. Moreover, when the skin is stimulated by friction, cracking of the thickened SC may occur, facilitating the development of pressure sores. In the case of a heel affected by pressure sores, walking becomes difficult, affecting bodily movement. Since recovery from skin injury requires a long period of time in elderly individuals, it is important to prevent the development of these skin conditions.

PROTECT X2 contains high concentrations of glycerin and dipropylene glycol, generally employed as moisturizing components, as well as glycereth-25 PCA isostearate, stearyl glycyrrhizinate, and tocophenyl acetate, which are widely used as anti-inflammatory components. In addition, it is worth noting that PROTECT X2 contains 3 other components, aminoethyl aminopropylmethylsiloxane-dimethylsiloxane copolymer from a silicon series, polyvinyl pyrrolidone from a vinyl series, and perfluoropolyether from a fluorine series, which are used to produce a protective covering for skin from external damaging factors such as hand washing and use of alcohol-based disinfectants.

In the present study, we examined the efficacy of this formulation for forming a protective skin covering, especially to enhance SC barrier function on the dorsum of the hand. We examined the effectiveness of PROTECT X2 for water holding when applied to the dorsum of the hands of elderly individuals. In addition, we examined its effectiveness on heel skin, the plantar area where the skin is covered by a uniquely thick SC, which requires sufficient hydration to remain soft and flexible, and resists strong external forces, for avoiding formation of cracking or deep fissures, which particularly occur in elderly individuals who tend to have thicker SC than young healthy individuals (11).

2. Materials and Methods

2.1. Test agent and measuring instruments

PROTECT X2 (Newhair Cosmetic Material Co., Ltd., Tokyo, Japan), a quasi-drug, was the agent examined in this study. It is mainly composed of glycerin, dipropylene glycol, glycereth-25 PCA isostearate, stearyl glycyrrhetinate, tocophenyl acetate, aminoethylaminopropylmethylsiloxane-dimethylsiloxane copolymer, polyvinyl pyrrolidone, and perfluoropolyether. To measure the hydration state of the skin surface, we used a SKICON-200EX (I.B.S Co., Ltd., Shizuoka, Japan). For determination of TEWL, a Tewameter[®] TM300 (Courage + Khazaka Electronics GmbH, Cologne, Germany) was employed. These instruments were operated in accordance with the enclosed instruction manuals and the instrumental measurements were made in an environment controlled to a constant temperature and humidity (21-23°C, 43-50% relative humidity).

2.2. Subjects

A total of 8 elderly individuals and their caretakers (1 male, 7 females) ranging from 29-85 years old (mean 52.8 years) participated in the study as the subjects. None had any special skin diseases, but demonstrated mild to moderate skin roughness. Informed consent was obtained after explaining verbally and in writing the purpose and methods of the experiment, as well as handling of the data obtained from the experimental results. The present study was approved by the Ethical Committee of Chiba Institute of Science (Approval No. 23-2).

2.3. Method of application of PROTECT X2

The study was performed in the period from December 2011 to January 2012. The subjects applied PROTECT X2 3-5 times daily to the dorsa of one of their hands and one of their heels for a period of 1 month, with the application amount set at 0.6 mL per dose. As a control, nothing was applied to the contralateral hand and heel throughout the 1-month study period. SC hydration state and TEWL in the SC were determined 5 times at each measuring site, from which the mean value was calculated after excluding the maximum and minimum values. The measurement obtained immediately before the start of the application was considered to be the initial value. Similar measurements were conducted again 1 week and 1 month after the start of the applications. The measurements were made in principle when the subjects were calm, in an environment controlled at constant temperature and humidity (21-23°C, 43-50% relative humidity). The maximum and minimum temperature and humidity at each measuring point were also recorded.

2.4. Statistical analysis

For testing the significance of the mean values between the groups, Student's paired *t*-test was used, while Pearson's correlation coefficient was used for analyzing correlations. For correlation analysis of the mean values with temperature and humidity, Pearson's correlation coefficient was used. The level of significance in Student's *t*-test was 5%. For testing the correlation coefficient (*r*), Fisher's *r* to *z* transformation was used. Microsoft[®] Office Excel 2007 (Microsoft Japan Co., Ltd., Tokyo, Japan) and KaleidaGraph[®] 3.6 (Hulinks Inc., Tokyo, Japan) were used, as appropriate, for statistical calculations.

3. Results

3.1. Changes in skin surface hydration state with PROTECT X2 applications

Before the start of the PROTECT X2 applications, there was no significant difference between the dorsum of the pre-treated and the untreated hands (96.8 ± 18.9 vs. 85.8 ± 20.2 μ S; mean \pm standard error), or between that of the pre-treated and the untreated heels (12.7 ± 3.9 vs. 8.4 ± 2.2 μ S). After 1 week of PROTECT X2 applications, the skin surface hydration state of the dorsum of the hands became 169.9 ± 54.8 μ S, which was 2.6-fold greater than that of the untreated side (66.5 ± 25.1 μ S) ($p < 0.05$). Furthermore, after 1 month of daily applications, the hydration state of the treated side was 68.0 ± 14.1 μ S, which was 1.5-fold greater than that of the untreated side (45.3 ± 12.3 μ S) ($p < 0.01$) (Figure 1A). Meanwhile, in the 7 subjects who applied PROTECT X2 to one of their heels daily for 1 week, the hydration state in the treated side was 16.7 ± 3.2 μ S, which was 3.0-fold greater than that of the untreated side (5.5 ± 1.2 μ S) ($p < 0.01$). One month after the start of the applications, the hydration state in the treated heel was 20.4 ± 4.2 μ S, or 2.8-fold greater than that of the untreated side (7.2 ± 1.3 μ S) ($p < 0.05$) (Figure

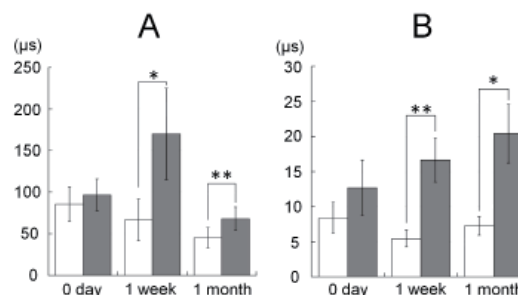


Figure 1. Changes in water content in corneocyte layer with PROTECT X2 application. A) Water content in dorsum of hand ($n = 8$). **B)** Water content in heel ($n = 7$). Open column, untreated side; closed column, treated with PROTECT X2. Error bar, mean \pm standard error. * $p < 0.05$, ** $p < 0.01$.

1B). These findings suggest that PROTECT X2 was effective to increase the SC hydration state in the dorsa of the hands and heels.

3.2. Changes in TEWL with PROTECT X2 applications

Before the start of the PROTECT X2 applications, there was no significant difference between the dorsum of the pre-treated and the untreated hands (13.4 ± 1.8 vs. 14.3 ± 1.7 g/hm²), or between that of the pre-treated and the untreated heels (30.6 ± 3.9 vs. 34.2 ± 5.4 g/hm²). We examined TEWL in the dorsum of the hands of 8 subjects. After 1 week of daily applications of PROTECT X2, that value was 13.7 ± 1.6 g/hm² in the treated side, which was 27.9% lower than that of the untreated side (19.0 ± 3.3 g/hm²) ($p < 0.05$). Furthermore, TEWL at 1 month after starting PROTECT X2 applications was 15.1 ± 2.4 g/hm² in the treated side, 17.0% lower than that in the untreated side (18.2 ± 2.2 g/hm²) ($p < 0.05$) (Figure 2A). In contrast, in the 7 subjects who applied PROTECT X2 to their heel, TEWL after 1 week was 35.4 ± 2.5 g/hm², which was 17.2% higher than that in the untreated side (30.2 ± 1.9 g/hm²). TEWL after 1 month of daily PROTECT X2 applications was 36.0 ± 5.0 g/hm² in the treated heel, 15.0% higher than that in the untreated side (31.3 ± 4.0 g/hm²) (Figure 2B). On the basis of these findings, we concluded that PROTECT X2 helped to decrease TEWL in the dorsum of the hand, whereas it increased TEWL in the heel skin in the present subjects.

4. Discussion

So-called healthy skin indicates a condition in which the skin surface is firmly and smoothly covered with SC, and an adequate amount of moisture is retained. Measurements of water content in the superficial portion of the SC as well as TEWL can be employed to objectively evaluate the condition of the skin surface. The former is used as an index for moisture-holding capacity, while the latter represents the barrier function

of skin (6-8). Accordingly, these measurements together are suitable for determining such conditions such as xerosis, in which moisture in the skin is lost during the dry period in winter, and exfoliation of the superficial portion of the SC occurs due to repeated movements of the skin that produce friction as well as cracking in the skin surface.

In the present subjects, the level of hydration of skin surfaces repeatedly applied with PROTECT X2 was frequently found to range from 1.5- to 3-fold greater in conductance measurements as compared to the untreated sides for both the hands and heels. The mean hydration state at 1 week after the start of applications was the highest at 169.9 ± 54.8 μ S, though the early values also showed the largest standard error ranges. Thus, we think that the extent of increase in SC hydration varies between individuals due to the fact that only 1 week had passed after the start of application. Although the water content in the SC of the heel was highest after 1 month of treatment (mean 20.4 μ S), it was only about one-tenth of the maximum value (169.9 μ S) measured in the dorsum of the hands. This corresponded to the fact that the SC of the heel is distinct from that of the other portions of the body except for the palms, because, like palmar skin, it is several times thicker than that of the dorsum of the hands and other areas of the body. Over time, hydration state in the heel tended to increase gradually from 16.7 μ S at 1 week to a peak value at 1 month after the start of the applications (Figure 1B) (12).

In our present investigation of the correlation between PROTECT X2 treated and untreated sites, strong correlations were confirmed after 1 week (0.89) and 1 month (0.96) (both, $p < 0.01$) in the dorsum of the hands, which were statistically significant. These findings indicate that higher levels before starting treatment resulted in higher levels after the applications. Thus, we think that the higher hydration state in the treated side was due to the daily applications of PROTECT X2 to the dorsum of the hands. Meanwhile, no such correlation was observed at any time points for the heels. Thus, it is important to consider the unique water distribution in the palmo-plantar SC, as a thick low hydrated portion has been found in the upper and middle part of the SC in that area (12). In addition, it is possible that perspiration due to physical and mental changes in the subjects (9), individual differences in the timing of putting on footwear such as socks after applications, or differences in moisture retention because of different footwear materials might have also affected our results. We found a large difference regarding hydration state in the SC between the treated and untreated sides at 1 week after the start of the applications in both hands and heels. However, our findings indicate that daily PROTECT X2 applications for 1 week are effective to enhance the moisture retention capacity of the SC. We already studied that the

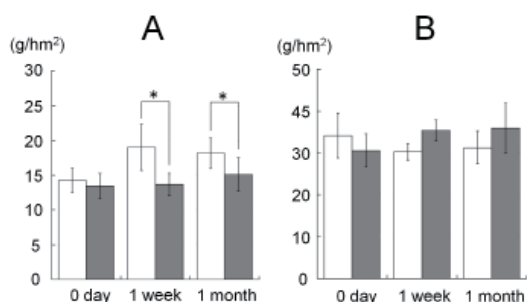


Figure 2. Changes in TEWL in corneocyte layer with PROTECT X2 application. A) TEWL in dorsum of hand ($n = 8$). **B)** TEWL in heel ($n = 7$). Open column, untreated side; closed column, treated with PROTECT X2. Error bar, mean \pm standard error. * $p < 0.05$.

moisture retention of the SC after its single application are continuous with 3 h at least (data not shown).

TEWL values for the dorsum of the hands applied with PROTECT X2 were 17.0-27.9% lower than those of the untreated hands, whereas TEWL values for the treated heels were 15.0-17.2% higher than those of the untreated heels. The mean TEWL of the treated side remained nearly constant throughout the experimental period (13.7 g/hm² at 1 week, 15.1 g/hm² at 1 month), whereas that of the untreated side showed an increasing tendency, suggesting a worsening of the barrier function when it remained untreated. We concluded that this was because the protective covering provided by PROTECT X2 on the SC prevented water loss from the dorsum of the hands, indicating that repeated applications of PROTECT X2 prevent weakening of the SC barrier function (Figure 2A). This has also been reported when measurements were done with dry skin (13,14). In contrast, TEWL in the treated heels remained higher than that in the untreated side throughout the experimental period. We speculated that this reflected the supply of water and moisturizing ingredients by PROTECT X2 to the SC of the heel. Because the SC of the heel is much thicker than that in the dorsum of the hands, it is likely that the SC cannot be replaced totally by new corneocyte layers within 1 month (15). Accordingly, we think that the barrier function of plantar skin might not be improved within the treatment period, as intercellular lipids such as ceramide did not become normalized within the 1-month experimental period. Thus, it may require more time to improve the barrier function in the heel (Figure 2B).

We also investigated the correlation between the treated and untreated sides over time. For the dorsum of the hands, the correlation was 0.86 ($p < 0.01$) at 1 week after the start of application and 0.88 ($p < 0.01$) at 1 month, which were statistically significant, suggesting that a smaller correlation before treatment resulted in a smaller correlation after the applications. We concluded that the lower TEWL value in the treated side of the hands was a result of barrier function improvement induced by PROTECT X2 applications. However, no such correlations were found for TEWL in the heel. It is possible that a total lack of sebum excretion and low amounts of intercellular lipids in addition to the unique sweat glands that have relatively abundant secretion in the heel areas might have affected these measurements (9), in addition to the thickness of the heel SC, as noted above.

Neither water content nor TEWL had any correlation with room temperature or humidity (water content: $p = 0.30-0.96$, TEWL: $p = 0.15-0.88$). Accordingly, we think that our study was performed under proper environmental conditions and obtained highly reliable results. In addition, visual assessments throughout the measurement period confirmed that skin in the untreated sides had greater amounts of scaling and



Figure 3. Visual observations throughout the measurement period. The untreated hands had greater amounts of scaling and chapped skin, as well as bleeding from cracks after 1 month (the left hand). Meanwhile, hands applied with PROTECT X2 maintained adequate moisture levels.

chapped skin, as well as bleeding from cracks over time (Figure 3). Meanwhile, hands and heels applied with PROTECT X2 maintained adequate moisture levels. Skin tenderness is closely related to water content in the SC (2), thus it is useful to measure skin surface hydration for evaluating skin roughness.

Based on the present findings, we concluded that daily applications of PROTECT X2 increases SC hydration state in the skin of patients with senile xerosis and improves the barrier function in the dorsum of the hand. Thus, it is reasonable to consider that this preparation is effective for not only protecting the hands from detergent and use of alcohol-based disinfects, but that it can also protect heels from winter dryness and friction.

Acknowledgements

I wish to thank Nozomi Suzuki (Bachelor of Pharmacology) and Mayumi Shibayama (Bachelor of Pharmacology) for their assistance with the measurements. I also gratefully acknowledge Dr. Hachiro Tagami, Professor Emeritus of Tohoku University, for the cooperation and guidance in designing the investigation and completing the study.

References

1. Elias PM. Structure and function of the stratum corneum permeability barrier. *Drug Dev Res.* 1988; 13:97-105.
2. Takenouchi M, Suzuki H, Tagami H. Hydration characteristics of pathologic stratum corneum – Evaluation of bound water. *J Invest Dermatol.* 1986; 87:574-576.
3. Middleton JD. The mechanism of water binding in stratum corneum. *Br J Dermatol.* 1968; 80:437-450.
4. Imokawa G, Hattori M. A possible function of structural lipids in the water-holding properties of the stratum corneum. *J Invest Dermatol.* 1985; 84:282-284.
5. Watanabe M, Tagami H, Horii I, Takahashi M, Kligman

- AM. Functional analyses of the superficial stratum corneum in atopic xerosis. *Arch Dermatol.* 1991; 127:1689-1692.
6. Obata M, Tagami H. Electrical determination of water content and concentration profile in a simulation model of *in vivo* stratum corneum. *J Invest Dermatol.* 1989; 92:854-859.
 7. Tagami H. Quantitative measurements of water concentration of the stratum corneum *in vivo* by high-frequency current. *Acta Derm Venereol Suppl (Stockh).* 1994; 185:29-33.
 8. Tagami H. Impedance measurement for evaluation of the hydration state of the skin surface. In: *Cutaneous investigation in health and disease. Noninvasive methods and instrumentation* (Leveque JL, ed.). Marcel Dekker, New York, 1989, pp. 79-111.
 9. Tagami H, Ohi M, Iwatsuki K, Kanamaru Y, Yamada M, Ichijo B. Evaluation of the skin surface hydration *in vivo* by electrical measurement. *J Invest Dermatol.* 1980; 75:500-507.
 10. Zou Y, Song E, Jin R. Age-dependent changes in skin surface assessed by a novel two-dimensional image analysis. *Skin Res Technol.* 2009; 15:399-406.
 11. Hara M, Kikuchi K, Watanabe M, Denda M, Koyama J, Nomura J, Horii I, Tagami H. Senile xerosis: Functional, morphological and biochemical studies. *J Geriatr Dermatol.* 1993; 1:111-120.
 12. Egawa M, Hirao T, Takahashi M. *In vivo* estimation of stratum corneum thickness from water concentration profiles obtained with Raman spectroscopy. *Acta Derm Venereol.* 2007; 87:4-8.
 13. Kikuchi K, Kobayashi H, Hirao T, Ito A, Takahashi H, Tagami H. Improvement of mild inflammatory changes of the facial skin induced by winter environment with daily applications of a moisturizing cream. A half-side test of biophysical skin parameters, cytokine expression pattern and the formation of cornified envelope. *Dermatology.* 2003; 207:269-275.
 14. Kikuchi K, Tagami H; Japanese Cosmetic Scientist Task Force for Skin Care of Atopic Dermatitis. Noninvasive biophysical assessments of the efficacy of a moisturizing cosmetic cream base for patients with atopic dermatitis during different seasons. *Br J Dermatol.* 2008; 158:969-978.
 15. Ya-Xian Z, Suetake T, Tagami H. Number of cell layers of the stratum corneum in normal skin-relationship to the anatomical location on the body, age, sex and physical parameters. *Arch Dermatol Res.* 1999; 291:555-559.

(Received May 31, 2012; Revised June 16, 2012; Accepted June 18, 2012)

Effect of surfactant on lycopene-loaded nanostructured lipid carriers

Pornthida Riangjanapatee, Siriporn Okonogi*

Faculty of Pharmacy, Chiang Mai University, Chiang Mai, Thailand.

ABSTRACT: Nanostructured lipid carriers (NLC) have gained high interest as enhancing drug delivery systems *via* topical application during the last few years. NLC can enhance stability of many active substances against environmental stress. The extremely small size of NLC plays an important role in skin penetration. The unchanged size of NLC upon storage indicates its physical stability. The aim of this work was to investigate the effect of surfactant type on physical properties and stability of lycopene-loaded NLC. The preparation of the NLC was achieved by means of high pressure homogenization. The results indicate that different types of surfactant yield NLC with different properties. We also explored the effect of contact angle on the size of the NLC. It was found that the small contact angle gave NLC with small size. Among two small contact angle surfactants, Plantacare 1200 gave lycopene-loaded NLC with smaller size, higher zeta potential and narrower size distribution. The particle size, size distribution, and zeta potential of lycopene-loaded NLC prepared with Plantacare 1200 was unchanged during 30 days of storage. It was concluded that Plantacare 1200 is the most suitable surfactant for lycopene-loaded NLC. The chemical stability of lycopene entrapped in the NLC was significantly enhanced.

Keywords: NLC, surfactant, orange wax, lycopene, stability

1. Introduction

Nanostructured lipid carrier (NLC), the second generation innovative lipid nanoparticle that acts as a bioactive carrier system, has been developed to overcome some potential limitations of the solid lipid nanoparticle (SLN). NLC has attracted increasing scientific and commercial attention during the last few years (1,2) due to the lower risk of systemic side effects and is suitable for transdermal

administration (3,4). It has benefits over SLN in improving release properties (5-7). NLC can reduce irritation, increase absorption of the active compound to skin, and protect photolabile agents from light. In addition, the expulsion of drug entrapped in NLC during storage is minimized or avoided. NLC is an alternative carrier to other drug carrier systems such as liposomes and polymeric nanoparticles because it has combined the advantages of other colloidal carriers and avoided their disadvantages. These include high amounts of drug payload, increasing drug stability, the possibility to control drug release and targeting, and avoidance of organic solvents (8).

Many water-insoluble active compounds were reported to be successfully incorporated in NLC and showed high advantages in skin permeation (9,10). Lycopene, a potential natural antioxidant found in tomatoes and tomato-based food products, watermelon, and pink grapefruit (11) has so far become one of the most interesting molecules. It is an acyclic carotene with 11 conjugated double bonds and possesses the highest antioxidant activity among common carotenoid compounds (12). Lycopene functions as an antioxidant, anti-inflammatory, anti-cancer, and anti-mutagenic agent and exhibits a high physical quenching rate constant for singlet oxygen *in vitro* (13-15). However, lycopene is water insoluble and hardly diffuses *via* the transdermal pathway when applied topically. Lycopene is an unstable molecule. Because of many conjugated double bonds in its molecule, it is very susceptible to oxidation when exposed to air and light (16). NLC were reported to give excellent protection to incorporated labile drugs from degradation (17). The utilization of NLC to increase stability of lycopene is a challenge and has not yet been reported anywhere. Moreover, it is known that for a sufficient residence time and optimal penetration *via* the transdermal route in order to obtain the maximum therapeutic efficiency, the size of NLC plays the most important role (18). The unchanged size of NLC upon storage indicates its physical stability as well as its effectiveness. As NLC is derived from the emulsion system, the NLC hence is mainly stabilized by a surface active molecule or a so-called surfactant. In the process of NLC production, the spreading of surfactant on the surface of an oil droplet of lipid is one of the main reactions required for desirable NLC. One impact for this interaction is contact angle, an angle which is created at the point where the three phases composed of gas, liquid and solid

*Address correspondence to:

Dr. Siriporn Okonogi, Faculty of Pharmacy, Chiang Mai University, Chiang Mai 50200, Thailand.
E-mail: sirioko@chiangmai.ac.th

meet (19). It is known that contact angle influences the spreading of liquid onto the solid substrate (20,21). At the present time, there are very few systematic investigations of the quantitative relationship between surfactant solution and the spreading behavior of the solid lipids.

In the present study, several surfactants which showed a different contact angle to the major lipid of NLC were first investigated. We hypothesized that contact angle might be a useful tool for selection of a suitable surfactant for a small size NLC within a short time. The main aim of this study was to evaluate the effect of surfactant type on stability of lycopene loaded NLC.

2. Materials and Methods

2.1. Materials

Orange wax was provided by Koster Keunen, LLC (Connecticut, USA). Plantacare 1200 (lauryl glucoside) were from Cognis (Dusseldorf, Germany). C-1216 (sucrose laurate), C-1816 (sucrose stearate), C-1616 (sucrose palmitate), C-1815 (sucrose stearate) surfactants were obtained from Surfhope® SE Cosme marketed by Mitsubishi-Kagaku Foods Corporation (Japan). Lycopene was obtained in the form of an oily solution containing 40-47 mg/L of tomato lycopene in rosemary oil under the trade name of "Lycosol" (LiBiol, Germany). Tetrahydrofuran (THF) was from Rankem, New Delhi, India. Ultra-purified water was obtained from a MilliQ Plus system, Millipore (Schwalbach, Germany).

2.2. Preparation of lycopene-loaded NLC

NLC formulations using orange wax as a major lipid core were produced using a high pressure homogenizer (HPH) (Micron LAB40, Homogenizer Systems, Germany). The melted lipid phase containing orange wax (90%, w/w) and lycopene oil solution (10%, w/w) was dispersed in a hot surfactant solution (75°C), obtaining a pre-emulsion by high speed stirring using an Ultra-Turrax T25 (Janke and Kunkel GmbH, Staufen, Germany) at 12,000 rpm for 30 sec. This hot pre-emulsion was further processed by HPH applying five cycles at 500 bar and 75°C. The lipid dispersion was cooled at ambient conditions to room temperature and solidified to obtain the aqueous NLC dispersions.

2.3. Contact angle measurement

Contact angle between lipid surface and surfactant was determined by means of goniometry. The solid surface was prepared on a microscopic glass slide using an appropriate amount of lipid mixture composed of 90% (w/w) orange wax and 10% (w/w) lycopene oil solution. The series of 0.1% (w/v) aqueous solutions of five different surfactants; C-1216, C-1816, C-1616, C-1815, and Plantacare 1200 were freshly prepared. The contact angle between the lipid surface and a single drop of

the surfactant solution was determined 15 sec after the droplet was put onto the lipid surface using a Contact Angle Meter G1 (Krüss, Hamburg, Germany).

2.4. Particle size and zeta potential measurement

Analysis of the particle size, size distribution, and zeta potential was carried out by means of photon correlation spectroscopy (PCS) with a Malvern Zetasizer IV (Malvern Instruments, UK). The PCS yielded mean particle size (z-ave) and polydispersity index (PDI) which indicated the width of the size distribution. The z-ave and PDI values were obtained by averaging at least ten measurements at a fixed angle of 90° in 10-mm diameter cells at 25°C. All samples were diluted with purified water to have a suitable scattering intensity before measurement. For measuring zeta potential the sample was dispersed in purified water adjusted with sodium chloride solution (0.9%, w/v) to a conductivity of 50 µS/cm. The experiments were done in triplicate.

2.5. Stability test

To evaluate the physical stability of lycopene-loaded NLC, the samples of NLC dispersions were stored at 25°C over a period of 30 days. The changes of particle size, size distribution, and zeta potential against storage time were determined using PCS. The chemical stability of lycopene-loaded NLC was investigated as follows. Lycopene-loaded NLC dispersion containing 40 µg/mL lycopene and lycopene solution in THF of equivalent lycopene concentration were exposed to light at 50°C for 24 h. The amount of lycopene remaining in each sample during storage time was determined periodically using UV/visible spectroscopy at 475 nm with a UV-2450 double-beam spectrophotometer (Shimadzu, America) and THF as a solvent for dissolving lycopene in the NLC.

2.6. Statistical analysis

Statistical analysis of differences between different treatments was performed using analysis of variance (ANOVA). In all cases, $p < 0.05$ indicates the level of significance.

3. Results and Discussion

It is well known that surfactant is a group of hydrophilic-lipophilic molecules which are active at the interface of two immiscible liquid phases. The surfactant can produce huge advantages in pharmaceutical fields. By chemical structure, surfactant can be divided into two main groups of ionic and non-ionic surfactants with different solubility properties defined by the value of hydrophilic-lipophilic balance (HLB). The lower HLB surfactants give a w/o emulsion while the higher HLB molecules provide an o/w emulsion. Because NLC is derived from an o/w

emulsion system, the surfactants used in this study were of a higher HLB group which are preferably dissolved in an aqueous external phase of the emulsion. Moreover, as we emphasized developing the lycopene-loaded NLC for transdermal application, the surfactants of non-ionic groups particularly with a basic chemical structure of a sugar ester group were used in this study because they were claimed to be skin friendly. Besides their good compatibility with the skin, these surfactants also showed a drug enhancement effect in percutaneous absorption (22,23).

3.1. Effect of surfactant on contact angle

The contact angle is defined geometrically as the angle formed by a liquid at the three phase boundary where a liquid, gas, and solid intersect. It can be determined by goniometry (24). This technique is based on analysis of the shape of a drop of a test liquid on a test solid. A low contact angle value indicates well spreading or wetting while a high value indicates poor wetting or incompatibility. A zero contact angle represents complete wetting. In this study, five different surfactant solutions dropped on the solid surface composed of orange wax and lycopene oil solution demonstrated different contact angles as shown in Figure 1. It was obviously seen that the smallest contact angle of 38° was obtained from C-1216 followed closely by Plantacare 1200 which showed a contact angle of 39°. The other three surfactants; C-1816, C-1616, and C-1815, exhibited contact angle values higher than 45°. Considering the properties of surfactant, it was found that they are similar in basic properties. All five surfactants are non-ionic sugar esters with similar HLB values. The different contact angles obtained from these surfactants therefore were considered to be due to the number of carbon atoms existing in the hydrophobic chain of each molecule. The chemical structure of C-1216 (sucrose laurate) and Plantacare 1200 (lauryl glycoside) as shown in Figure 2 indicate that these two surfactants have 12 carbon atoms per molecule whereas the other surfactants such as sucrose stearate (C-1815 and C-1816) and sucrose palmitate (C-1616) possess 18 and 16 carbon atoms, respectively. It was considered that the surfactants with the shorter hydrocarbon chain length of C12 were more appropriate for the surface of lycopene-orange wax than that of C15-C18.

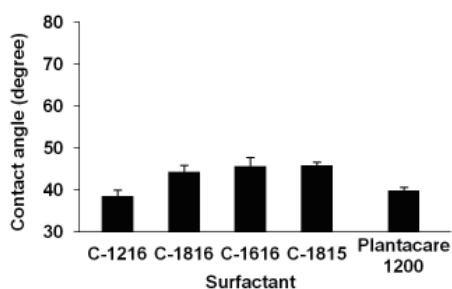


Figure 1. Contact angle between surfactant solution and lipid surface of orange wax and lycopene mixture.

3.2. Effect of surfactant on the particle size of the NLC

In this study, lycopene loaded NLC formulations of five different surfactants were produced. The orange wax was used as a major lipid component. Orange wax is light reddish-brown to orange in color with properties of sunscreen-enhancing (25), antioxidant (26), and antimicrobial activities (27). Lycopene also has an anti-stress effect related to inhibition of harmful effects from UV exposure, because it is an effective agent against solar stress (28,29). The development of lycopene loaded NLC in this study was expected to promote an additional biological action of both orange wax and lycopene as well as to enhance their bioavailability *via* the NLC system. Moreover, lycopene was used as the oil solution in order to reduce the degree of organization of lipid matrix of orange wax after the process of NLC production by hot high pressure homogenization. The results of this study revealed that the five different surfactants produced lycopene-loaded NLC with different sizes as shown in Figure 3. It was found that only two surfactants, C-1216

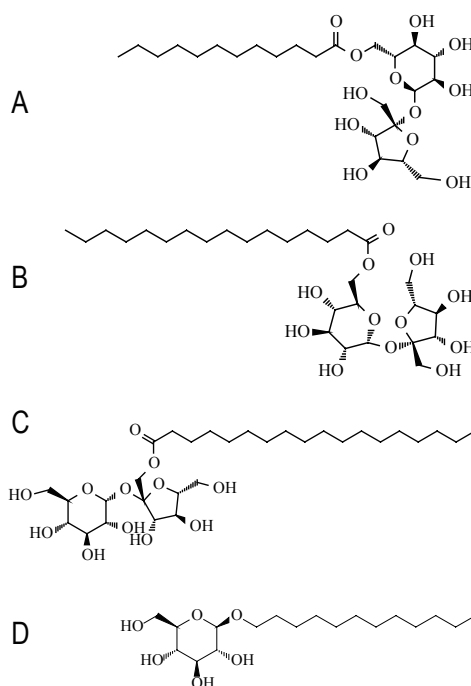


Figure 2. Chemical structure of sucrose laurate (A), sucrose palmitate (B), sucrose stearate (C), and lauryl glycoside (D).

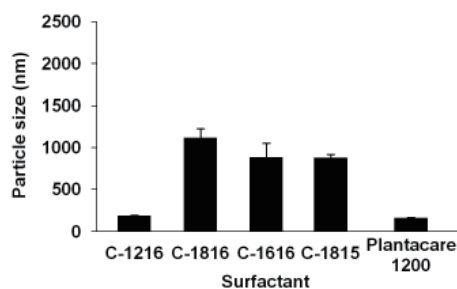


Figure 3. Particle size of lycopene-loaded NLC stabilized by different surfactants.

and Plantacare 1200, could yield the extremely smallest size NLC with z-ave of approximately 170-190 nm. The NLC particles obtained from C-1616, C-1816, and C-1815 were obviously greater with a z-ave higher than 900 nm. Considering this effect with the contact angle values obtained from the five surfactants mentioned above, it was found that the contact angle value and the particle size of the NLC were closely related. The results demonstrated that the small particle size of lycopene-loaded NLC was obtained from the surfactants with small contact angles of less than 40°. According to the famous Young equation (30), surfactants with lower surface tension give smaller contact angles. Moreover, a surfactant solution with lower surface tension can reduce more surface or interfacial free energy. Considering the data obtained from this experiment, it could be presumed that the small particle size of the lycopene-loaded NLC obtained from the small contact angle surfactants was due to the high capacity of decreasing interfacial free energy between the two immiscible lipid and aqueous phases during the emulsion forming process.

3.3. Effect of surfactant on physical stability of the NLC

Two surfactants, C-1216 and Plantacare 1200, were selected to use in this study because they showed the smallest contact angle value and high ability to produce the smallest size lycopene-loaded NLC. The NLC formulations obtained from both surfactants were evaluated for their particle size (z-ave), size distribution (PDI), and zeta potential. The results demonstrated that the mean size of the freshly prepared NLC of both formulations was not significant different with a z-ave of approximately 170-190 nm. However, the PDI and zeta potential of these particles were different. The PDI of lycopene-loaded NLC obtained from C-1216 was 0.3 whereas that of Plantacare 1200 was 0.1. The zeta potential of the NLC obtained from C-1216 was -52 mV whereas that obtained from Plantacare 1200 was -62 mV. Keeping these formulations at 25°C for 30 days caused the zeta potential of the NLC obtained from C-1216 to decrease to -47 mV whereas no significant change of zeta potential in the NLC was obtained from Plantacare 1200 as seen in Figure 4. The particle size and size distribution of the

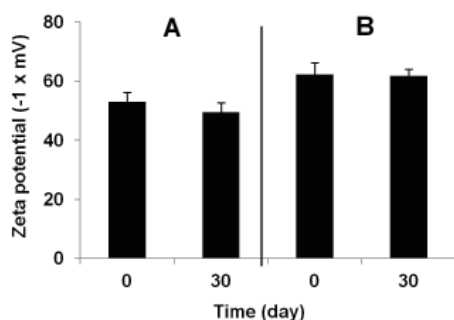


Figure 4. Effect of storage time on zeta potential of lycopene-loaded NLC stabilized by C-1216 (A) and Plantacare 1200 (B).

lycopene-loaded NLC were observed at day 7, day 14, and day 30 in comparison with those freshly prepared (day 0). The results are shown in Figures 5 and 6, respectively. It was found that the particle size of the NLC obtained from C-1216 was increased obviously during 30 days of

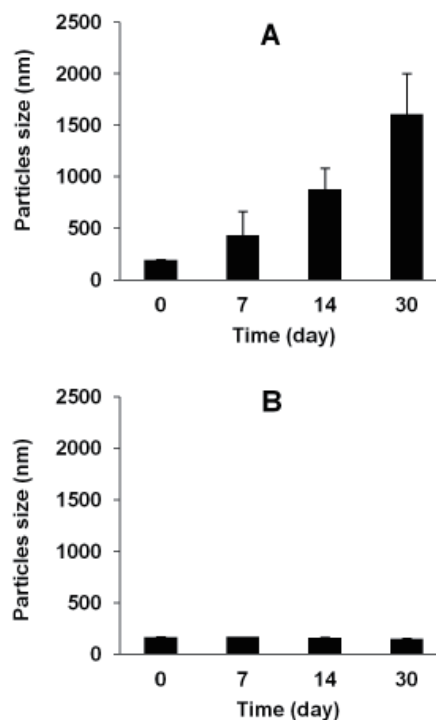


Figure 5. Effect of storage time on particle size of lycopene-loaded NLC stabilized by C-1216 (A) and Plantacare 1200 (B).

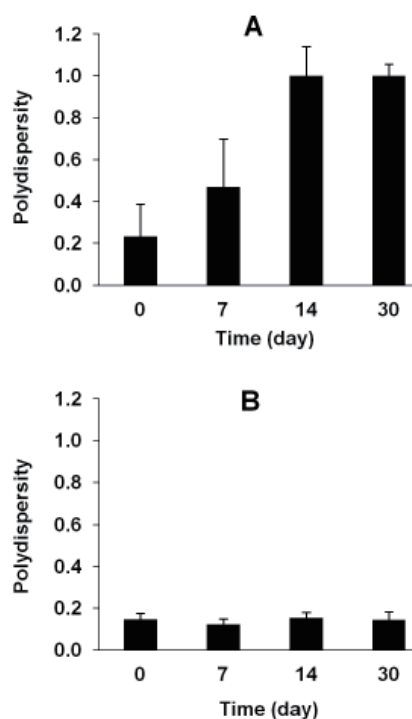


Figure 6. Effect of storage time on size distribution of lycopene-loaded NLC stabilized by C-1216 (A) and Plantacare 1200 (B).

storage whereas the size and PDI of that obtained from Plantacare 1200 showed no significant change. Therefore the lycopene-loaded NLC obtained from Plantacare 1200 were revealed to be more stable than that from C-1216. The good narrow size distribution with constant small particle size of the NLC obtained from Plantacare 1200 throughout the period of 30 days might be due to the strong effect of Plantacare 1200 to produce an extremely high zeta potential at the surface of the NLC system. The high zeta potential of the Plantacare 1200 based NLC was considered to be due to the hydroxyl ions caused by Plantacare 1200 molecules surrounding the surface of the NLC nanoparticles. The high zeta potential resulted from the electrical charge on this particle surface which repulsed the charge from other particles, and therefore made a stable NLC system. This is a reason why the lycopene-loaded NLC stabilized by Plantacare 1200 showed higher stability overtime than those made from C-1216. The results of this investigation demonstrated the influence and mechanism of the surfactant on enhancing NLC stability. Moreover, it can be assumed that Plantacare 1200 is the most suitable surfactant for producing lycopene-loaded NLC having orange wax as a major lipid at this moment.

3.4. Chemical stability of the lycopene

This experiment was done in order to study the chemical stability of lycopene in solution in comparison with that loaded in the NLC. The results revealed that lycopene in solution decreased rapidly during the first 4 h of storage and further gradually decomposed as demonstrated in Figure 7A. The plot of log lycopene versus the storage time showed a linear regression with $y = 1.674 - 0.072x$ ($r^2 = 0.995$). It was found that the degradation profile of lycopene was extremely slowed when incorporated in the NLC stabilized by C1216 and Plantacare 1200 as shown in Figures 7B and 7C, respectively. The plot of log lycopene during the storage time showed a linear regression with $y = 1.596 - 0.006x$ ($r^2 = 0.992$) and $y = 1.599 - 0.004x$ ($r^2 = 0.997$) for C1216 and Plantacare 1200 systems, respectively. These results suggest that lycopene in the samples followed a first-order chemical degradation. The first-order kinetic calculation demonstrated that the half life of lycopene in solution was 9.6 h whereas that entrapped in the NLC was 117.5 and 192.5 h stabilized by C-1216 and Plantacare 1200, respectively. This result revealed that lycopene was most chemically stable when entrapped in the Plantacare-1200 NLC.

4. Conclusion

It was found that surfactant type influenced the quality of lycopene loaded NLC. The results of this study demonstrate that the contact angle is a key tool to overcome the small size NLC. Surfactant type also showed an important role on the zeta potential of

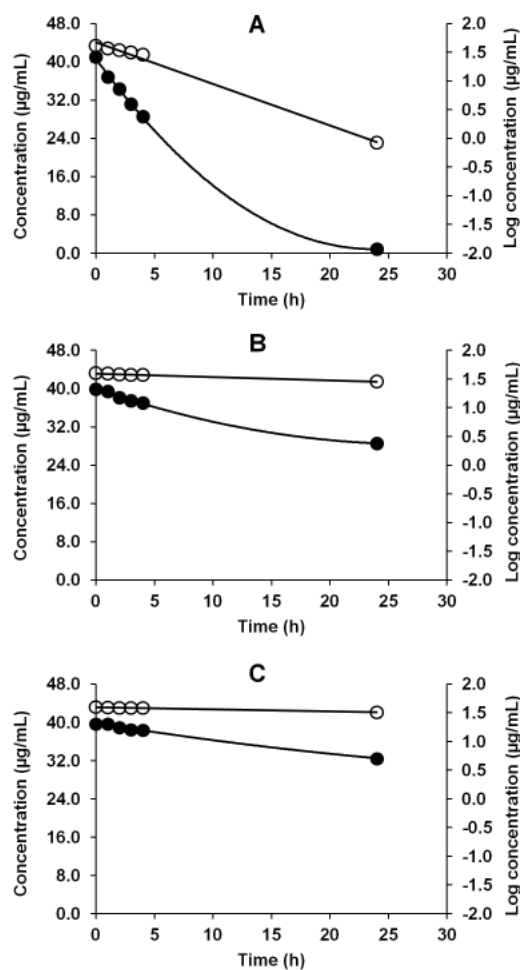


Figure 7. Stability profiles of lycopene concentration (●) and log concentration (○) in solution (A), C-1216 (B) and Plantacare-1200 (C) NLC dispersions.

the NLC. Plantacare 1200 was proven to be the best surfactant for lycopene-loaded NLC using orange wax as a major lipid. Lycopene was chemically stabilized by entrapping in the NLC.

Acknowledgements

The authors are grateful for financial support received from the Thailand Research Fund. We also thank the Graduate School, Chiang Mai University for their support.

References

- Schäfer-Korting M, Mehnert W, Korting HC. Lipid nanoparticles for improved topical application of drugs for skin diseases. *Adv Drug Deliv Rev.* 2007; 59:427-443.
- Souto EB, Müller RH. Investigation of the factors influencing the incorporation of clotrimazole in SLN and NLC prepared by hot high-pressure homogenization. *J Microencapsul.* 2006; 23:377-388.
- Fang JY, Fang CL, Liu CH, Su YH. Lipid nanoparticles as vehicles for topical psoralen delivery: Solid lipid

- nanoparticles (SLN) versus nanostructured lipid carriers (NLC). *Eur J Pharm Biopharm.* 2008; 70:633-640.
4. Souto EB, Müller RH. SLN and NLC for topical delivery of ketoconazole. *J Microencapsul.* 2005; 22:501-510.
 5. Pardeike J, Hommoss A, Müller RH. Lipid nanoparticles (SLN, NLC) in cosmetic and pharmaceutical dermal products. *Int J Pharm.* 2009; 366:170-184.
 6. Muller RH, Radtke M, Wissing SA. Solid lipid nanoparticles (SLN) and nanostructured lipid carriers (NLC) in cosmetic and dermatological preparations. *Adv Drug Deliv Rev.* 2002; 54:S131-S155.
 7. Muller RH, Petersen RD, Hommoss A, Pardeike J. Nanostructured lipid carriers (NLC) in cosmetic dermal products. *Adv Drug Deliv Rev.* 2007; 59:522-530.
 8. Puglia C, Blasi P, Rizza L, Schoubben A, Bonina F, Rossi C, Ricci M. Lipid nanoparticles for prolonged topical delivery: An *in vitro* and *in vivo* investigation. *Int J Pharm.* 2008; 357:295-304.
 9. Hentschel A, Gramdorf S, Müller RH, Kurz T. β -carotene-loaded nanostructured lipid carriers. *J Food Sci.* 2008; 73:N1-N6.
 10. Pardeike J, Müller RH. Coenzyme Q10 loaded NLCs: Preparation, occlusion properties and penetration enhancement. *Pharm Technol Eur.* 2007; 19:46-49.
 11. Olives Barba AI, Camara Hurtado M, Sanchez Mata MC, Fernandez Ruiz V, Lopez Saenz de Tejada M. Application of a UV-vis detection-HPLC method for a rapid determination of lycopene and β -carotene in vegetables. *Food Chem.* 2006; 95:328-336.
 12. Bramley PM. Is lycopene beneficial to human health? *Phytochemistry.* 2000; 54:233-236.
 13. Giovannucci E. Tomatoes, tomato-based products, lycopene, and cancer: A review of the epidemiologic literature. *J Natl Cancer Inst.* 1999; 91:317-331.
 14. Heber D, Lu QY. Overview of mechanisms of action of lycopene. *Exp Biol Med (Maywod).* 2002; 227:920-923.
 15. Shi J, Le Maguer M, Bryan M, Kakuda Y. Kinetics of lycopene degradation in tomato puree by heat and light irradiation. *J Food Process Eng.* 2003; 25:485-498.
 16. Sharma SK, Le Maguer M. Kinetics of lycopene degradation in tomato pulp solids under different processing and storage conditions. *Food Res Int.* 1996; 29:309-315.
 17. Wissing SA, Kayser O, Müller RH. Solid lipid nanoparticles for parenteral drug delivery. *Adv Drug Delivery Rev.* 2004; 56:1257-1272.
 18. Souto EB, Almeida AJ, Müller RH. Lipid nanoparticles (SLN[®], NLC[®]) for cutaneous drug delivery: Structure, protection and skin effects. *J Biomed Nanotechnol.* 2007; 3:317-331.
 19. Xie X, Morrow NR, Buckley JS. Contact angle hysteresis and the stability of wetting changes induced by adsorption from crude oil. *J Petro Sci Eng.* 2002; 33:147-159.
 20. Decker EL, Frank B, Suo Y, Garoff S. Physics of contact angle measurement. *Colloid Surface A.* 1999; 156:177-189.
 21. Kwok DY, Neumann AW. Contact angle measurement and contact angle interpretation. *Adv Colloid Interface Sci.* 1999; 81:167-249.
 22. Okamoto H, Sakai T, Tokuyama C, Danjo K. Sugar ester J-1216 enhances percutaneous permeation of ionized lidocaine. *J Pharm Sci.* 2011; 100:4482-4490.
 23. Arellano A, Santoyo S, Martn C, Ygartua P. Surfactant effects on the *in vitro* percutaneous absorption of diclofenac sodium. *Eur J Drug Metab Pharmacokinet.* 1998; 23:307-312.
 24. Dove JW, Buckton G, Doherty C. A comparison of two contact angle measurement methods and inverse gas chromatography to assess the surface energies of theophylline and caffeine. *Int J Pharm.* 1996; 138:199-206.
 25. Reynhardt EC, Riederer M. Structure and molecular dynamics of the cuticular wax from leaves of *Citrus aurantium* L. *J Phys D: Appl Phys.* 1991; 24:478-486.
 26. Puleo S, Rit TP. Natural waxes: Past, present, and future. *Lipid technol.* 1992; 4:82-90.
 27. Caccioni DR, Guizzardi M, Biondi DM, Renda A, Ruberto G. Relationship between volatile components of citrus fruit essential oils and antimicrobial action on *Penicillium digitatum* and *Penicillium italicum*. *Int J Food Microbiol.* 1998; 43:73-79.
 28. Stahl W, Sies H. Carotenoids and flavonoids contribute to nutritional protection against skin damage from sunlight. *Mol Biotechnol.* 2007; 37:26-30.
 29. Sies H, Stahl W. Carotenoids and UV Protection. *Photochem Photobiol Sci.* 2004; 3:749-752.
 30. Good RJ. Contact angle, wetting, and adhesion: A critical review. In: *Contact Angle, Wetting and Adhesion* (Mittal KL, ed.). Utrecht: VSP, The Netherlands, 1993; pp. 3-36.

(Received November 19, 2011; Revised April 19, 2012; Accepted May 8, 2012)

Guide for Authors

1. Scope of Articles

Drug Discoveries & Therapeutics welcomes contributions in all fields of pharmaceutical and therapeutic research such as medicinal chemistry, pharmacology, pharmaceutical analysis, pharmaceuticals, pharmaceutical administration, and experimental and clinical studies of effects, mechanisms, or uses of various treatments. Studies in drug-related fields such as biology, biochemistry, physiology, microbiology, and immunology are also within the scope of this journal.

2. Submission Types

Original Articles should be well-documented, novel, and significant to the field as a whole. An Original Article should be arranged into the following sections: Title page, Abstract, Introduction, Materials and Methods, Results, Discussion, Acknowledgments, and References. Original articles should not exceed 5,000 words in length (excluding references) and should be limited to a maximum of 50 references. Articles may contain a maximum of 10 figures and/or tables.

Brief Reports definitively documenting either experimental results or informative clinical observations will be considered for publication in this category. Brief Reports are not intended for publication of incomplete or preliminary findings. Brief Reports should not exceed 3,000 words in length (excluding references) and should be limited to a maximum of 4 figures and/or tables and 30 references. A Brief Report contains the same sections as an Original Article, but the Results and Discussion sections should be combined.

Reviews should present a full and up-to-date account of recent developments within an area of research. Normally, reviews should not exceed 8,000 words in length (excluding references) and should be limited to a maximum of 100 references. Mini reviews are also accepted.

Policy Forum articles discuss research and policy issues in areas related to life science such as public health, the medical care system, and social science and may address governmental issues at district, national, and international levels of discourse. Policy Forum articles should not exceed 2,000 words in length (excluding references).

Case Reports should be detailed reports of the symptoms, signs, diagnosis, treatment, and follow-up of an individual patient. Case reports may contain a demographic profile of the patient but usually describe an unusual or novel occurrence. Unreported or unusual side effects or adverse interactions involving medications will also be considered. Case

Reports should not exceed 3,000 words in length (excluding references).

News articles should report the latest events in health sciences and medical research from around the world. News should not exceed 500 words in length.

Letters should present considered opinions in response to articles published in Drug Discoveries & Therapeutics in the last 6 months or issues of general interest. Letters should not exceed 800 words in length and may contain a maximum of 10 references.

3. Editorial Policies

Ethics: Drug Discoveries & Therapeutics requires that authors of reports of investigations in humans or animals indicate that those studies were formally approved by a relevant ethics committee or review board.

Conflict of Interest: All authors are required to disclose any actual or potential conflict of interest including financial interests or relationships with other people or organizations that might raise questions of bias in the work reported. If no conflict of interest exists for each author, please state "There is no conflict of interest to disclose".

Submission Declaration: When a manuscript is considered for submission to Drug Discoveries & Therapeutics, the authors should confirm that 1) no part of this manuscript is currently under consideration for publication elsewhere; 2) this manuscript does not contain the same information in whole or in part as manuscripts that have been published, accepted, or are under review elsewhere, except in the form of an abstract, a letter to the editor, or part of a published lecture or academic thesis; 3) authorization for publication has been obtained from the authors' employer or institution; and 4) all contributing authors have agreed to submit this manuscript.

Cover Letter: The manuscript must be accompanied by a cover letter signed by the corresponding author on behalf of all authors. The letter should indicate the basic findings of the work and their significance. The letter should also include a statement affirming that all authors concur with the submission and that the material submitted for publication has not been published previously or is not under consideration for publication elsewhere. The cover letter should be submitted in PDF format. For example of Cover Letter, please visit <http://www.ddtjournal.com/downloadcentre.php> (Download Centre).

Copyright: A signed JOURNAL PUBLISHING AGREEMENT (JPA) must be provided by post, fax, or as a scanned file before acceptance of the article. Only forms with a hand-written signature are accepted. This copyright will ensure the widest possible dissemination of information. A form facilitating transfer of copyright can be downloaded by clicking the appropriate link and can be returned to the e-mail address or fax number noted on the form (Please visit

Download Centre). Please note that your manuscript will not proceed to the next step in publication until the JPA form is received. In addition, if excerpts from other copyrighted works are included, the author(s) must obtain written permission from the copyright owners and credit the source(s) in the article.

Suggested Reviewers: A list of up to 3 reviewers who are qualified to assess the scientific merit of the study is welcomed. Reviewer information including names, affiliations, addresses, and e-mail should be provided at the same time the manuscript is submitted online. Please do not suggest reviewers with known conflicts of interest, including participants or anyone with a stake in the proposed research; anyone from the same institution; former students, advisors, or research collaborators (within the last three years); or close personal contacts. Please note that the Editor-in-Chief may accept one or more of the proposed reviewers or may request a review by other qualified persons.

Language Editing: Manuscripts prepared by authors whose native language is not English should have their work proofread by a native English speaker before submission. If not, this might delay the publication of your manuscript in Drug Discoveries & Therapeutics.

The Editing Support Organization can provide English proofreading, Japanese-English translation, and Chinese-English translation services to authors who want to publish in Drug Discoveries & Therapeutics and need assistance before submitting a manuscript. Authors can visit this organization directly at <http://www.iacmhr.com/iac-eso/support.php?lang=en>. IAC-ESO was established to facilitate manuscript preparation by researchers whose native language is not English and to help edit works intended for international academic journals.

4. Manuscript Preparation

Manuscripts should be written in clear, grammatically correct English and submitted as a Microsoft Word file in a single-column format. Manuscripts must be paginated and typed in 12-point Times New Roman font with 24-point line spacing. Please do not embed figures in the text. Abbreviations should be used as little as possible and should be explained at first mention unless the term is a well-known abbreviation (e.g. DNA). Single words should not be abbreviated.

Title page: The title page must include 1) the title of the paper (Please note the title should be short, informative, and contain the major key words); 2) full name(s) and affiliation(s) of the author(s); 3) abbreviated names of the author(s); 4) full name, mailing address, telephone/fax numbers, and e-mail address of the corresponding author; and 5) conflicts of interest (if you have an actual or potential conflict of interest to disclose, it must be included as a footnote on the title page of the manuscript; if no conflict of interest exists for each author, please state "There is no conflict of interest to disclose"). Please visit [Download Centre](#) and refer to the title page of the manuscript sample.

Abstract: A one-paragraph abstract consisting of no more than 250 words must be included. The abstract should briefly state the purpose of the study, methods, main findings, and conclusions. Abbreviations must be kept to a minimum and non-standard abbreviations explained in brackets at first mention. References should be avoided in the abstract. Key words or phrases that do not occur in the title should be included in the Abstract page.

Introduction: The introduction should be a concise statement of the basis for the study and its scientific context.

Materials and Methods: The description should be brief but with sufficient detail to enable others to reproduce the experiments. Procedures that have been published previously should not be described in detail but appropriate references should simply be cited. Only new and significant modifications of previously published procedures require complete description. Names of products and manufacturers with their locations (city and state/country) should be given and sources of animals and cell lines should always be indicated. All clinical investigations must have been conducted in accordance with Declaration of Helsinki principles. All human and animal studies must have been approved by the appropriate institutional review board(s) and a specific declaration of approval must be made within this section.

Results: The description of the experimental results should be succinct but in sufficient detail to allow the experiments to be analyzed and interpreted by an independent reader. If necessary, subheadings may be used for an orderly presentation. All figures and tables must be referred to in the text.

Discussion: The data should be interpreted concisely without repeating material already presented in the Results section. Speculation is permissible, but it must be well-founded, and discussion of the wider implications of the findings is encouraged. Conclusions derived from the study should be included in this section.

Acknowledgments: All funding sources should be credited in the Acknowledgments section. In addition, people who contributed to the work but who do not meet the criteria for authors should be listed along with their contributions.

References: References should be numbered in the order in which they appear in the text. Citing of unpublished results, personal communications, conference abstracts, and theses in the reference list is not recommended but these sources may be mentioned in the text. In the reference list, cite the names of all authors when there are fifteen or fewer authors; if there are sixteen or more authors, list the first three followed by *et al.* Names of journals should be abbreviated in the style used in PubMed. Authors are responsible for the accuracy of the references. Examples are given below:

Example 1 (Sample journal reference):
Nakata M, Tang W. Japan-China Joint Medical Workshop on Drug Discoveries and Therapeutics 2008: The need of Asian pharmaceutical researchers' cooperation. *Drug Discov Ther.* 2008; 2:262-263.

Example 2 (Sample journal reference with more than 15 authors):
Darby S, Hill D, Auvinen A, *et al.* Radon in homes and risk of lung cancer: Collaborative analysis of individual data from 13 European case-control studies. *BMJ.* 2005; 330:223.

Example 3 (Sample book reference):
Shalev AY. Post-traumatic stress disorder: Diagnosis, history and life course. In: *Post-traumatic Stress Disorder, Diagnosis, Management and Treatment* (Nutt DJ, Davidson JR, Zohar J, eds.). Martin Dunitz, London, UK, 2000; pp. 1-15.

Example 4 (Sample web page reference):
World Health Organization. The World Health Report 2008 – primary health care: Now more than ever. http://www.who.int/whr/2008/whr08_en.pdf (accessed September 23, 2010).

Tables: All tables should be prepared in Microsoft Word or Excel and should be arranged at the end of the manuscript after the References section. Please note that tables should not in image format. All tables should have a concise title and should be numbered consecutively with Arabic numerals. If necessary, additional information should be given below the table.

Figure Legend: The figure legend should be typed on a separate page of the main manuscript and should include a short title and explanation. The legend should be concise but comprehensive and should be understood without referring to the text. Symbols used in figures must be explained.

Figure Preparation: All figures should be clear and cited in numerical order in the text. Figures must fit a one- or two-column format on the journal page: 8.3 cm (3.3 in.) wide for a single column, 17.3 cm (6.8 in.) wide for a double column; maximum height: 24.0 cm (9.5 in.). Please make sure that artwork files are in an acceptable format (TIFF or JPEG) at minimum resolution (600 dpi for illustrations, graphs, and annotated artwork, and 300 dpi for micrographs and photographs). Please provide all figures as separate files. Please note that low-resolution images are one of the leading causes of article resubmission and schedule delays. All color figures will be reproduced in full color in the online edition of the journal at no cost to authors.

Units and Symbols: Units and symbols conforming to the International System of Units (SI) should be used for physicochemical quantities. Solidus notation (*e.g.* mg/kg, mg/mL, mol/mm²/min) should be used. Please refer to the SI Guide www.bipm.org/en/si/ for standard units.

Supplemental data: Supplemental data might be useful for supporting and enhancing your scientific research and

Drug Discoveries & Therapeutics accepts the submission of these materials which will be only published online alongside the electronic version of your article. Supplemental files (figures, tables, and other text materials) should be prepared according to the above guidelines, numbered in Arabic numerals (*e.g.*, Figure S1, Figure S2, and Table S1, Table S2) and referred to in the text. All figures and tables should have titles and legends. All figure legends, tables and supplemental text materials should be placed at the end of the paper. Please note all of these supplemental data should be provided at the time of initial submission and note that the editors reserve the right to limit the size and length of Supplemental Data.

5. Submission Checklist

The Submission Checklist will be useful during the final checking of a manuscript prior to sending it to Drug Discoveries & Therapeutics for review. Please visit [Download Centre](#) and download the Submission Checklist file.

6. Online submission

Manuscripts should be submitted to Drug Discoveries & Therapeutics online at <http://www.ddtjournal.com>. The manuscript file should be smaller than 5 MB in size. If for any reason you are unable to submit a file online, please contact the Editorial Office by e-mail at office@ddtjournal.com

7. Accepted manuscripts

Proofs: Galley proofs in PDF format will be sent to the corresponding author *via* e-mail. Corrections must be returned to the editor (proof-editing@ddtjournal.com) within 3 working days.

Offprints: Authors will be provided with electronic offprints of their article. Paper offprints can be ordered at prices quoted on the order form that accompanies the proofs.

Page Charge: A page charge of \$140 will be assessed for each printed page of an accepted manuscript. The charge for printing color figures is \$340 for each page. Under exceptional circumstances, the author(s) may apply to the editorial office for a waiver of the publication charges at the time of submission.

(Revised October 2011)

Editorial and Head Office:

Pearl City Koishikawa 603
2-4-5 Kasuga, Bunkyo-ku
Tokyo 112-0003
Japan
Tel: +81-3-5840-9697
Fax: +81-3-5840-9698
E-mail: office@ddtjournal.com

JOURNAL PUBLISHING AGREEMENT (JPA)

Manuscript No.:

Title:

Corresponding author:

The International Advancement Center for Medicine & Health Research Co., Ltd. (IACMHR Co., Ltd.) is pleased to accept the above article for publication in Drug Discoveries & Therapeutics. The International Research and Cooperation Association for Bio & Socio-Sciences Advancement (IRCA-BSSA) reserves all rights to the published article. Your written acceptance of this JOURNAL PUBLISHING AGREEMENT is required before the article can be published. Please read this form carefully and sign it if you agree to its terms. The signed JOURNAL PUBLISHING AGREEMENT should be sent to the Drug Discoveries & Therapeutics office (Pearl City Koishikawa 603, 2-4-5 Kasuga, Bunkyo-ku, Tokyo 112-0003, Japan; E-mail: office@ddtjournal.com; Tel: +81-3-5840-9697; Fax: +81-3-5840-9698).

1. Authorship Criteria

As the corresponding author, I certify on behalf of all of the authors that:

- 1) The article is an original work and does not involve fraud, fabrication, or plagiarism.
- 2) The article has not been published previously and is not currently under consideration for publication elsewhere. If accepted by Drug Discoveries & Therapeutics, the article will not be submitted for publication to any other journal.
- 3) The article contains no libelous or other unlawful statements and does not contain any materials that infringes upon individual privacy or proprietary rights or any statutory copyright.
- 4) I have obtained written permission from copyright owners for any excerpts from copyrighted works that are included and have credited the sources in my article.
- 5) All authors have made significant contributions to the study including the conception and design of this work, the analysis of the data, and the writing of the manuscript.
- 6) All authors have reviewed this manuscript and take responsibility for its content and approve its publication.
- 7) I have informed all of the authors of the terms of this publishing agreement and I am signing on their behalf as their agent.

2. Copyright Transfer Agreement

I hereby assign and transfer to IACMHR Co., Ltd. all exclusive rights of copyright ownership to the above work in the journal Drug Discoveries & Therapeutics, including but not limited to the right 1) to publish, republish, derivate, distribute, transmit, sell, and otherwise use the work and other related material worldwide, in whole or in part, in all languages, in electronic, printed, or any other forms of media now known or hereafter developed and the right 2) to authorize or license third parties to do any of the above.

I understand that these exclusive rights will become the property of IACMHR Co., Ltd., from the date the article is accepted for publication in the journal Drug Discoveries & Therapeutics. I also understand that IACMHR Co., Ltd. as a copyright owner has sole authority to license and permit reproductions of the article.

I understand that except for copyright, other proprietary rights related to the Work (e.g. patent or other rights to any process or procedure) shall be retained by the authors. To reproduce any text, figures, tables, or illustrations from this Work in future works of their own, the authors must obtain written permission from IACMHR Co., Ltd.; such permission cannot be unreasonably withheld by IACMHR Co., Ltd.

3. Conflict of Interest Disclosure

I confirm that all funding sources supporting the work and all institutions or people who contributed to the work but who do not meet the criteria for authors are acknowledged. I also confirm that all commercial affiliations, stock ownership, equity interests, or patent-licensing arrangements that could be considered to pose a financial conflict of interest in connection with the article have been disclosed.

Corresponding Author's Name (Signature):

Date:

